Process and Tool Development for Friction Stir Welding of Steels

A thesis submitted for the degree of

Doctor of technical sciences

(Doktor der technischen Wissenschaften)

By

Thomas Weinberger

Graz University of Technology

Institute for Materials Science and Welding

June, 2010

Statutory Declaration

I declare that I have authored this thesis independently, that I have not used other than the declared sources / resources, and that I have explicitly marked all material which has been quoted either literally or by content from the used sources.

……………………………   ……………………………………………..
date   (signature)

Preface

This thesis is submitted for the Doctoral Degree at Graz University of Technology, Austria. The research described herein was conducted under the supervision of Professor H. Cerjak at the Institute for Materials Science and Welding, Graz University of Technology between March 2006 and December 2009.

Some parts of this work have been published in the following conference proceedings and journals.

T. Weinberger, S. U. Khosa, B. Führer, N. Enzinger, Analysis of Tool Wear and Failure Mechanism during Friction Stir Welding of Steel, 7th International Symposium 'Friction Stir Welding', 2008, Paper on CD

T. Weinberger, Research Activities in the Area of Friction Stir Welding at IWS, Verarbeitungs- und Gebrauchseigenschaften von Werkstoffen - Heute und Morgen, 2008, Pages 97-98

T. Weinberger, B. Führer, S. U. Khosa, N. Enzinger, H.-H. Cerjak, H. Schröttner, S. Mitsche, Evolution of Microstructure and Properties for Friction Stir Welded Martensitic Precipitation-Hardening Steels, 8th International Conference on Trends in Welding Research Conference, 2009, Pages 398-402

T. Weinberger, N. Enzinger, H.-H. Cerjak, Microstructural and Mechanical Characterization of Friction Stir Welded 15-5PH Steel, Science and Technology of Welding and Joining 14, 2009, Pages 210-215

T. Weinberger, Device and Method for the Friction Stir Spot Welding of Two Workpieces with a Hollow Cylinder having a Detachable Friction Liner and with a Tool, Patent Application WO/2009/126981, 22.10.2009

T. Weinberger, N. Enzinger, Rührreibschweißen von Stahl: Momentaner Status, Schweiss- & Prüftechnik, Sonderband, 2009, Pages 32-34

T. Weinberger, N. Enzinger, C. Kuttin, C. Kolbeck, Werkzeugentwicklung für das Rührreibschweißen hochfester Werkstoffe, Schweiss- & Prüftechnik, Sonderband, 2009, Pages 35-37

Thomas Weinberger

June, 2010

Acknowledgements

First I would like to thank Prof. Horst Cerjak for the opportunity to perform this work in the area of friction stir welding under his supervision at the Institute for Materials Science and Welding. His encouragement, support and advice during the last years is gratefully acknowledged. I would also like to thank Prof. Jesper Henri Hattel for his review and valuable suggestions.

I would like to express my especially thanks to Dr. Norbert Enzinger for his guidance, help and support during the whole project period. My colleagues Gunter Figner and Saleem Khosa deserve special thanks for the valuable discussions and help.

I am sincerely grateful to all members of the Institute for the collegial and friendly atmosphere. I also wish to express my thanks to Kurt Kerschbaumer, Leander Herbitschek, Herbert Penker, Gernot Stöfan and Christian Schlieber for their support in the lab.

I gratefully acknowledge the financial support of the whole work as a part of the projects B6 and B7 of K-net JOIN granted by the Federal Ministry of Economy, Family and Youth, Austria.

Further, I would like to give my special thanks to the diploma students Bernhard Führer and Christof Kuttin who did excellent work within their master thesis.

All the help from Hartmuth Schröttner, Dr. Stefan Mitsche and Dr. Mihaela Albu from the Austrian Centre for Electron Microscopy and Nanoanalysis is gratefully acknowledged.

Finally I would like to thank my parents for their endless support throughout my life.

Abstract

Friction Stir Welding (FSW), a solid state welding technique which was developed by TWI in 1991, was initially used for metals with low strength and melting point e.g. aluminium alloys. But welding of steels is from production point of view one of the most significant area for many industrial applications. Due to this fact, the application of FSW and friction stir spot welding (FSSW) for steels has been intensively researched in the last years, but industrial applications are still missing due to extensive tool wear and/or tool fracture.

The aim of this study is the tool and process development for FSW and FSSW of steels and the characterization of the joints. The development was made using a state of the art friction stir welding machine with a water cooled welding head and different sensors to measure and record parameters like spindle torque or forces.

To select and develop proper tool materials which can be applied for FSW and FSSW of steels, the special requirements were determined by experiments and modeling. Candidate tool materials were selected, tested and evaluated. Based on this knowledge a tungsten carbide based tool was developed which fulfills the requirements. Therefore grain size, binder content and tool coating were optimized together with the tool geometry. The tool wear was analyzed for FSW and FSSW of different steels. The active wear and failure mechanisms that occur during friction stir welding of steel were evaluated.

After tool development, the process parameters were optimized for a butt weld of 2.6 mm thick 15-5PH steel. For the understanding of the microstructural development during FSW, the thermal and strain profile in the workpiece is essential. The hardening of 15-5PH steels is achieved by a martensitic matrix and the formation of submicroscopic copper rich particles in the matrix. To study the precipitation effects, samples from different locations were prepared and investigated using transmission electron microscopy (TEM) and energy-filtered transmission electron microscopy (EFTEM). With the combination of several methods, it was possible to identify the hardening mechanism and the influence of the thermal cycle on the precipitation process. Additionally, effects of post weld heat treatment on microstructure and properties of the joint have been analyzed.

Contents

List of Abbreviations

AHSS	Advanced high strength steels
AS	Advancing side
BM	Base metal
C	Symbol of the chemical element Carbon
Co	Symbol of the chemical element Cobalt
Cr	Symbol of the chemical element Chromium
Cu	Symbol of the chemical element Copper
EDXS	Energy Dispersive X-ray Spectroscopy
Fe	Symbol of the chemical element Iron
FSSW	Friction Stir Spot Welding
FSW	Friction Stir Welding
HAZ	Heat affected zone
HV	Vicker hardness
Ni	Symbol of the chemical element Nickel
PH	Precipitation hardening
RS	Retreating side
SEM	Scanning electron microscope
Si	Symbol of the chemical element Silicon
SZ	Stirzone
TEM	Transmission electron microscope
TMAZ	Thermo mechanically affected zone
W	Symbol of the chemical element Tungsten

1 Introduction

1.1   Fundamentals

The solid state welding process Friction Stir Welding (FSW) was invented at "The Welding Institute Ltd.", United Kingdom, in 1991 [1,2], and was initially applied to aluminium alloys. The basic concept of FSW is remarkable simple. A non consumable rotating tool with a specially designed pin and shoulder is inserted into the edges of sheets or plates to be joined and subsequently traversed along the joint line which is illustrated in Fig. 1-1.

The advancing and retreating side orientations require knowledge of the tool rotation and travel directions. In Fig. 1-1, the FSW tool rotates in the counterclockwise direction and travels into the page (or left to right). Therefore the advancing side is on the right, where the tool rotation direction is the same as the tool travel direction, and the retreating side is on the left, where the tool rotation is opposite the tool travel direction [3].
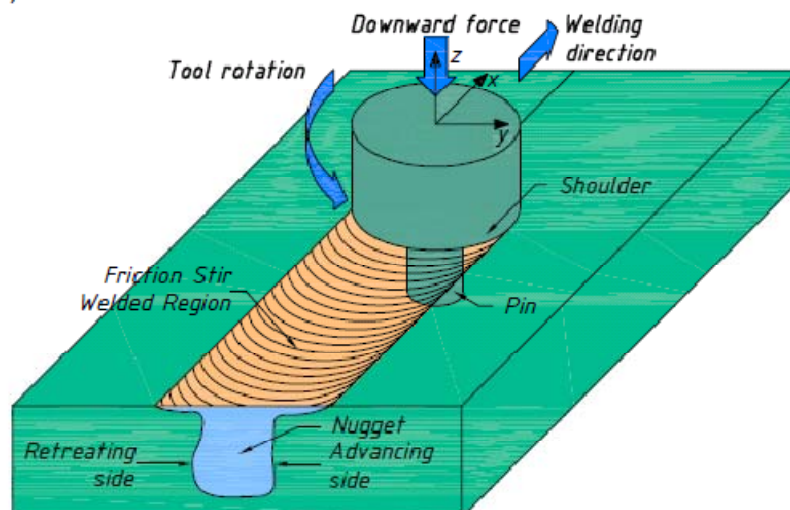
Fig. 1-1 Schematic drawing of friction stir welding

Because friction stir welding is a solid state welding process, following benefits are achieved compared to fusion welding processes:

- The weld is made in the solid phase, so it reduces the risk of cracking and/or avoids the emergence of porosities
- Additional filler materials are not necessary
- Excellent metallurgical properties
- Low distortion of work piece compared to fusion welding
- No significant surface and edge pre-weld preparations are necessary
- Easy to automate and monitor
- High quality reproducibility
- No smoke and radiations → Environment friendly process and pollution free working
- Avoiding of harmful chromium gases (when welding steel)

However, the friction stir welding process has also some disadvantages:

- Asymmetrical weld
- Remaining hole at the end of the weld when retracting the tool
- High axial forces
- Less flexibility than fusion welding processes

Due to the numerous advantages of the process and the excellent properties of the joints there is an increasing interest to use the process also for other materials like titanium, steel, etc. But these materials reach higher temperatures during welding than aluminium alloys and increased demands are requested to tool material and tool design. At the moment, the major factor limiting the implementation of the process into industrial applications for steels is the lack of a tool with sufficient service life at acceptable costs. Therefore the selection / development of appropriate tool materials is the most critical aspect.

Further, very limited literature is published about FSW of (high strength) steels. Especially these steel types are attractive for engineers because the performance of fusion welded joints is often very low. Beside the weldability of different steel types, the

joint properties and the microstructural development is of interest. Therefore deeper knowledge of the process like thermal field, peak temperatures, and strain rates in the workpiece is required.

The friction stir welding process can be divided into following stages:

1. Touch down of the tool (contact with workpiece)

2. Plunge phase

3. Welding Phase

4. Retracting of the tool

During the initial tool plunge, the lateral forces are fairly large, and extra care is required to ensure that plates in the butt configuration do not separate. To accomplish the weld, the rotating tool is plunged into the joint line and traversed along this line, while the shoulder of the tool is maintained in contact with the plate surface. Tool position and penetration depth are maintained by either position control or control of the applied normal force (Fig. 1-2) [3].
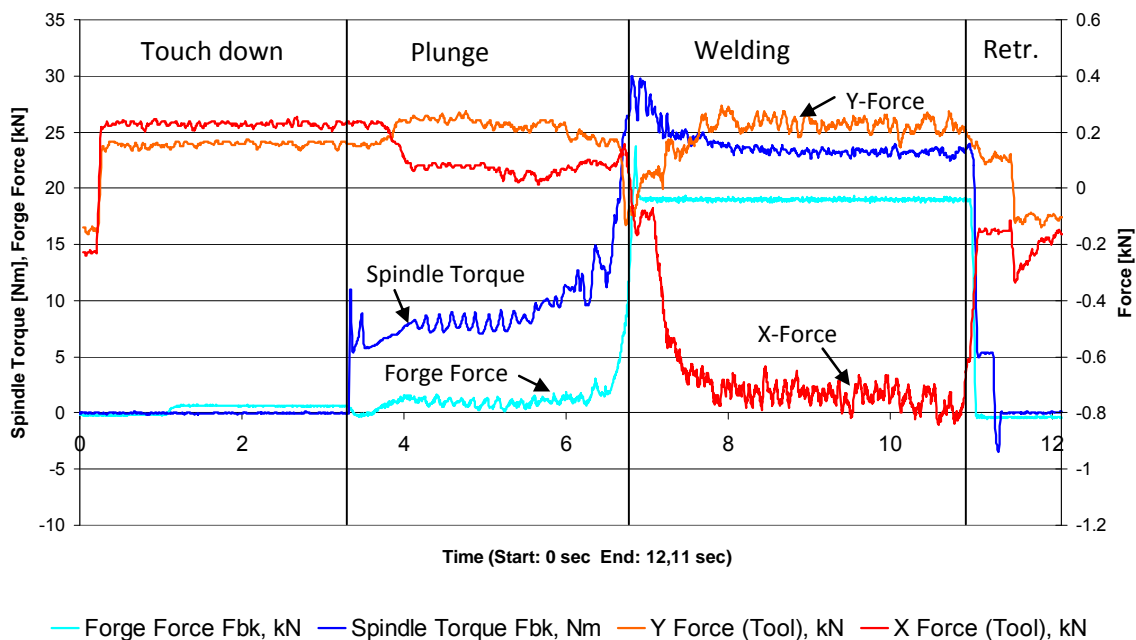
Fig. 1-2 Different stages during friction stir welding, X Forces are in welding direction, Y Forces are across welding direction

1.2   Welding parameters

The main welding parameters are **tool rotation rate (rpm)** and **tool traverse speed (mm/min)** along the line of joint they are influencing the heat input and peak temperature, and torque.

The rotation of tool results in stirring and mixing of material around the rotating pin and the translation of tool moves the stirred material from the front to the back of the pin and finishes welding process. Higher tool rotation rates generate higher temperature because of higher friction heating and result in more intense stirring and mixing of material [3].

In addition to the tool rotation rate and traverse speed, another important process parameter is the **angle of spindle or tool tilt (°)** with respect to the workpiece surface (Fig. 1-3). A suitable tilt of the spindle towards welding direction ensures that the shoulder of the tool holds the stirred material by the pin and move material from the front to the back of the pin.

| 1 … workpiece |
| 2 … probe |
| 3 … shoulder |
| 4 … heel |
| 5 … plunge |
| 6 … tool rotation |
| 7 … downward force |
| 8 … tool tilt |
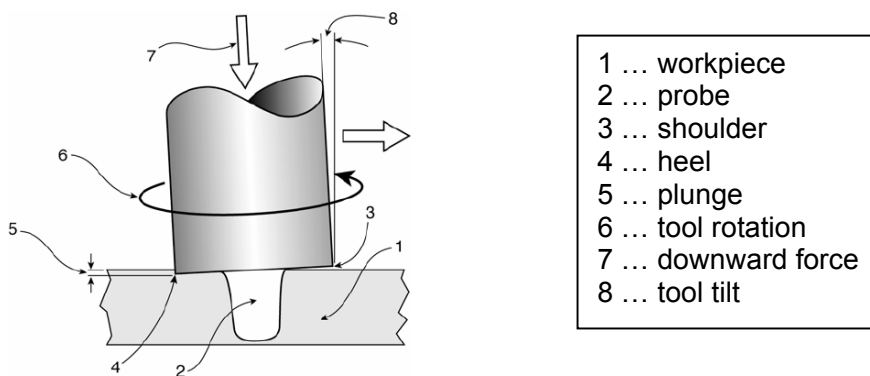
Fig. 1-3 Illustration of tool tilt during friction stir welding [4]

Further, the **insertion depth of pin (mm)** into the workpieces (also called plunge depth) is important for producing sound welds with smooth tool shoulders. The insertion depth of pin is associated with the pin height. When the insertion depth is too low, the shoulder of tool does not contact the workpiece surface. This may result in generation of welds with channel or surface groove [5]. When the insertion depth is too deep, the shoulder of tool plunges into the workpiece creating excessive flash. In this case, a

significantly concave weld is produced, leading to local thinning of the welded plates. It should be noted that the recent development of 'scrolled' tool shoulder allows FSW with 0° tool tilt. Such tools are particularly preferred for curved joints [6].

1.3   Weld configuration

FSW can be applied to most geometric structural shapes and to various types of joints, such as butt, lap, T -butt, and fillet shapes, see Fig. 1-4 [7]. The most convenient joint configurations for FSW are butt and lap joints. Two plates or sheets with the same thickness are placed on a backing plate and clamped firmly to prevent the abutting joint faces from being forced apart. The backing plate is required to resist the normal forces associated with FSW and the workpiece [3].
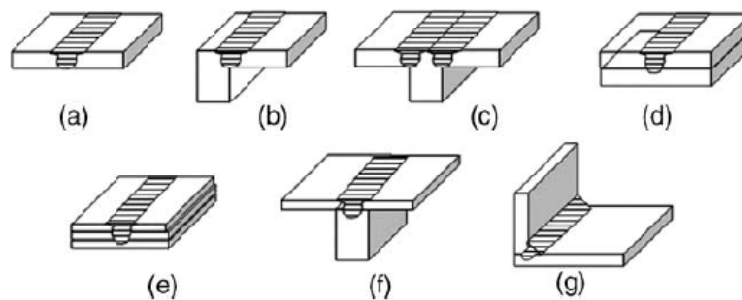
Fig. 1-4 Joint configurations for friction stir welding: (a) square butt, (b) edge butt, (c) T butt joint, (d) lap joint, (e) multiple lap joint, (f) T lap joint, and (g) fillet joint [8]

1.4   Industrial applications

Friction stir welding is considered to be the most significant development in metal joining in decades and, in addition, is a "green" technology due to its energy efficiency, environmental friendliness, and versatility. As compared to the conventional welding methods, FSW consumes considerably less energy, no consumables such as a shielding gas or flux are used, and no harmful emissions are created during welding,

thereby making the process environmentally friendly. Further, because FSW does not involve the use of filler metal and because there is no melting, any aluminum alloy can be joined without concern for compatibility of composition or solidification cracking issues associated with fusion welding. Also, dissimilar aluminum alloys and composites can be joined with equal ease [9-11].

Friction stir welding is already used by some industrial companies. In particular, the use of FSW for aluminum welding has developed rapidly. Potentials are given in the areas of automotive, aircraft manufacturing, shipbuilding, fuel tanks, trains, etc. [12]. Industrial application of FSW includes aluminium 2014 propellant tanks of the Delta II and Delta IV space launch vehicles. Lockheed Martin and NASA MSFC have developed and implemented FSW on the longitudinal welds of the 2195 Al-Li liquid hydrogen and liquid oxygen barrel segments of the external tank for Space Shuttle. Ford Motor Company has produced several thousand Ford GT automobiles with a FSW central tunnel assembly. The use of FSW results in improved dimensional accuracy and a 30% increase in strength over similar GMAW welded assemblies [13].

2 Objectives

The aim of this work is to develop friction stir welding tools and process parameters with which friction stir welding of steels is possible.

In order to achieve a deeper understanding of the process and the tool demands during friction stir welding of steel, the development of bead on plate welding process for a 4 mm thick austenitic stainless steel has to be carried out. The influence of welding parameters on forces, spindle torque and temperatures should be investigated.

The next part of the work is focused on the development of a competitive tool for friction stir welding of steel. A systematic selection of potential tool materials has to be carried out considering the defined requirements. The tool material has to be developed together with a tool coating and suitable process parameters. The tool wear and weld quality of the developed tool have to be analyzed and documented. Moreover, the effect of tool geometry on forces has to be investigated. Additionally, the wear and failure mechanism of a tool during friction stir welding of steel is analyzed and discussed.

Up to date, a 2.6 mm thick martensitic stainless steel plate 15-5PH is welded with the tungsten inert gas (TIG) welding process. For the application of friction stir welding for a butt weld of this material, the tool geometry and process parameters are developed. The investigations of the joint are made using metallographic investigations, hardness analysis and tensile tests. After achieving satisfactory results, bending tests are carried out to analyze the fatigue properties of the friction stir weld. The minimum tool life for a butt weld is defined by the company partner and must exceed 2.0 m, which is the weld length for the planned application.

3 Literature Review

3.1   Process Variants

As described in chapter 1.1, the friction stir welding process has also some disadvantages, particularly the **high process forces**, the **asymmetrical seam** and the **remaining hole** at the end of the weld. To eliminate or reduce these disadvantages, process variations have been developed and are presented in the following chapter.

3.1.1 Com-Stir[TM]

In this process variant a rotation and an orbital motion are combined to achieve better joint properties. The principle of this method is shown in Fig. 3-1. With this process variation, a larger stirring zone and a reduction of asymmetry can be achieved [14].
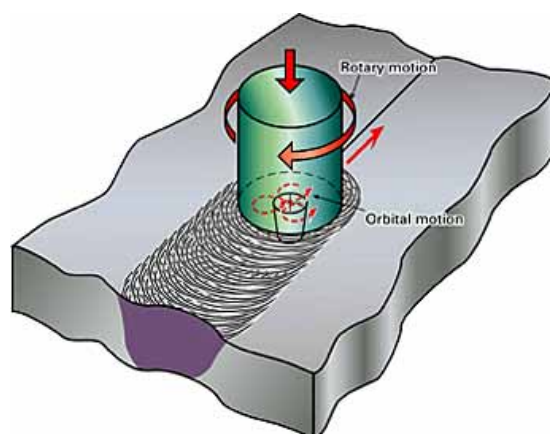
Fig. 3-1 Schematic principle of Com-Stir[TM]-process [14]

3.1.2 Reversal Stir Welding (Re-Stir[TM])

In the Re-Stir[TM] process, the direction of rotation of the tool is changed at frequent intervals. By changing the direction of rotation, an asymmetry of the weld can be avoided [15]. The process is schematically shown in Fig. 3-2.
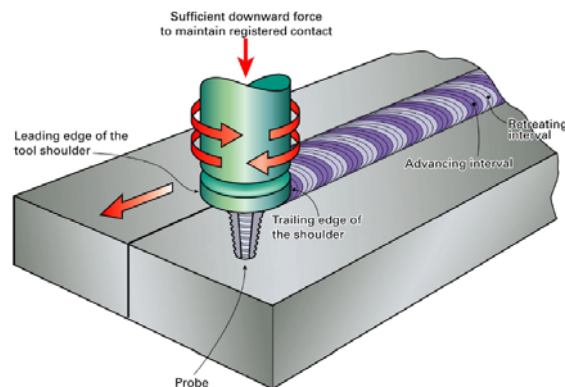
Fig. 3-2 Schematic principle of Re-Stir[TM]-process [15]

3.1.3 Multi-stir

The multi-stir process is characterized by using two or more spindles simultaneously. Through an arrangement of two tools with spindles which rotate in opposite directions (Figure 3-3 (a)) a balance of momentums can be achieved [16]. The welding of multiple extrusions simultaneously is possible when using adjacent spindles (Figure 3-3 (b)) [17].
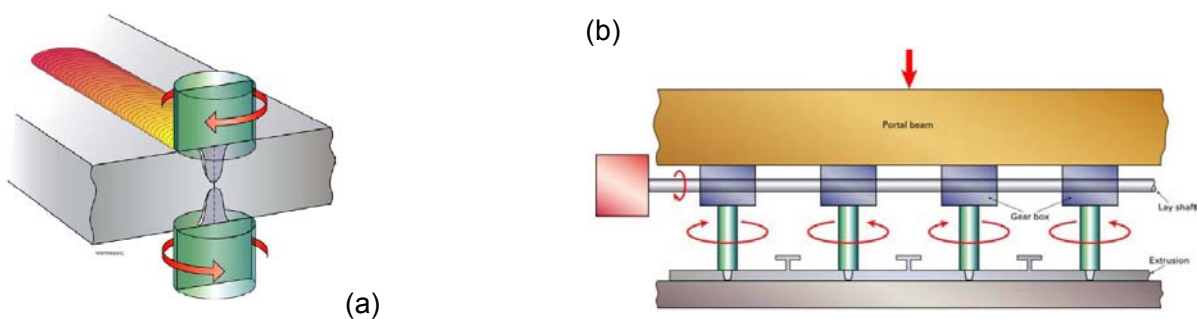
Fig. 3-3 Schematic principle of Multi-Stir[TM]-process with one (a) and multiple (b) spindles axes [16, 17]

3.1.4 Dual-rotation FSW

The rotation of the friction stir welding pin and shoulder is controlled separately; the direction and speed can be changed. In Fig. 3-4 two variants of the dual-rotation FSW are shown.

(a)   (b)

Fig. 3-4 Schematic principle of Dual-rotation FSW with equal rotation direction (a) and (b) different rotation direction [18]

When using conventional FSW, the speed in the center is zero and increases linearly with the radius. By using the dual-rotation FSW it is possible to adapt the velocity of the shoulder and the pin successive to get a perfect weld. Thus, overheating of the surface area of shoulder-piece is avoided [18]. Other advantages are a reduction of the torque and hardness loss in the joint [19].

3.1.5 Skew-stir^{TM}

The Skew-stir^{TM} variant of friction stir welding is characterized that the rotational axis of tool is slightly inclined to the spindle (Fig. 3-5 b)). But the shoulder surface is perpendicular to the spindle of the welding machine.
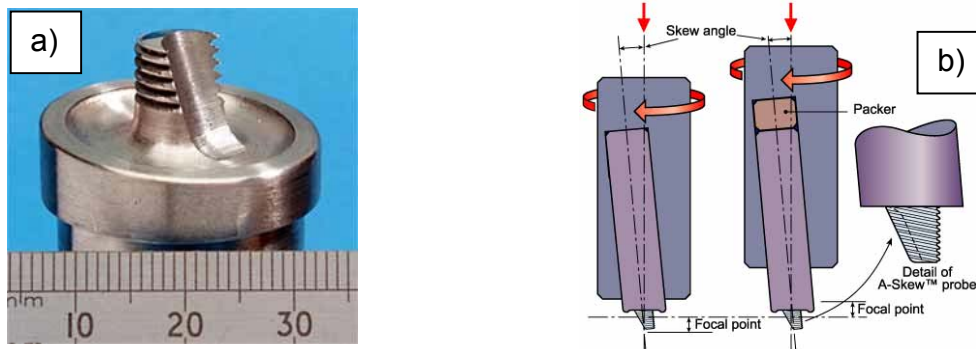
Fig. 3-5 a) Tool prototype and b) schematic principle of Skew-stir[TM]-tool [20]

The tool is moved with a slight orbital movement to improve the material flow around the pin [20]. For stirring of the material, only the outer part of the pin is used because the tool does not rotate around its own axis. Therefore, the inner part of the pin can be machined away, which also affects positively the material flow. Due to a diagonal arrangement of the tool, a larger stirring zone and a reduction of the asymmetry can be achieved [19]. A prototype of an asymmetric Skew-stir[TM] tool is shown in Fig. 3-5 a).

3.1.6 Twin-stir[TM]

The Twin-stir or stir tandem method is used for lap welding. Two tools are arranged side by side or moved laterally to produce an increase of the stir zone (Fig. 3-6). The tools rotate in opposite directions and thus the asymmetry can be avoided [16].

Fig. 3-6 Schematic principle of Twin-stir[TM]-process (a), cross view (b) in welding direction [16]

3.1.7 Friction stir spot welding (FSSW)

Friction stir spot welding (FSSW) is a new process that recently has received considerable attention from the automotive and other industries. A novel variant of the "linear" friction stir welding (FSW) process, FSSW creates a spot, lap-weld without bulk melting (see Fig. 3-7). The process has gained recognition by becoming competitor for related techniques e.g. Resistance Spot Welding (RSW), cl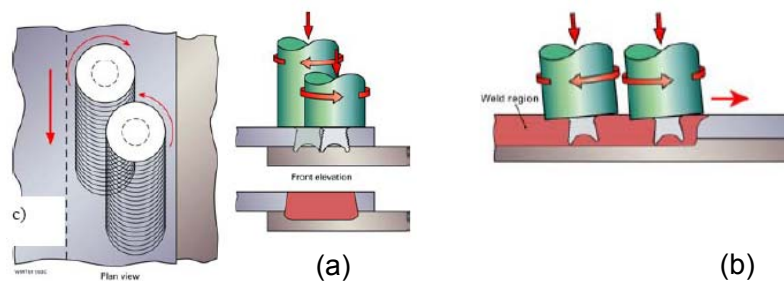inching and riveting etc. [21, 22]. For example, for a recent model of MAZDA, FSSW has been opted during its fabrication [23].
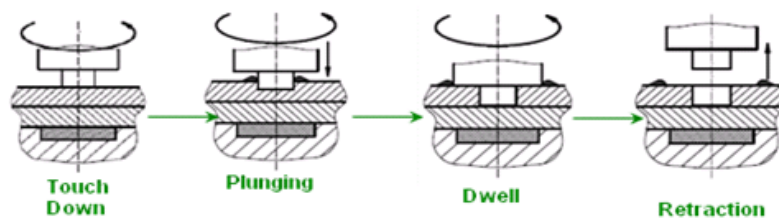
Fig. 3-7 Different steps during FSW and FSSW process [24]

Two distinctive variants of the FSSW process have been reported in the open literature. The first approach, used by Mazda, employs fixed pin tool geometry [25, 26]. The protruded pin leaves a characteristic exit hole in the middle of the joint.

The second approach [19] utilizes delicate relative motions of the pin and the shoulder to refill the pinhole. Based on the information available, the second approach would require relatively long processing time to accommodate the complex motions of the tool to fill the hole. In comparison, the fixed pin approach is very fast.

For Al alloys, a weld can be made in less than one second [25]. In addition, the welding machine and control system for the fixed pin approach is simple and easy to integrate on a high-volume mass production assembly line. Mazda reported over 90 percent operation energy savings and over 40 percent capital investment reductions when compared to the conventional resistance spot welding of Al alloys.

The reason why automotive and other industries have such great interest in application of FSSW lies in many advantages of that process over resistance spot welding (widely used now).

Some of them are:

• Fatigue life 5x better and very consistent

• Stronger and more consistent welds with reduced downtime

• Reduced services required

• Environmentally friendly (no fumes)

• Can place welds closer together

• Can weld through contaminants

• No metallurgical degradation

• No restriction to conventionally "weldable" alloys

The success of FSSW in Al alloy body structures has led to tremendous interest in applying the technology to weld advanced high strength steels. However, past research and development activities on linear friction stir welding have shown that steels are much more difficult to friction stir weld than Al alloys [27]. The technical difficulties stem from the very fundamental aspect of the FSW process – compared to aluminium alloys, FSW of advanced high strength steels (AHSS) must operate at much higher temperatures and it requires much higher mechanical loading for plunging and stirring. These technical difficulties are also expected for FSSW. The high-volume, high-speed, and cost-conscious requirements of auto-body assembly lines make the development of FSSW even more challenging.

3.2   Weld Structure

Friction stir welding is a solid state welding process and the material around the pin experiences different thermal, strain and strain rate histories. Accordingly, the resulting stir zone microstructure reflects these different thermomechanical histories and is not homogeneous. In spite of the local microstructural inhomogeneity, one of the significant benefits of this solid-state welding technique is the fully recrystallized, equiaxed, fine grain microstructure created in the stir zone by the intense plastic deformation at elevated temperature [3, 29-31]. This fine grain microstructure produces excellent mechanical properties and enhanced formability.

Like at many new technologies, a new nomenclature is required to accurately describe observations. In FSW, new terms are necessary to adequately describe the postweld microstructures. The first attempt at classifying friction stir welded microstructures was made by Threadgill [3, 32]. Fig. 3-8 identifies the different microstructural zones existing after FSW in aluminium, and a brief description of the different zones is presented. The structure of a friction stir weld can be divided into the following regions:
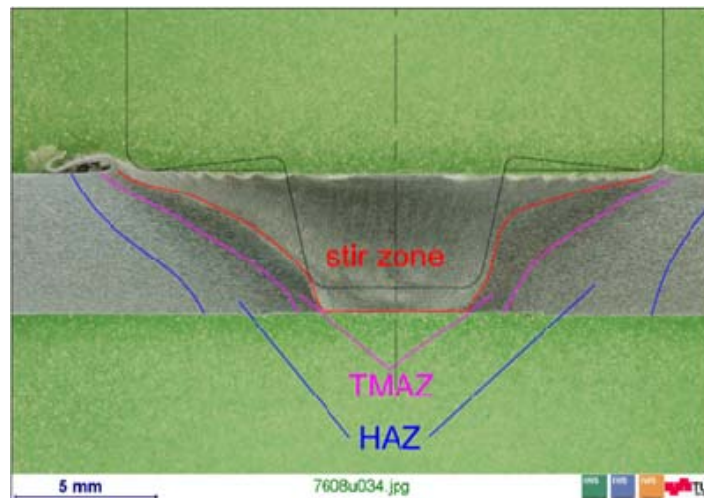
Fig. 3-8 Different zones of an aluminium friction stir weld

Base metal (BM) or unaffected material

This is material remote from the weld that has not been deformed and that, although it may have experienced a thermal cycle from the weld, is not affected by the heat in terms of microstructure or mechanical properties [3].

Heat affected zone (HAZ)

In this region, which lies closer to the weld center, the material has experienced a thermal cycle that has modified the microstructure and/or the mechanical properties. However, there is no plastic deformation occurring in this area [3].

Thermomechanically affected zone (TMAZ)

In this region, the FSW tool has plastically deformed the material, and the heat from the process will also have exerted some influence on the material. In the case of

aluminum, it is possible to obtain significant plastic strain without recrystallization in this region, and there is generally a distinct boundary between the recrystallized zone (weld nugget) and the deformed zones of the TMAZ [3].

Weld nugget or stir zone (SZ)

The fully recrystallized area, sometimes called the stir zone, refers to the zone previously occupied by the tool pin. The term stir zone is commonly used in friction stir processing, where large volumes of material are processed [3].

3.3   Tool geometry

The tool serves three primary functions, that is, **heating of the workpiece**, **movement of material** to produce the joint, and **containment** of the hot metal beneath the tool shoulder. Heating is created within the workpiece both by friction between the rotating tool pin and shoulder and by severe plastic deformation of the workpiece [6].

3.3.1 Tool shoulder

Tool shoulders are designed to produce heat (through friction and material deformation) to the surface and subsurface regions of the workpiece. The tool shoulder produces a majority of the deformation and frictional heating in thin sheet, while the pin produces a majority of the heating in thick workpieces. Also, the shoulder produces the downward forging action necessary for weld consolidation [6].

3.3.1.1   Concave Shoulder

The first shoulder design was the concave shoulder, commonly referred to as the standard-type shoulder, and is currently the most common shoulder design in friction stirring [6]. Concave shoulders produce quality friction stir welds, and the simple design is easily machined. The shoulder concavity is produced by a small angle between the edge of the shoulder and the pin, between 6 and 10°. During the tool plunge, material

displaced by the pin is fed into the cavity within the tool shoulder. This material serves as the start of a reservoir for the forging action of the shoulder. Forward movement of the tool forces new material into the cavity of the shoulder, pushing the existing material into the flow of the pin. Proper operation of this shoulder design requires tilting the tool 2 to 4° from the normal of the workpiece away from the direction of travel (see Fig. 1-3); this is necessary to maintain the material reservoir and to enable the trailing edge of the shoulder tool to produce a compressive forging force on the weld. A majority of the friction stir welds produced with a concave shoulder are linear; nonlinear welds are only possible if the machine design can maintain the tool tilt around corners (i.e., multiaxis FSW machine) [6].

3.3.2 Shoulder Features

The FSW tool shoulders can also contain features to increase the amount of material deformation produced by the shoulder, resulting in increased workpiece mixing and higher-quality friction stir welds. These features can consist of scrolls, ridges or knurling, grooves, and concentric circles (Fig. 3-9) and can be machined onto any tool shoulder profile (concave, flat, and convex). Currently, there are published examples of three types of shoulder features: scoops, concentric circles, and scrolls [6].
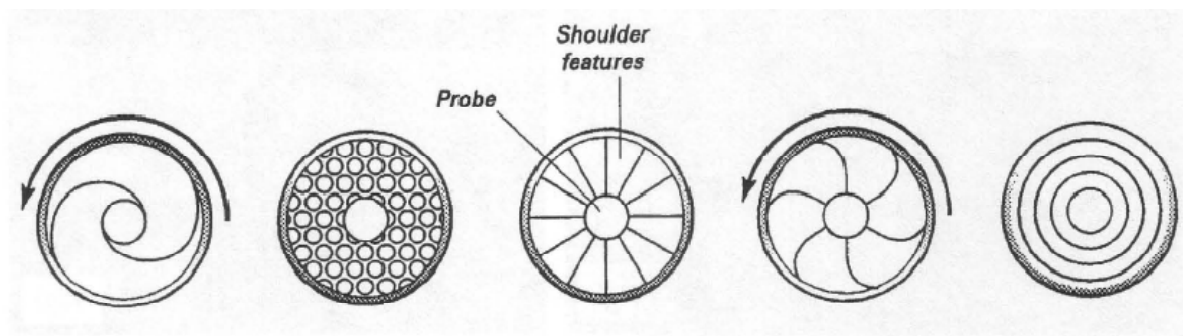

Fig. 3-9 Different shoulder features used to improve material flow and shoulder efficiency [8]

3.3.2.1   Convex Shoulders

Friction stir tool shoulders can have a convex profile. The advantage of the convex shape is that the outer edge of the tool need not be engaged with the workpiece, so the shoulder can be engaged with the workpiece at any location along the convex surface. Thus, a sound weld is produced when any part of the scroll is engaged with the workpiece, moving material toward the pin. This shoulder design allows for a larger flexibility in the contact area between the shoulder and workpiece (amount of shoulder engagement can change without any loss of weld quality), improves the joint mismatch tolerance, increases the ease of joining different-thickness workpieces, and improves the ability to weld complex curvatures. The profile of the convex shoulder can be either tapered or curved [6].

3.3.3 Tool pin

The pin of a tool produces deformational and frictional heating to the joint surfaces. The pin is designed to disrupt the faying, or contacting, surfaces of the workpiece, shear material in front of the tool, and move material behind the tool. In addition, the depth of deformation and tool travel speed are governed by the pin design [6].

3.3.3.1   Cylindrical Pin

The pin cited in the original FSW patent [1] consists of a cylindrical, threaded pin with a round bottom. Threads are used to transport material from the shoulder down to the bottom of the pin; for example, a clockwise tool rotation requires a left handed thread. A round or domed end to the pin tool reduces the tool wear upon plunging and improves the quality of the weld root directly underneath the bottom of the pin. The best dome radius was specified as 75% of the pin diameter. Also, machining a radius at the bottom of the threads will increase tool life by eliminating stress concentrations at the root of the threads [6].

3.3.3.2   Flat-Bottom Cylindrical Pin

Contrary to the statements made in the previous section about the negative aspects of the flat-bottom cylindrical pin, the flat-bottom pin design is currently the most commonly used pin design [6].

3.3.3.3   Tapered Pins

Cylindrical pins were found to be sufficient for aluminum plate up to 12 mm thick, but researchers wanted to friction stir weld thicker plates at faster travel speeds. A simple modification of a cylindrical pin is a tapered cone. Tapered cone pins have lower transverse loads (when compared to a cylindrical pin), and the largest momentum load on a truncated cone is at the base of the cone, where it is the strongest. A variation of the tapered cone pin is the stepped spiral pin, a design developed for high-temperature materials [33].

During the friction stir processing (FSP) of Ni-Al bronze, a threaded profile distorted, and threadless tools did not produce sufficient material flow to obtain 6 mm deep deformation regions. Thus, the stepped spiral tool (Fig. 3-10) was designed with robust features that survived the 1000°C temperatures. The stepped spiral has a square edge and never forms a recess between a step and the following step. Also, the stepped spiral profile can be ground into ceramic tools, where threaded features are not possible. Thus, some polycrystalline cubic boron nitride (PCBN) tools contain a stepped spiral pin that increases the volume of material deformed by the pin [6].
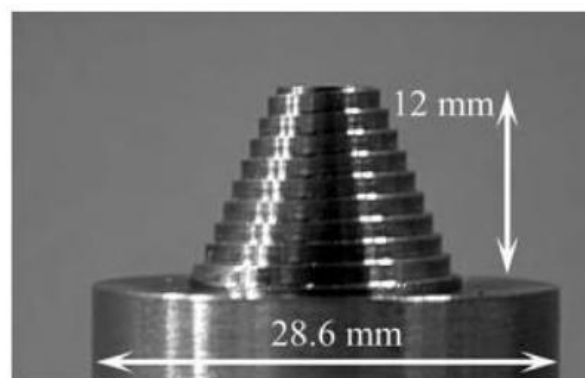

Fig. 3-10 Photograph of a stepped spiral pin tool [6]

3.4   **Material Flow**

The thermally softened material is transported around the tool in the direction of rotation and deposited in bands in the wake of the weld. Viewed in the plane section of FSW, the spacing of the bands left in the wake of the FSW are equivalent to the longitudinal distance the weld tool travels during a single rotation. Geometric and microstructural differences within the refined weld nugget reflect asymmetrical flow processes that occur around the weld centerline [34].

The "onion ring" pattern [35] observed in the weld nugget is not always apparent in the weld macrostructure. Studies document visible patterns in colder welds, with no discernable ring pattern at hotter welds [36]. The disappearance of the onion rings may result from slide conditions existing at the tool/workpiece interface at higher temperatures, when the FSW process becomes dominated by extrusion [35]. Crystallographic orientation texture maps have shown the onion ring pattern corresponds to bands of shear induced fiber texture in the weld nugget [37-38]. Although the onion ring pattern is of benefit in interpreting the thermomechanical processing of the metal in the FSW process, there has been no reported correlation with the resulting quality of the weld nugget [38].

Although the coupling between metal flow, heat-generation model, weld tool material and features of the shoulder and pin is complicated, some generalizations have been made regarding the mechanisms of the metal flow. Most of what is known about the deformation flow path is deduced from the asymmetric flow patterns inferred from tracer studies.
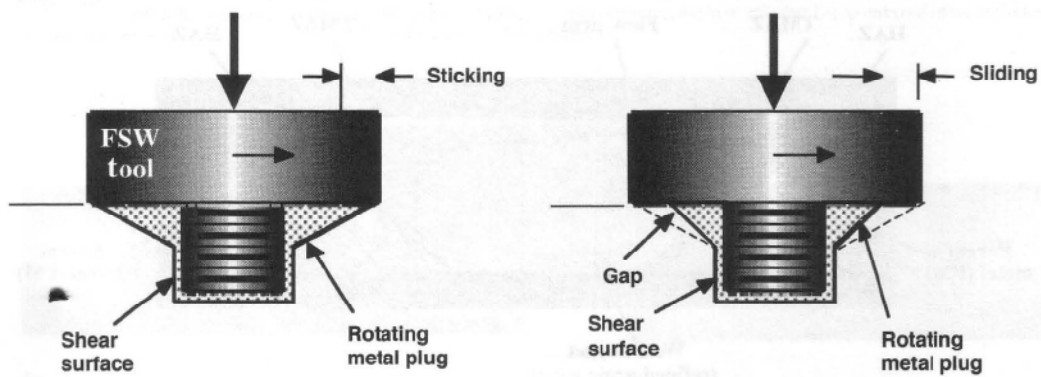
Fig. 3-11 Alternating boundary conditions at the interface of the weld tool shoulder and the workpiece affect the boundary conditions for heat generation [34]

Initial tracer studies used preferential etching to study the mixing of dissimilar alloys [38-41]. Definition of the flow paths in the FSW process was first obtained in a study by Colligan [42], in which the faying surface of the weld joint was embedded with 0.38 mm diameter steel balls placed at various linear positions through the weld thickness and to either side of the weld tool. Postweld positioning of the steel balls, as investigated by x-ray radiography, suggested an orderly flow of the metal around the pin tool. Based on the entrance into the weld zone, only some of the metal flow appeared to be forced downward by the threaded pin, while the rest appeared to be simply rotated from the front to the back of the pin tool [42].

Subsequent studies have looked at inserted copper foil, plated surfaces, and composite markers to further investigate the mechanisms [43 – 44]. All studies indicated that the flow was orderly, with the weld metal appearing to flow along defined paths or streamlines. Variations were observed in individual streamlines at some weld parameters, with differences observed in the deposition dependent on advancing side (AS) versus retreating side (RS) insertion into the weld zone. These variations were attributed to metal either being stirred or extruded around the pin.

Based on the experimental studies using tracers, two models have been published that describe the metal flow as influenced by the processing parameters and weld tool geometry [46, 47]. Nunes [39, 46] has based his physical model of the metal flow in the friction stir process in terms of kinematics describing the metal motion. Figure 3-12 illustrates the deconvolution of the FSW process into three incompressible flow

fields that combine to form two distinct currents. In this model, a rigid body rotation field imposed by the axial rotation of the pin tool is modified by a superimposed ring vortex field encircling the pin imposed by the pitch of the weld pin threads. These two flow fields, bound by a shear zone, are uniformly translated down the length of the weld panel. Metal not entrained in the ring vortex flow simply passes around the pin tool in a straight-through current, while metal entrained in the ring vortex flow experiences a high degree of thermomechanical processing, because it may pass around the pin tool more than once. Variations in features on the pin tool are reflected in the upward or downward motion of the metal as described by the vortex flow [34].
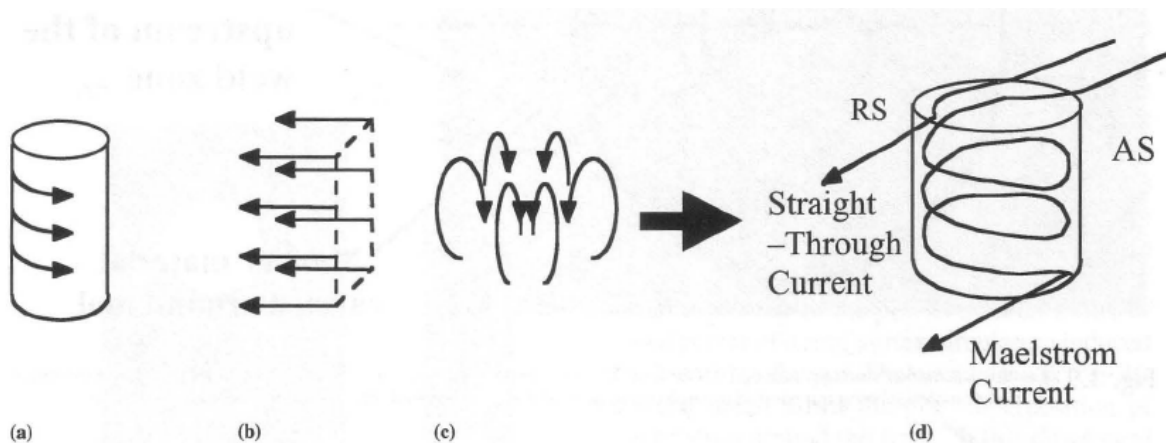

Fig. 3-12 Three incompressible flow fields of the friction stir weld. (a) Rigid body rotation, (b) uniform translation, and (c) ring vortex combine to form (d) two flow currents. RS, retreating side; AS, advancing side [34]

The Arbegast model [47] treats the FSW as a metal-working process that involves five zones: preheat, initial deformation, extrusion, forging, and postweld cooldown. These zones are illustrated in Fig. 3-13. The heat generated by the rotating weld tool preheats the metal in advance of the weld tool. The rotating motion of the weld tool forms the initial deformation zone in the softened metal. In this zone, the metal is forced upward into the shoulder and then downward into the extrusion zone. In the extrusion zone, the metal in front is moved around the pin tool to the exiting wake of the weld in the cavity being vacated by the pin as it moves forward. This model provides for an interleaving effect between the upper and lower extrusion zones. The back or heel of the

shoulder passes over the metal exiting the extrusion zone and forges it, ensuring consolidation. As the weld tool leaves the area, the metal is cooled by either passive or forced means, analogous to quenching during heat treating operations.

Marker studies by Reynolds [43, 48] also describe the process as one of extrusion followed by forging.

The Arbegast model can be used to explain two of the more common weld defects in terms of the processing parameters. The first is a wormhole or tunnel defect that runs the length of the weld and is attributed to insufficient forming pressure under the tool shoulder, which prevents the material from consolidating. The second defect is a lack of penetration on the root surface next to the anvil. This can result when the weld tool does not sufficiently penetrate into the metal plates, most likely from a too short pin tool [47].
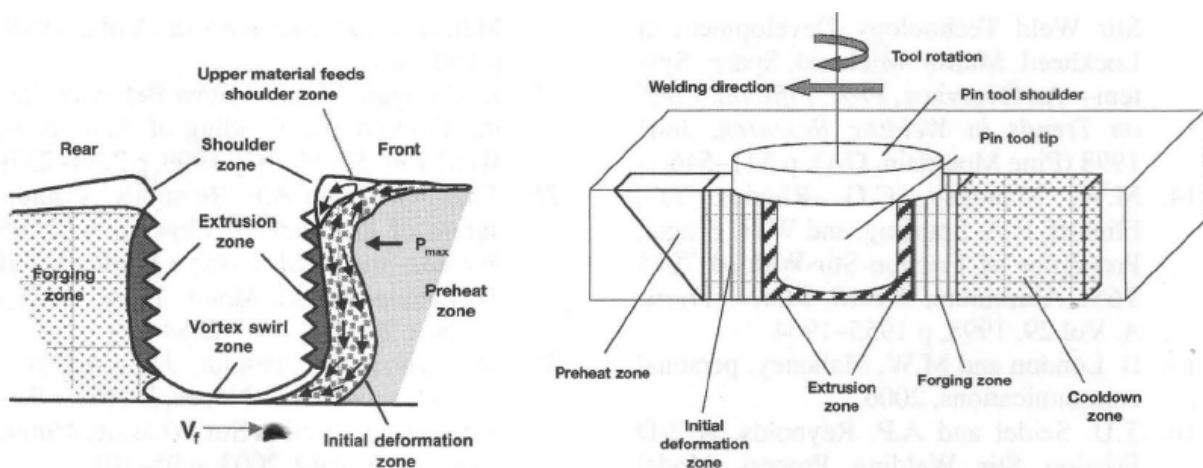

Fig. 3-13 Metallurgical processing zones developed during friction stir joining [47]

3.5   Friction Stir Welding of Steels

In recent years, a number of authors have shown the possibility of friction stir welding of different steel types [49]. Because friction stir welding is a solid state welding process, benefits are achieved compared to fusion welding processes (e.g. avoiding of harmful chromium gases and hydrogen cracks). In 1999, Thomas [50] has analyzed the applicability of friction stir welding of 12% chromium steel and low carbon steel. Further

studies on the microstructure and mechanical properties of friction stir welded steels followed [51, 52].

But the friction stir welding of steels has not progressed as rapidly as for aluminium for important reasons. First, the material from which the tool is made has to survive much more strenuous conditions because of the strength of steel. Second, there are also numerous ways in which steel can be satisfactorily and reliably welded. Third, the consequences of phase transformations accompanying FSW have not been studied in sufficient depth. Finally, the variety of steels available is much larger than for any other alloy system, requiring considerable experiments to optimize the weld for a required set of properties [53].

3.5.1 Tool material

In the published literature, friction stir welding of steels and other high temperature alloys have been performed using primarily the following tool materials:

- Refractory metals
- Polycrystalline cubic boron nitride (PCBN)
- Silicon nitride (Si_3N_4)

3.5.1.1   Refractory metals

Refractory metals include tungsten (W), molybdenum (Mo), niobium (Nb), tantalum (Ta) and their alloys. They are used for high temperature (e.g. light bulb filament) and high density applications (e.g. ballistic projectiles). Many of these alloys are produced as single phase, so strength is maintained to nearly the melting point temperature. Therefore refractory alloys are among the strongest alloys between 1000 and 1500°C. However tantalum and niobium have high solubility of oxygen at elevated temperatures, which quickly degrades the ductility. The drawbacks using refractory alloys include limited material availability, long lead times, cost, and difficult machining. Powder processing is the primary production method for refractory alloys [6].

Tungsten-rhenium (WRe)

Tungsten-rhenium is produced using a powder metallurgical routine. By addition of rhenium, the material obtains higher heat resistance and increased toughness at high temperatures [54]. For friction stir welding of steel, alloys with 25% to 26% rhenium content are mainly used. Better ductility and higher strength can be achieved using special production routines like hot isostatic pressing (HIP) and swaging. The microstructure of a W25Re tool is shown in Fig. 3-14. Tool life of tungsten-rhenium tools is mainly limited by tool wear.
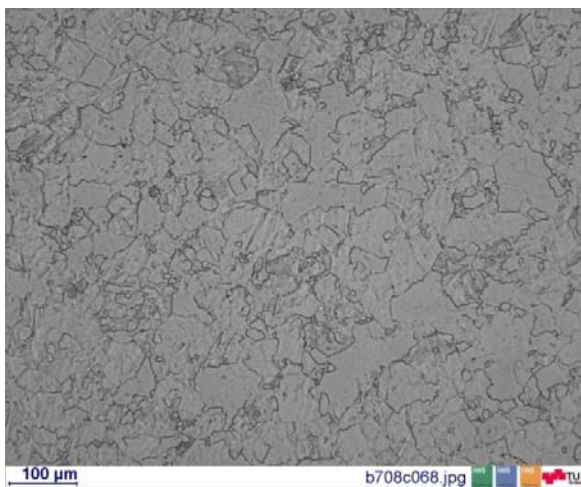

Fig. 3-14 Microstructure W25Re tool

Lanthanated Tungsten (WL)

Another tungsten based alloy is lanthanated tungsten. Doping with 1 - 1.5 weight % lanthanum oxide (LaO_2) increases the creep strength and recrystallization temperature in comparison to pure tungsten. In addition the oxide particles in the structure help to eliminate the poor machinability associated with pure tungsten [55]. Mahoney et. al. reported on friction stir processing of cast NiAl bronze with a W-1%LaO_2 tool [56].

The ultimate tensile strength temperature dependence of tungsten, W-26%Re and W-1%LaO$_2$ is shown in Fig. 3-15 [55].
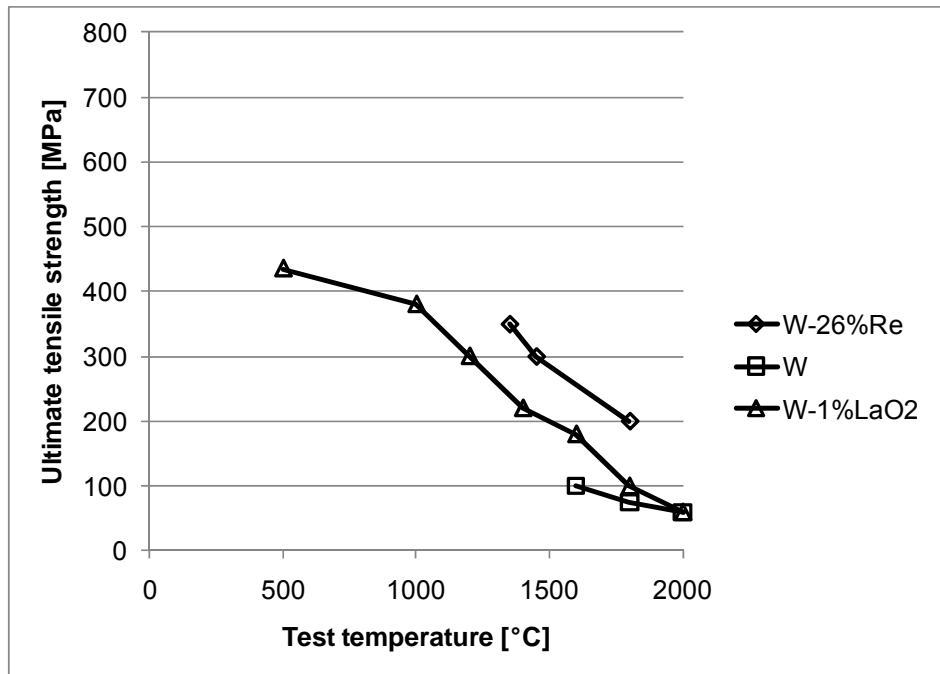

Fig. 3-15 Temperature dependent properties for W, W-26%Re and W-1%LaO$_2$ [55]

3.5.1.2   Polycrystalline cubic Boron nitride (PCBN)

PCBN is a metastable material produced much like synthetic diamond under high pressure (~7000MPa) and high temperatures (~1400°C). Improved PCBN grades for friction stir welding of steel have been developed in the past years [57]. The fabrication process is very difficult and hence the tools are costly. Only the pin and the shoulder of the tool are produced from PCBN; the shank is made from tungsten carbide and both are held together by a superalloy locking collar [58]. Since PCBN is a very hard, wear resistance material, it seems to be an optimal material for friction stir welding of steel. But premature cracking and high costs are limiting factors for its application (Fig. 3-16) [59]. Previous studies [60] have reported that the PCBN tool wear results in a significant deterioration of corrosion properties in the stir zone of austenitic stainless steel due to formation of Cr-rich borides through a reaction between the PCBN tool debris and the steel matrix.
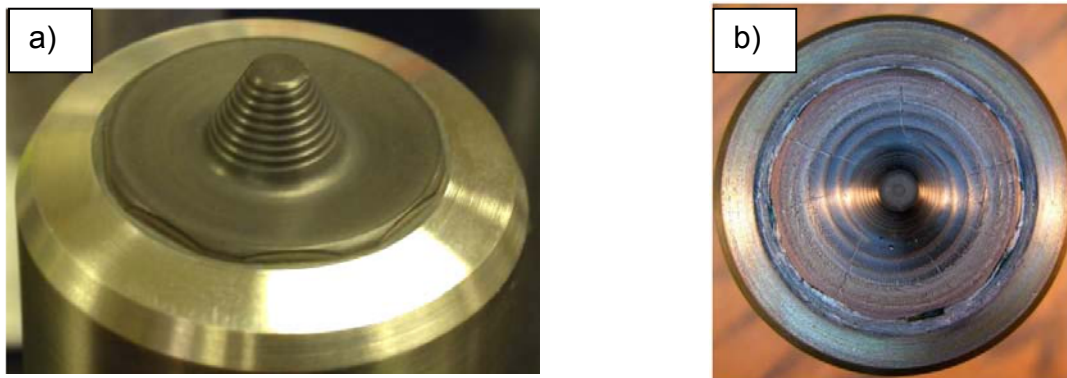
Fig. 3-16 PCBN tools used to friction stir weld HSLA-65 steel. a) a smooth concave shoulder (7°) with a step spiral conical pin and b) illustration of radial cracking in a PCBN FSW tool. [59]

Fischer et. al. analyzed the thermal stresses due to heat generation in a PCBN tool. It was found, that thermal stresses are high enough to generate cracks by one heating / cooling cycle. Therefore PCBN should not undergo thermal shock but kept at a certain constant temperature [61].

Friction stir processing of a typical heat-treated D2 knife steel using PCBN tools was reported by [62]. The process was then implemented into industrial production by the company Diamond Blade.

3.5.1.3   Silicon nitride (Si_3N_4)

TWI reported on the successful friction stir spot welding of steel with a silicon nitride tool (Si_3N_4) [63]. However, no details were reported about tool wear and tool failure. Silicon nitride is a ceramic material and widely used as cutting tool because of its high hardness, high thermal conductivity and low thermal expansion coefficient, that give better thermal shock resistance than other ceramic materials [64]. A disadvantage may be the limited fracture toughness.

3.5.2 FSW Equipment

The FSW equipment for high-temperature materials requires improved cooling, higher precision spindles, and increased machine stiffness compared to that required for aluminum [65].

3.5.2.1 Tool Cooling

The welding zone temperature reaches up to 1200°C, depending on the material to be welded. Further, the materials used for the tool (either tungsten alloys or tungsten carbide shanks) have high thermal conductivity relative to the tool steel commonly used for aluminum welding. To prevent damage to the spindle bearings and to establish a consistent thermal environment for the tool (heat removal), cooling of the tool shank is required.

Two different methods for cooling the tool have been used. In the first, a hollow drawbar is used to conduct coolant directly onto the back end of the tool shank. The second method used for cooling the tool is to mount a cooled tool holder in the machine spindle. The holder can be designed for any spindle configuration, and the cooling is consistent from machine to machine. The major disadvantage of this cooling method is that the cooled tool holder is generally less stiff than the machine spindle and a precise spindle runout is not guaranteed [65]. For example, this system is used by MTS for the steel friction stir welding head.

3.5.2.2 Precision Spindles

Strengths of metallic tools at process temperatures are substantially higher than the aluminum alloys being welded. In contrast, for high-temperature materials, the tool strengths are only marginally higher than the alloys being welded. Thus, tool deformation for metallic tools and fracture for PCBN tools are common [65].

Spindle runout has been demonstrated to be a significant factor limiting the life of PCBN tools. Many FSW machines built for aluminum alloys have relatively high spindle runout, because they were designed primarily to accommodate high process loads. Producers of PCBN tools have recognized the importance of precise spindles and specify a maximum spindle runout of 0.01 m [57]. Failure to meet this spindle runout requirement has led to premature tool fracture [65].

3.5.2.3   Stiff Machines

Increased demands are required to machine technology for friction stir welding of steel. Especially for brittle tool materials, the machine must have sufficient stiffness and good runout performance of the spindle (see chapter 3.5.2.2). Instabilities and vibrations have a negative effect on the wear and the life of the tool [57, 65].

Deflections under load can lead to problems with fatigue failure, particularly with PCBN tools. To minimize these problems, the stiffness for the machine is specified. A maximum deflection of 0.75 mm under a load of 45 kN is suggested by [65].

3.5.3 Weld Metal Properties

A few studies have carefully examined the metallurgy of welds produced in a broad variety by FSW. A summary of steels that have been studied using FSW is given in Table 3-1 [53].

Table 3-1 Compositions of steels (wt%) that have been studied using FSW. The Vickers hardness values represent approximate mean values within the zone concerned; more detail can be found in the original references. Peak hardness values are reported in brackets. In some cases the compositions are assumed from the published specification range [53].

Alloy	C	Si	Mn	Ni	Mo	Cr	V	Others	Plate	HAZ	TMAZ
										Hardness / HV	
1	0.01	0.38	1.09	0.55	0.03	11.2	0.01	Nb 0.27	158	280	230
2	0.1	0.16	0.69	0.08	0.01	0.06			131	149	158
3	0.002		0.1					Ti 0.04	90	100	130
4	0.12		0.29						110		130 (160)
5	0.21	0.24	0.5						125		230 (500)
6	0.34	0.21	0.69					Cu 0.01	155		280 (360)
7	0.5	0.2	0.7					Cu 0.01	200		360 (520)
8	0.18		0.82						135		165
9	0.1	0.2	1.4						180		200
10	0.18	0.3	1.25			0.08	0.35		175		320
11	0.14	0.02	0.64			0.08	0.35		280-460		150
12	0.13	0.26	1.52	0.03	0.17	0.03	0.06		200		300
13	0.32	0.35	1.2	0.2	0.65	1.3	0.05	B 0.0025	250		360
14	0.32	0.35	1.2	0.2	0.65	1.3	0.05	B 0.0025	250		450

3.5.3.1   Austenitic Stainless Steel

This section summarizes the detailed property and structure results for friction stir welded austenitic stainless steels.

Reynolds et.al [51] welded 304L stainless using a tungsten alloy tool. They reported extrapolated peak temperatures in the weld zone of approximately 1200°C. They reported equiaxed grains in the stir zone, with a grain size slightly reduced compared to the base metal. They also noticed narrow bands in the stir zone but made no determination as to the origin or detailed structure of the bands. The weld material was found to be stronger than the base metal and to exhibit excellent ductility, with elongation to fracture of more than 50%. Longitudinal residual stresses were found to be close to the base material yield strength.

Researchers [66] reported on welding of 304L and AL-6XN stainless steels. They found a highly refined stir-zone microstructure, with an unidentified dark banded structure in the stir zone. They reported increased microhardness in the weld zone and excellent ductility for both 304L and AL-6XN. They also described the difficulty of achieving sound welds in AL-6XN, because a number of pores were found in the resulting weld.

A later report [67] gave properties of friction stir welds and AL-6XN base metal. The weld metal was higher in yield strength (700 MPa compared to 430 MPa in base metal) and ultimate strength (930 MPa compared to 780 MPa in base metal) but lower in ductility (50 to 60% reduction in area compared to 75%; 28% elongation compared to 46%). The elongation of the friction stir welds was only slightly below the 30% minimum elongation specified for the base metal.

Park et.al. [68] analyzed friction stir welds made in 304 stainless steel. They found a banded structure similar to that identified by Reynolds et al. [51]. The dark bands were found to be narrow regions of ultrafine grains. The advancing side of the stir zone was found to contain fine sigma phase particles as well as even finer carbide precipitates.

Sorensen and Nelson [69] investigated sigma phase formation in FSW of various stainless alloys with compositions at various distances from the sigma + austenite region according to the Fe-Ni-Cr ternary diagram. They were able to predict the propensity for sigma phase formation and hypothesized that sigma phase formation was a marker for

recrystallization in 304L. They also demonstrated that welding parameter changes affected the amount and location of sigma phase.

Later studies [70] with a convex shoulder, step spiral (CS4) pin tool showed dramatically reduced sigma phase formation in 304L with the new tool design. No sigma phase has yet been identified in welds with the new tool geometry [67].

Because the temperature of the weld zone exceeds 800°C, the possibility of sensitization exists. Clark [71] explored both sensitization and stress-corrosion cracking (SCC) in FSW 304L. The welds analyzed qualified as nonsensitized during an oxalic acid etch test. Double-loop electrochemical potentiokinetic reactivation testing showed regions of increased corrosion susceptibility away from the surface of the specimen. U-bend specimens in boiling 25% NaCl showed no increased SCC susceptibility compared with the base metal [65].

3.6 Precipitation Hardening Steels

In general, precipitation hardening stainless steels are chromium and nickel containing steels. Hardening is achieved through the addition of one or more of the elements copper, aluminium, titanium, niobium, and molybdenum [72].

The most well known precipitation hardening steel is 17-4 PH. The name comes from the additions 17% chromium and 4% nickel [72]. Steel 15-5 PH is the ferrite-free version of 17-4 PH Stainless Steel. The nominal chemical composition of precipitation hardening stainless steels is given in the following table.

Table 3-2 Chemical composition of PH stainless steels [73-74]

PH types	UNS number	Composition [%] Single values are maximum values							other
		C	Mn	Si	Cr	Ni	P	S	
15-5PH	S15500	0.07	1.00	1.00	14.00-15.50	3.50-5.50	0.040	0.030	2.50-4.50Cu
17-4PH	S17400	0.07	1.00	1.00	15.00-17.50	3.00-5.00	0.040	0.030	3.00-5.00Cu

Martensitic precipitation hardening stainless steels have a predominantly austenitic structure at annealing temperatures of around 1040 to 1065°C. Upon cooling to room temperature, they undergo a transformation that changes the austenite to martensite [72].

Martensite is the desired predominant phase in martensitic stainless steels. Its presence is a consequence of the diffusionless transformation of austenite during cooling to room temperature. In alloys containing less than about 0.6 wt% C, the martensite forms as laths which are aligned parallel to one another. The laths are grouped into larger structural entities, called blocks and packets. The microstructure of lath martensite is generally too fine to be revealed using optical microscopy, necessitating the use of electron microscopy [75].

15-5 PH is a low-carbon martensitic precipitation-hardening stainless steel that provides an outstanding combination of high strength, good corrosion resistance, good mechanical properties at temperature up to 320°C and toughness in both the longitudinal and traverse directions in both base metal and welds. Short-time, low temperature heat treatments minimize distortion and scaling [73].

The strength obtained by heat treatment depends on the carbon content of the alloy. Increasing carbon content increases strength but decreases ductility and toughness. So, the low carbon content of the martensitic PH stainless steels is especially critical for toughness and good ductility. Wear resistance for martensitic stainless steel is very dependent on carbon content [72].

Molybdenum and nickel can be added to martensitic stainless steel to improve corrosion and toughness properties. Nickel also serves to maintain the desired microstructure, preventing excessive free ferrite when higher chromium levels are used to improve corrosion resistance. Copper is added in order to age hardening [75].

Due to the high strength of precipitation hardening stainless steels, these alloys are most used in the aerospace and other high-technology industries like chemical, petrochemical, food processing, paper and general metalworking industries. Applications include gears, valves and other engine components, high strength shafts, turbine blades, moulding dies and nuclear waste casks [72 - 74].

3.6.1 The heat treatment of the PH martensitic stainless steel

Garrison and Brooks [76] showed that 15-5PH solidify as essentially 100% ferrite. During cooling, the ferrite transforms almost entirely to austenite. Ferrite stringers can be found in directions parallel to the rolling direction (parallel to the surface) [76].

A homogenization treatment can be used as part of the annealing process when the steel is in the austenite phase. This homogenization, accomplished by holding at temperatures above 850°C, tends to reduce the ferrite content. The austenite subsequently transforms to martensite on cooling to temperatures approaching ambient. The M_s temperature for both is reported as approximately 132°C and the M_f temperature is reported as approximately 32°C [76].

During the aging treatment austenite reversion can take place. Aging at 595°C or 621°C resulted in about 15% austenite after cooling to room temperature. Likewise, Anthony [77] also noted an increase in austenite content of 17-4PH stainless steel form about 1.5% in the solution annealed condition or age at 480°C, to 5.5% after aging at 595°C. Subsequent exposure to lower temperatures such as 425 to 480°C for a few thousands of hours resulted in as much as 18% austenite [77].

Higher aging temperatures are accompanied by higher ductility. Lower strength with increasing aging temperature was thought to be due to precipitate coarsening and loss of precipitate coherency with a matrix. However, Hochanadel [78] dispute this. Instead, the reduction of strength is attributed to formation of reverted austenite in this alloy. The austenite has much lower strength than martensite.

Where ductility in the hardened condition is of importance, better toughness can be obtained by raising the temperature of the hardening heat treatment.

By varying the heat-treating procedure between 482°C-621°C for one to four hours, a wide range of properties can be obtained (Table 3-3) [73, 74].

Table 3-3 Standard heats treatments of 15-5PH [73, 74]

Condition	Heat to	Time at Temperature [hours]	Type of cooling
H 900	900°F(482°C)	1	Air
H 925	925°F(496°C)	4	Air
H 1025	1025°F(551°C)	4	Air
H 1075	1075°F(580°C)	4	Air
H 1100	1100°F(593°C)	4	Air
H 1150	1150°F(621°C)	4	Air
H 1150 + 1150	1150°F(621°C) 1150°F(621°C)	4 followed by 4	Air Air
H 1150-M	1400°F(760°C) 1150°F(621°C)	2 Followed by 4	Air Air

If the alloy is not sufficiently ductile in any given hardened condition, it can be reheated at a higher temperature to increase impact strength and elongation [73, 74].

For hot-worked or overaged material, a solution treatment at 1024°C to 1052°C for three minutes for each 2.5 mm of thickness, must be done prior to hardening. The solution treatment refines the grain size and makes hardened material more uniform [73, 74].

Because of this characteristic, it is necessary to cool parts in process at least to 32°C prior to applying subsequent heat treatments if normal final properties are to be obtained. This practice is essential to assure grain refinement and to assure good ductility [73, 74].

3.6.2 Mechanical properties

15-5PH and 17-4PH provide excellent mechanical properties (see Table 3-4). For applications requiring high strength and hardness plus corrosion resistance, this alloy is an outstanding choice. In addition, it is more cost effective than many high-nickel, non ferrous alloys [73, 74].

Table 3-4 Mechanical property of PH steels [72]

PH steel	Condition	Tensile strength		0,2% Yield strength		Elongation	Hardness
		Ksi	MPa	Ksi	MPa	%	Rockwell
15-5PH	H900	190	1310	170	1172	10	C44
	H1150	135	931	105	724	16	C32
17-4PH	H900	200	1379	178	1227	12	C44
17-4PH	Sol.Ann.	150	1034	110	758	10	C33

3.6.3 Welding

Several studies have been published reporting the microstructure and mechanical properties of fusion welded PH steels [79, 80]. Generally the steels show a good weldability but overaging in the heat affected zone takes place and softens the material. Therefore weldments in 15-5 PH steel are not usually put into service in the as welded condition. In order to obtain weld properties approximating those of the base material, post weld heat treatment (PWHT) is necessary [72].

4 Tool Development

The objective of this chapter is to provide details about the tool functions, necessary requirements for potential tool materials, the selection of tool materials, the tool development performed in this work, the optimization of process parameters and the analysis of tool life and failure mechanism.

4.1 Tool function

As discussed in chapter 1.1, the friction stir welding tool consists of a protruding pin (often called probe), which is plunged into the work pieces, and a larger concentric shoulder which is maintained on the surface of the joint (Fig. 4-1). The functions of both probe and shoulder are discussed in the following chapter.
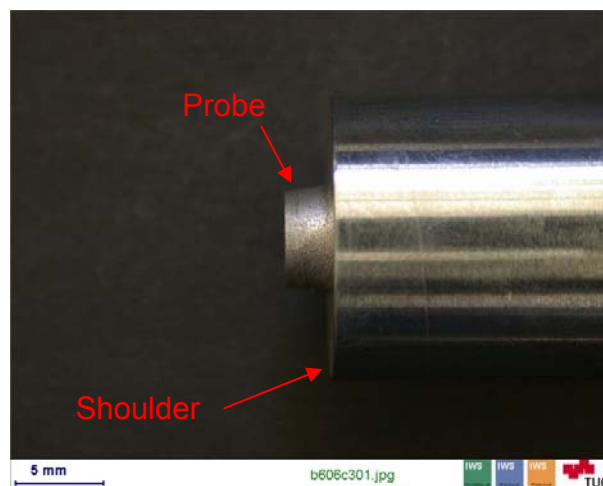
Fig. 4-1 Tungsten 25% Rhenium tool, showing tool probe and tool shoulder

4.1.1 Shoulder

The main task of the shoulder is to generate heat by frictional heating and to apply a sufficient pressure (downforce) onto the workpiece during welding. Another

function is to feed the plasticized material towards the probe, where the probe will be able to stir the material. This is realized by using a concave or spiral shoulder as discussed in chapter 3.3.2 The shoulder also has an influence on the material flow and microstructure of the upper part of the weld.

Due to the high axial forces during welding, the tool shoulder must have high compressive strength at room and process temperature. The contact speed with the workpiece surface is quite high and a good abrasive wear resistance is required.

4.1.2 Probe (Pin)

The main function of the probe is to move the material from ahead of the tool to behind of the tool. In some cases, especially when welding thicker sheets, the probe has to provide also a vertical movement of material and heat generation of the workpiece.

Whereas the probe for welding of aluminium is designed with a threated or fluted design, only smooth or tapered probes are used for welding of steels (chapter 3.3.3).

4.2   Tool Material Properties

By analysing the conditions of the tool and workpiece during the welding process, following requirements can be made. A suitable tool material for friction stir welding of steel must have a high compressive strength, sufficient fracture toughness and shock strength at room and process temperature. Furthermore, good wear resistance at the working temperature and the avoidance of chemical reactions with the welded material and the ambient medium is necessary. The requirements of the tool material are discussed in detail:

<u>Compressive strength</u>

A suitable tool material must have sufficient compressive strength at room and process temperature. As a minimum requirement, the yield strength at the process temperature of the tool material must be higher than the load applied by the downforce. Insufficient yield strength will lead to plastic deformation of the shoulder and/or probe. Considering fatigue as further criteria the yield strength has to be even higher. Wei Gan

et. al analysed the tool mushrooming in friction stir welding of L80 steel and suggested a yield strength of the tool material of 400 MPa at 1000°C to avoid mushrooming [81].

Fracture toughness

Some of the applied tool materials have a high hardness but only low fracture toughness, especially at room temperature (e.g. Si_3N_4). But an insufficient toughness can cause tool failure during plunge or welding phase by brittle fracture [82]. Therefore a potential tool material should have sufficient fracture toughness at room and process temperature. The author proposes that the minimum toughness for potential tool materials should be the value of PCBN.

Thermal shock resistance

Thermal shock failure occurs when too high stresses due to temperature gradient or temperature rate is created in a piece of material during the heating and cooling process. Small to large cracks in the piece occurs, or the piece may actually break. Due to the simultaneous heat generation and cooling of the tool during friction stir welding, thermal shock within the tool may appear. This can cause brittle fracture. Therefore thermal shock should be avoided by keeping the tool at a constant process temperature.

Wear resistance

Extensive tool wear changes the tool shape (normally by removing tool features), thus changing the weld quality and increasing the probability of defects. In friction stir welding, wear can occur by adhesive, abrasive or chemical wear mechanisms. The exact wear mechanism depends on the interaction between the workpiece and tool materials and the selected tool parameters [83].

Thermal conductivity

The thermal conductivity of both tool material and workpiece can be significant for the friction stir welding process. When using tool materials with low thermal conductivity, most of the heat generated at the tool / workpiece interface will diffuse into the workpiece. When welding the same material with high thermal conductivity alloys, most of the heat generated ends up in the tool. This may cause overheating of the tool and

weakening of the tool material. A possibility to influence the effect is the use of a thermal barrier (e.g. coating).

Thermal expansion

Thermal expansion should be considered when designing multimaterial tools. Large differences in the coefficient of thermal expansion between the pin and the shoulder material lead to either expansion of the shoulder relative to the probe or expansion of the probe relative to the shoulder. Both of these situations increase the stresses between the probe and the shoulder, thus leading to tool failure [83].

Additional consideration should be made when the probe and shoulder are made of one material, while the tool shank (portion of the tool within the spindle) is a different material. One way to mitigate this situation is with a thermal barrier designed to prevent heat removal from the tool into the shank. An example is the PCBN tool, where a thermal barrier prevents heat from moving into the tungsten carbide shank [83].

The thermal expansion differences between the tool and workpiece are not found to have a significant influence on friction stir welding [83].

Uniform microstructure and density

It is important to ensure that the tool material has a uniform microstructure. Slight variations in microstructure or density produce a weak region within the tool where premature fracture occurs [83]. Powder metallurgy tools are often fabricated using special techniques like swagging. But the density in a swaged material is less in the centre, which is the area where the tool probe is located.

Oxidation resistance

Whereas it is not necessary to use a shielding from the atmosphere when welding aluminium or copper, welding of steel or titanium requires shielding of the workpiece material. Due to the high temperatures a potential interaction between the tool and the surrounding medium should be considered. It should be noted that some materials produce toxic oxides. Since the tools are used in a production environment, the tool material and the oxides should be non toxic.

Machinability

Many friction stir welding tools are designed with features that must be machined, ground or electrodischarged machined into the tool [83]. Since most of the friction stir welding tools for steel do not have complex shapes, as a minimum requirement the fabrication of simple tool shapes should be possible (e.g. tapered probe). For some tool materials it is possible to reshape them after welding. This should be also considered in the material selection.

Availability of materials

A tool material is not useful if a steady supply of tool material is not available. This is especially true in a production environment, where production specifications dictate the use of a specific material [83].

From the discussion above, a list of required material properties for potential tool materials was created (Table 4-1). Since the welded material will have an influence on the defined properties, the importance of properties may vary. Therefore no ranking of properties was set.

Table 4-1 List of required material properties for friction stir welding tools

Required material properties	Unit
Compressive strength	[MPa]
Fracture toughness	[MPa m$^{1/2}$]
Service temperature	[°C]
Oxidation resistance at 500°C	[ ]
Thermal conductivity	[W/mK]
Thermal expansion coefficient	[µstrain/K]
Non Toxic	[ ]
Hardness	[HV]
Availability	[ ]
Material price	[€/kg]

4.2.1 Criteria definition

In the following section the limits of the material properties described in chapter 4.2 are assigned. These limits were determined by analyzing the loading conditions and the properties of existing tool materials. The relevant properties of PCBN and tungsten - 25% rhenium (W-25%Re) are shown in Table 4-2.

Table 4-2 Material properties of PCBN and W-25%Re tool materials [84, 85]

Property	Unit	PCBN [81]	W-25%Re [82]
Compressive strength	[MPa]	2700 - 3500	1150
Fracture toughness	[MPa m$^{1/2}$]	3.5 - 6.7	135
Service temperature	[°C]	1500 - 2000	600 - 900
Oxidation resistance at 500°C	[ ]	Very good	Very good
Thermal conductivity	[W/mK]	100 - 250	30 – 40
Thermal expansion coefficient	[µstrain/K]	4.6 - 4.9	4.4 – 4.6
Non Toxic	[ ]	Very good	Very good
Hardness	[HV]	2600 - 3500	400 – 635
Availability	[ ]	Low, 1 Supplier	Low, 2 Suppliers
Material price	[€/kg]	(High)	385.8 – 462.9

It can be seen from Table 4-2 that PCBN has a high compressive strength and hardness, but a significant lower fracture toughness than W-25%Re. Since the thermal conductivity of PCBN is much higher, more heat will go into the tool. If too much heat is removed from the joint, temperatures required to friction stir weld will not be achieved.

Based on the properties of Table 4-2 and the known strength and weaknesses of both materials, following limits for the selection of tool materials were defined (Table 4-3):

Table 4-3 Selected limits for the preselection of tool materials

Property	Unit	desired value	required (must) value
Compressive strength	[MPa]		> 800
Fracture toughness	[MPa m$^{1/2}$]		> 5
Service temperature	[°C]		> 600
Oxidation resistance at 500°C	[ ]		Very good
Thermal conductivity	[W/mK]	> 40	
Thermal expansion coefficient	[µstrain/K]	< 10	
Non Toxic	[ ]		Good
Hardness	[HV]	> 1000	
Material price	[€/kg]	Low	

4.3   Material Selection

In this chapter, the software package "CES Selector Version 4.0" was used to review the must-defined criteria in order to receive an appropriate pre-selection of tool materials. Later the results were analyzed and a ranking of materials was done using the weighted property index method. The material with the highest value was selected as a starting point for further studies.

4.3.1 Required properties (must criteria)

The first two must criteria which were verified in the selection are the compressive strength and the fracture toughness of the material. The minimum value for the compressive strength was defined as shown in Table 4-3 with 800 MPa and the minimum value for the fracture toughness was estimated at 5 MPa m$^{1/2}$. The result of this first selection is shown in Fig. 4-2.
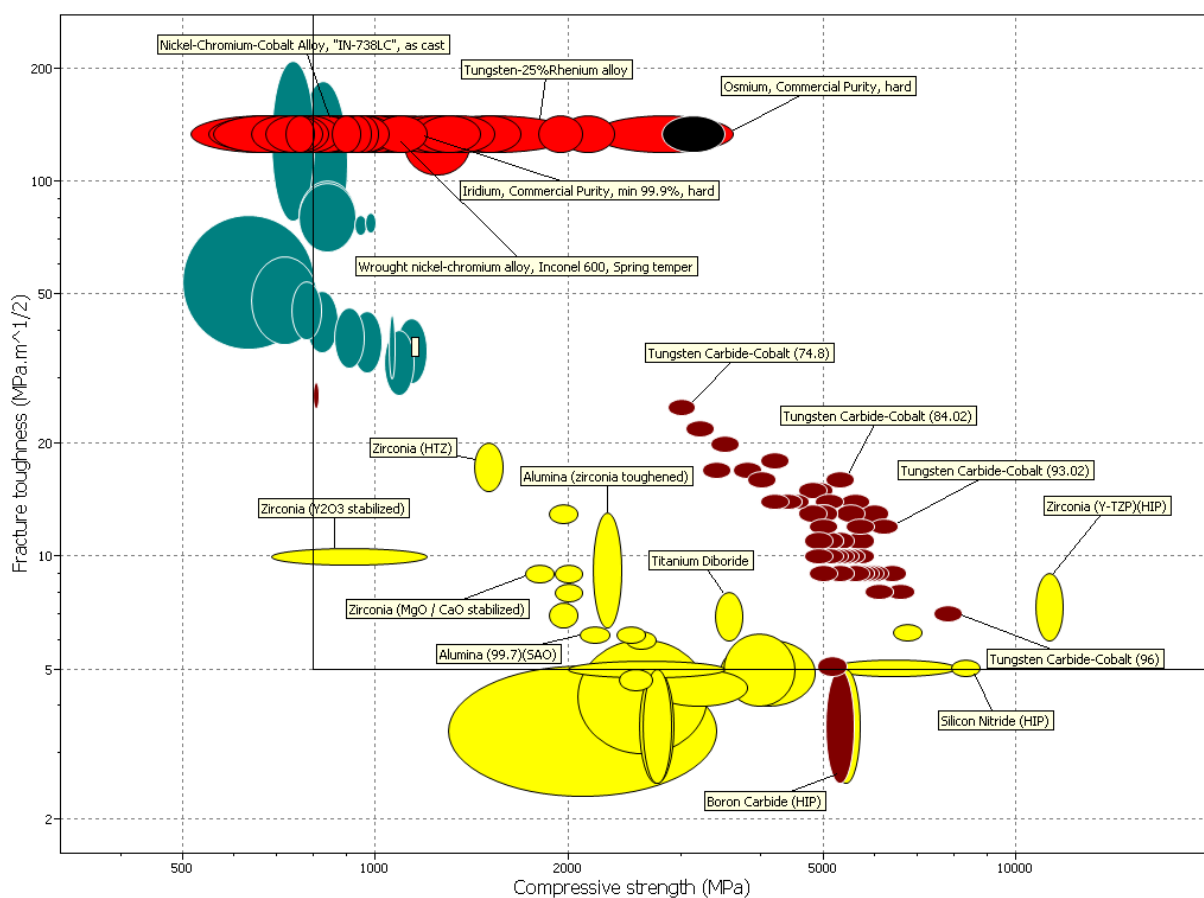
Fig. 4-2 Result of stage 1 of the material selection using CES

All materials which passed the first selection were considered for the second step. The next criteria are the maximum service temperature and the oxidation at 500°C. The limits for the selection were set as defined in Table 4-3. The minimum value of the maximum service temperature must be 600°C, the oxidation at 500°C must be "very

good" (that means no oxidation). The resulting materials out of the selection are shown in Fig 4-3.
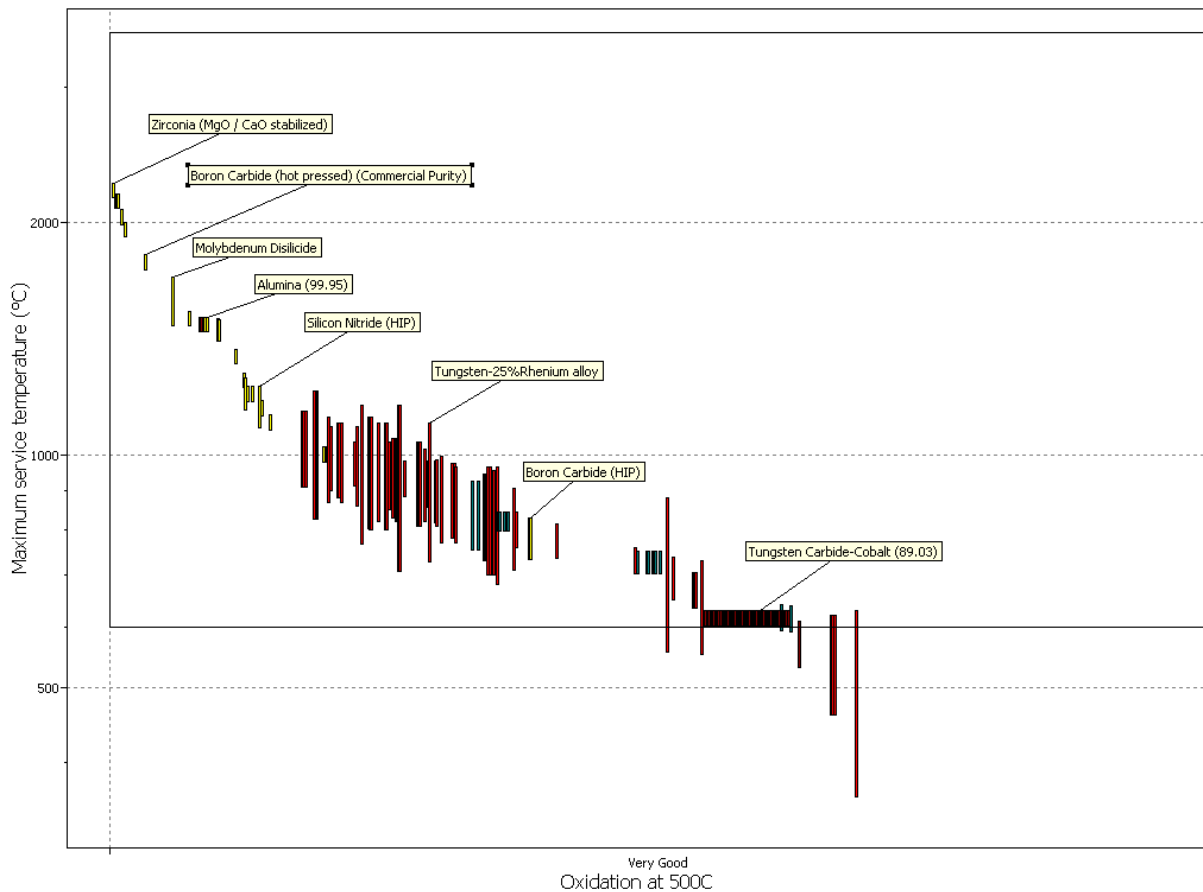
Fig. 4-3 Result of stage 2 of the material selection using CES

It can be seen in Fig. 4-4 that a number of materials passed this step. The resulting materials from the second step are shown in a graph with thermal conductivity on the abscissa and thermal expansion coefficient on the ordinate.
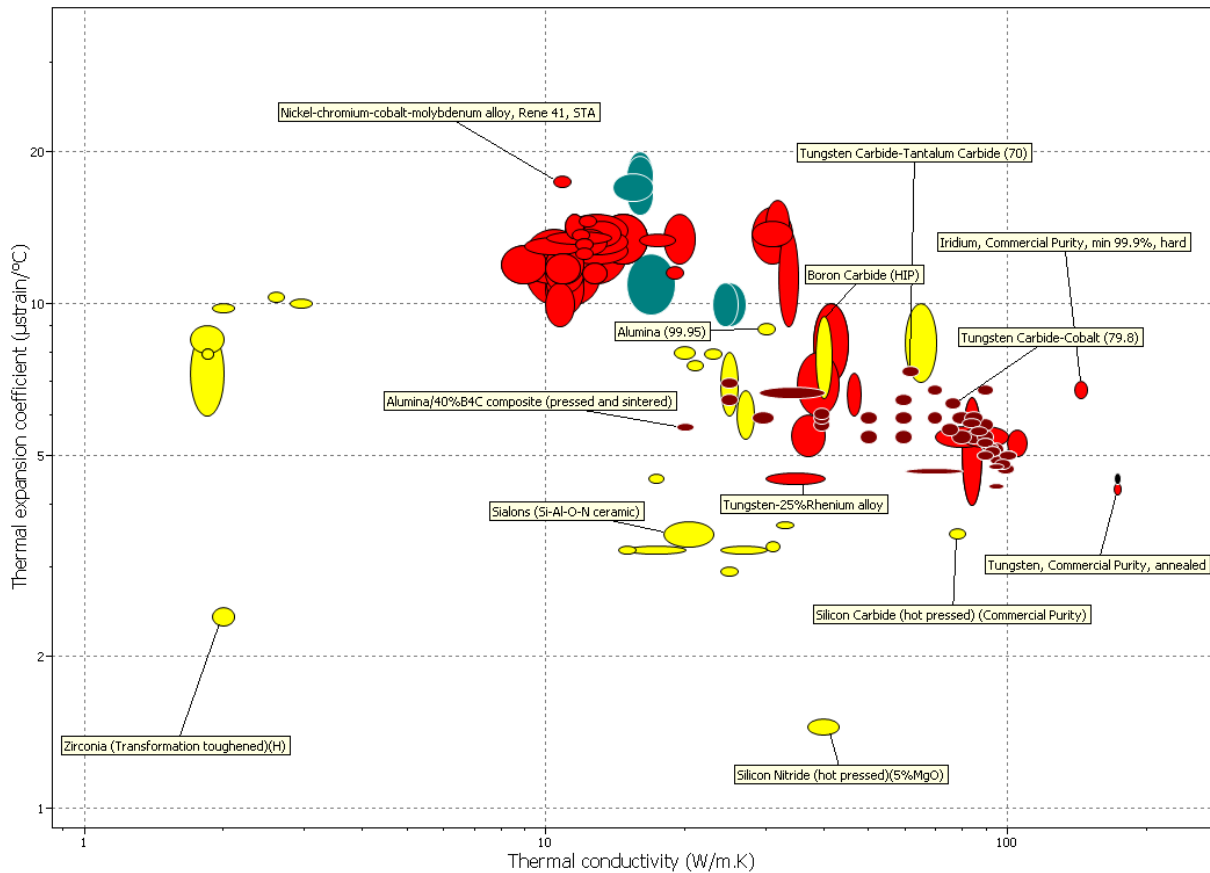
Fig. 4-4 Plot of resulting materials from stage 2 with thermal conductivity on the abscissa and thermal expansion coefficient on the ordinate

For further consideration, following materials out of the results were selected:

➢ Diamond

➢ Molybdenum – Titanium Alloy

➢ Molybdenum – Tungsten Alloy

➢ Osmium

➢ Iridium

➢ Silicon Nitride

➢ Tantalum - 10% Tungsten – 2.5% Hafnium Alloy

➢ Tungsten – Carbide

➢ Tungsten – 25% Rhenium

➢ Wrought Nickel-Chromium alloy

The result of the selection using the software package "CES Selector Version 4.0" was critically analyzed and some of the potential materials were eliminated. The reasons are discussed in the next paragraph.

<u>Tungsten – 25% Rhenium</u>

Since this material is already used for friction stir welding of steels, it will not be considered for the selection of **new** potential tool materials.

<u>Iridium, Osmium</u>

Iridium and osmium alloys are materials which have excellent high temperature properties and therefore they would be an ideal tool material for FSW of steels. But both materials are very rarely and thus the price is high. Due to the **limited availability** they are not considered in this work.

<u>Wrought Nickel-Chromium alloy</u>

Nickel-Chromium alloys were especially developed for high temperature applications like engines, power plants, etc. They show very good mechanical properties up to 600°C, but **at higher temperatures, they fall rapidly**. At temperatures, which are expected during FSW of steels, they have poor mechanical properties and therefore they will not be considered in this study. But they may be used for friction stir welding of aluminium alloys, especially when welding high strength alloys like EN AW7075.

The properties of the remaining materials are shown in Table 4-4. The description of the columns is as follow:

1. Service temperature [°C]
2. Hardness [HV]
3. Toxic
4. Compressive strength [MPa]
5. Fracture toughness [MPa m$^{1/2}$]
6. Oxidation resistance at 500°C
7. Thermal conductivity [W/mK]
8. Thermal expansion coefficient [μstrain/K]
9. Availability
10. Material price [Euro/kg]

The properties 3. (Toxic), 6. (Oxidation resistance at 500°C) and 9. (Availability) were ranked using the school grading system (1 to 5; 1 means excellent).

Table 4-4 Material properties for the selected tool materials

Material	1	2	3	4	5	6	7	8	9	10
Diamond	1700	4900	1	10000-20000	3-7	1	200-400	0.8-1.2	3	462900
Molybdenum - Titanium Alloy	1300	360	2	770-950	30-50	1	129-147	4.7-5.5	2	38.58
Molybdenum - Tungsten Alloy	1300	300	2	650-800	20-60	1	100-130	4-6	2	38.58
Silicon Nitride	1200	2200	1	7935-8750	4.8-5.3	1	31.7-34.3	3.6-3.7	1	40.12
Tantalum - 10% Tungsten – 2.5% Hafnium Alloy	900	320	1	650-880	120-150	1	30-55	5-6.5	2	694.4
Tungsten Carbide	1150	1800	1	3000-8000	7-25	1	95-103	4.6-4.8	1	23.15

In the next step of the selection the material properties were ranked using the weighted property index method shown in Table 4-5.

Table 4-5 Weighted material properties for the weight property index (WPI) table

Material properties	(pairwise comparison cells)	Sum	Weight Index
Service temperature [°C]	0 1 0 0 1 1 1 1 1	6	0,13
Hardness [HV]	1 ... 1 0 0 1 1 1 1	7	0,16
Toxic	0 ... 0 ... 0 0 1 1 1 1	5	0,11
Compressive strength [MPa]	1 ... 1 ... 1 ... 1 1 1 1 1	9	0,20
Fracture toughness [%]	1 ... 1 ... 1 ... 0 ... 1 1 1 1	8	0,18
Oxidation at 500°C	0 ... 0 ... 0 ... 0 ... 0 1 1 1 0	3	0,07
Thermal conductivity [W/mK]	0 ... 0 ... 0 ... 0 ... 0 ... 1 0 0	1	0,02
Thermal expansion coefficient [µstrain/K]	0 ... 0 ... 0 ... 0 ... 0 ... 0 ... 0 0	0	0,00
Availability	0 ... 0 ... 0 ... 0 ... 0 ... 1 1 0	2	0,04
Price [Euro/kg]	0 ... 0 ... 0 ... 0 ... 0 ... 1 1 1 1	4	0,09
		45	1

Following boundary conditions were set:

- maximum hardness: 2000 HV
- maximum thermal conductivity: 200 W/mK

Table 4-6 Weighted property index (WPI) table for the selected tool materials

Material	WPI
Diamond	67
Molybdenum - Titanium Alloy	40
Molybdenum - Tungsten Alloy	40
Silicon Nitride	68
Tantalum - 10% Tungsten – 2.5% Hafnium Alloy	50
Tungsten Carbide	*71*

As shown in Table 4-6, the material with the highest WPI is tungsten carbide, followed by silicon nitride and diamond. Due to the results of the material selection, tungsten carbide (WC) with cobalt binder (Co) was selected for further studies.

4.3.2 Tungsten Carbide

WC-Co cemented carbides, also commonly referred to as hardmetals are well known as highly wear-resistant materials, being especially useful for various applications (cutting tools, drilling and mining equipment). They exhibit an exceptional combination of strength, hardness, toughness and wear resistance as a result of extremely different properties of their two interpenetrating constitutive phases: hard, brittle carbides and a relatively soft, ductile, metallic binder [86, 87].

Another big advantage is the ability to tailor the properties of WC-Co to the requirements of the application:

- By changing the grain size of the tungsten carbide (<0.1 to >30 μm)
- By changing the amount of cobalt binder phase (<1 to >30wt. %)
- By adding other types of hard phase (e.g. TiC, Ta(Nb)C, Cr_3C_2)
- By using different binder metals (e.g. Co-, Ni-, Fe-, Cr- alloy binders)
- By special processing technologies (e.g. gradient sintering)
- By creating new sub-classes of hardmetals (e.g. carbonitride-based cermets)

The use of WC-Co for FSW of MMC was reported to friction stir 5 mm thick AC4A (aluminium-silicon alloy) + 30% vol% SiC [88]. But WC-Co can also exhibit high temperatures, the use as a cutting plate with measured peak temperatures up to 1200°C was reported (Fig. 4-5) [89].
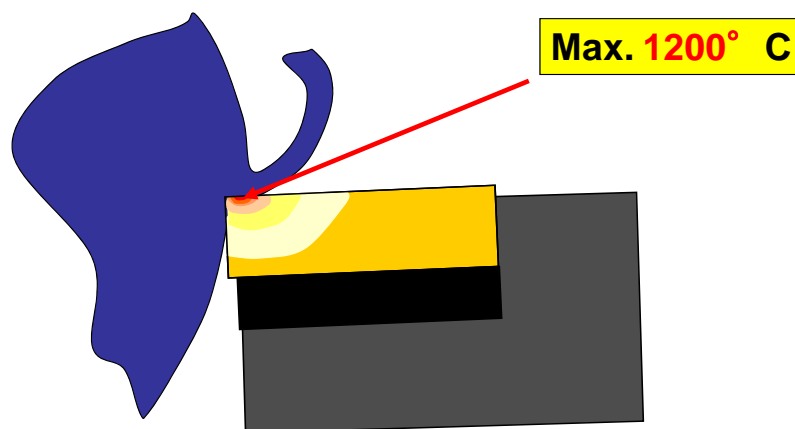
Fig. 4-5 Temperature distribution in a cutting plate [89]

Formation of WC-Co structure

WC-Co is produced by sintering usually in a region between 1350 and 1500°C. Even during heating (from about 700°C), up to 80% of the required densification is achieved by solid phase sintering. During sintering the hard material phase is dissolved by the molten binder metal and reprecipitated. During the solidification of the liquid phase the majority of the dissolved WC crystallizes back on hard particles [90]. The structure of WC-Co cemented carbides is illustrated in Fig. 4-6.
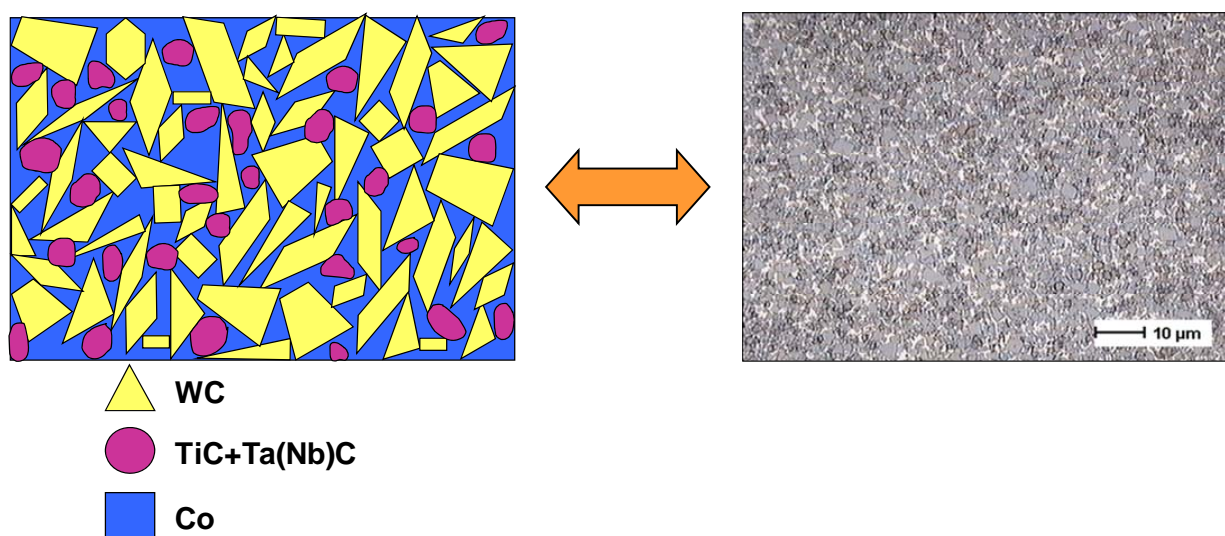
Fig. 4-6 Structure of WC-Co cemented carbides a) schematic and b) macrograph

In the system W-C-Co, the stoichiometric range for this area is limited to 6.08 to 6.20 weight %C in WC [90]. The Co content depends on applications. It is well known that the cermets with higher binder content have higher thermal conductivity [86].

Mechanical properties

The knowledge of the influence of different parameters on the mechanical properties is essential for the selection / development of friction stir welding tools. The relationships can be described as follow:

The structure of a WC-Co hardmetal can be characterized by the linear average grain size l_{WC} and average thickness of the intermediate cobalt layers p_{Co} ; these are also called mean free path or average distance. The fracture toughness of the WC-Co

hardmetals (which is within the limits of 7 to 20 MPa m$^{1/2}$) is related by the following expression [90]:

$$G_{1C} = \frac{K_{1C}^2}{\pi \cdot E} = \frac{p_{Co}^2}{l_{WC}} \quad (4\text{-}1)$$

Hardness depends on the same parameter p^2_{Co}/l_{WC} and shows the reverse relationship:

$$HV = 877 \cdot (p_{Co}^2 / l_{WC})^{-1/5} \quad (4\text{-}2)$$

This means that in any given compound system **hardness and fracture toughness** can only be **optimized at the expense of each other**. The variation of hardness and fracture toughness in relation to the grain size of the tungsten carbide and the amount of cobalt binder phase is given in Fig. 4-7.
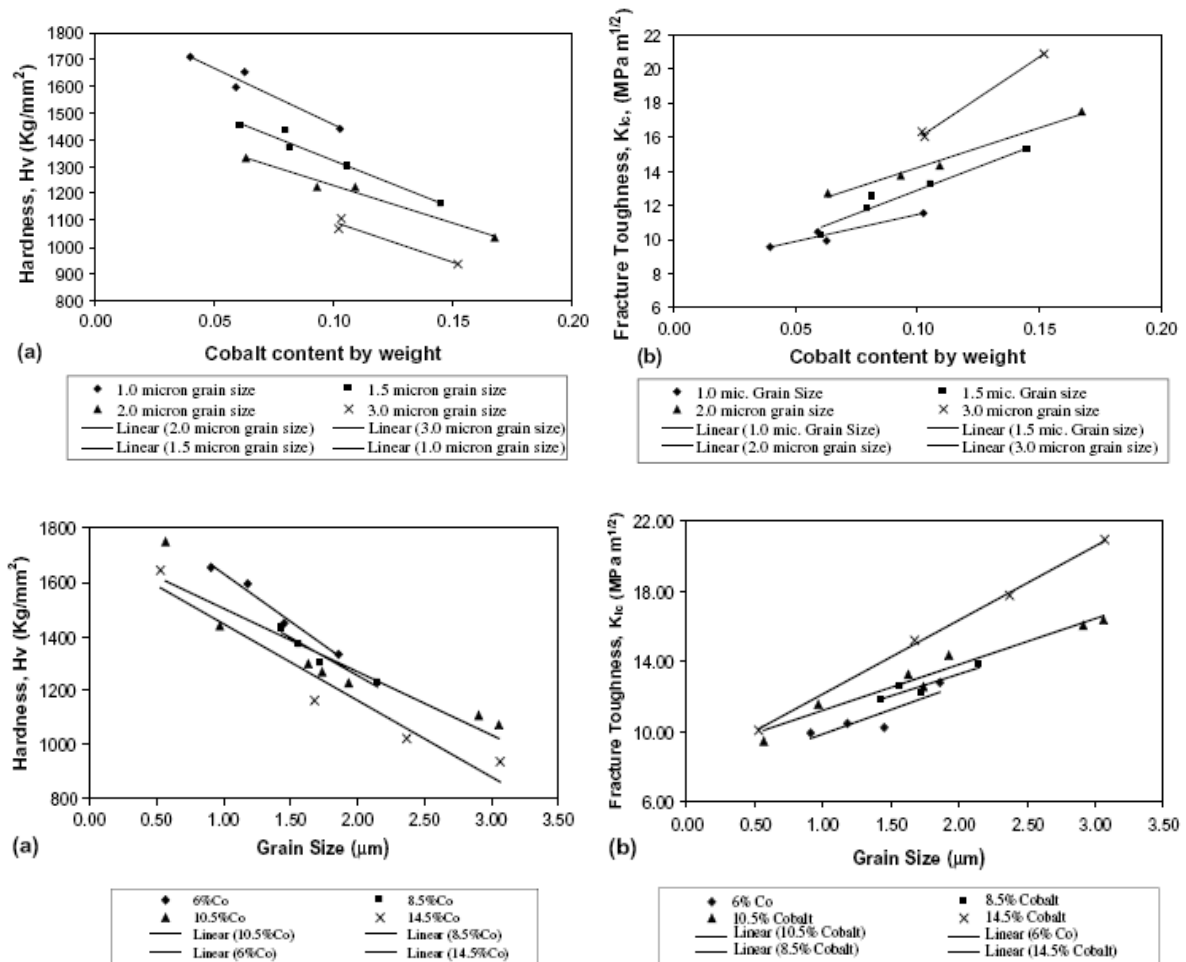
Fig. 4-7 Influence of cobalt content and average carbide grain size on hardness and fracture toughness [91]

By adding TiC, hardness is increased at the expense of bending fracture strength, due to the solid solution hardening. This sometimes also increases the warm strength of the WC-TiC(TaC) solid solution in comparison with WC and above all TiC (Fig 4-8). This is especially relevant at higher working temperatures [90].
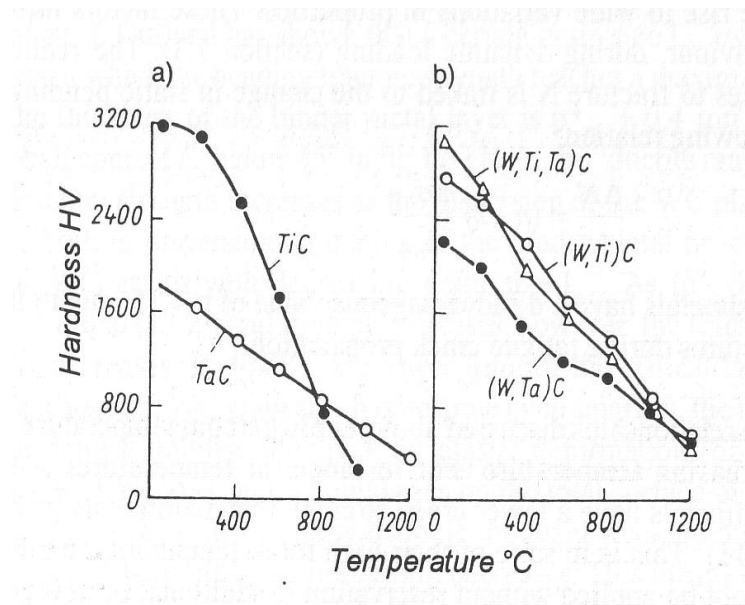
Fig. 4-8 Warm strength a) cubic carbides b) cubic mixed carbides [90]

4.4   Experimental Setup

4.4.1 Friction Stir Welding Machine

For the friction stir welding experiments, the 2D research and development machine ISTIR BR4 from MTS Systems Corporation at the Institute for Materials Science and Welding was used (Fig. 4-9). The I-STIR BR4 system is based on a proven machine platform. The three-axis gantry utilizes a stiff crossbeam construction with a moving table. The manipulation system consists of the X, Y, and Z axes. The machine also has a manually adjustable pitch axis. These axes position the weld head in space and essentially run in position control. The weld head performs pin penetration and load control. The forces and torque were measured by high accuracy pressure cells and recorded simultaneously during each welding operation.

Fig. 4-9 MTS ISTIR BR4 Friction Stir Welding Machine at the Institute for Materials
Science and Welding of TU Graz

The ISTIR BR4 has an integrated cooling tool holder for welding steel or other high temperature alloys (Fig. 4-10). It is important to note that the temperature range for FSW high temperature materials is generally above 900°C for most applications. Since these temperatures are significantly higher than aluminum FSW, the welding process is more dynamic and subject to temperature and load gradients. This also means that the FSW tool governs the heat flow of the welding process rather than the material being friction stir welded. For this reason, a tool cooling system is needed to manage the heat transferred out of the tool. The liquid-cooled tool holder removes just enough heat from the tool shank to ensure stiffness and protects the welding head. A slip ring will allow a thermal couple to be mounted with the tool holder. This is required for continuous real time temperature data acquisition and control. This verifies steady state FSW conditions when used with z-axis and x-axis load control.
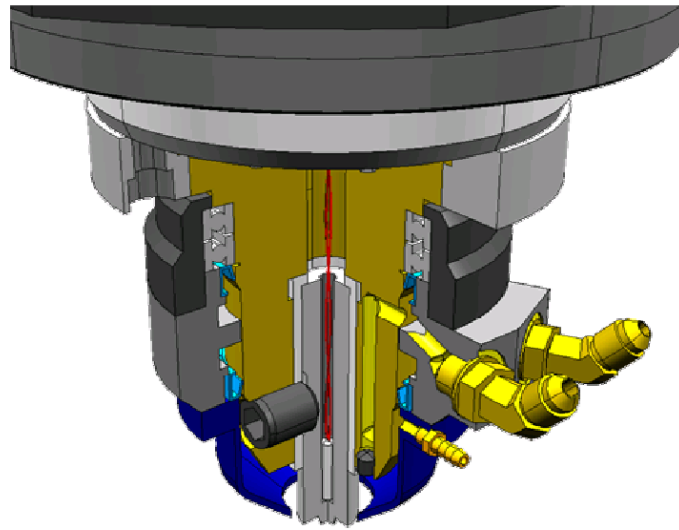
Fig. 4-10 Schematic of the watercooled welding head [92]

The system will also provide a special chamber for performing the welds in an argon (or other gas) atmosphere (Fig. 4-11). The inert gas assists in improving tool life by preventing oxidation of the base and tool material. Oxidation surfaces are harder and reduce flow characteristics of the base metal.
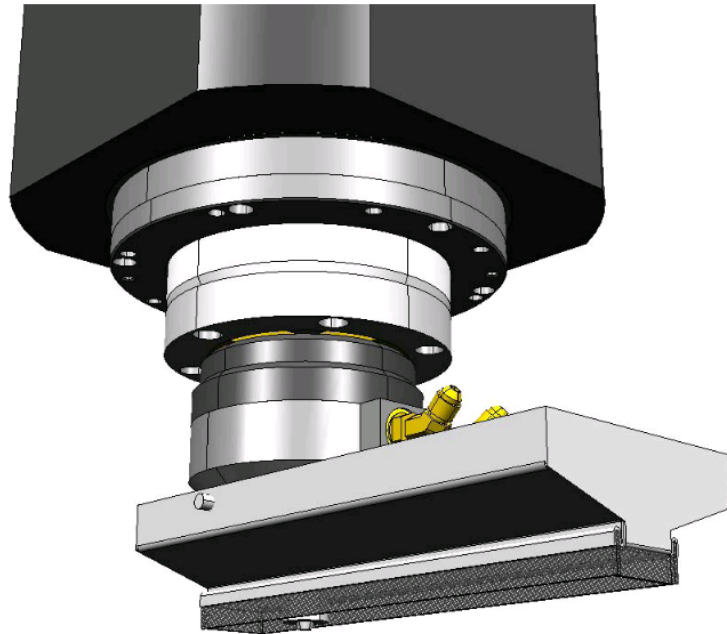
Fig. 4-11 Schematic of the watercooled welding head and the argon chamber [92]

The specifications of the machine are as follow [92]:

- Travel range - 2450 x 1250 mm

- Max. welding speed - 6.4 m/min

- Max. spindle speed - 3200 U/min

- Max Axial force - 35.6 kN

- Max. spindel torque - 180 Nm

- Pitch – 5°

- Separate Pin- and Forge axis (self reacting pin tool [SRPT] possible)

- Position or force control mode possible

- Measure, control and monitor of the parameters - pin rotation, forge force and traverse loads, displacement

In addition to the machine technology, clamping devices were designed and fabricated. The pneumatic and mechanical clamping devices which were used within this work are shown in Fig. 4-12. The clamping will ensure that the plates are rigidly fixed during the welding process.
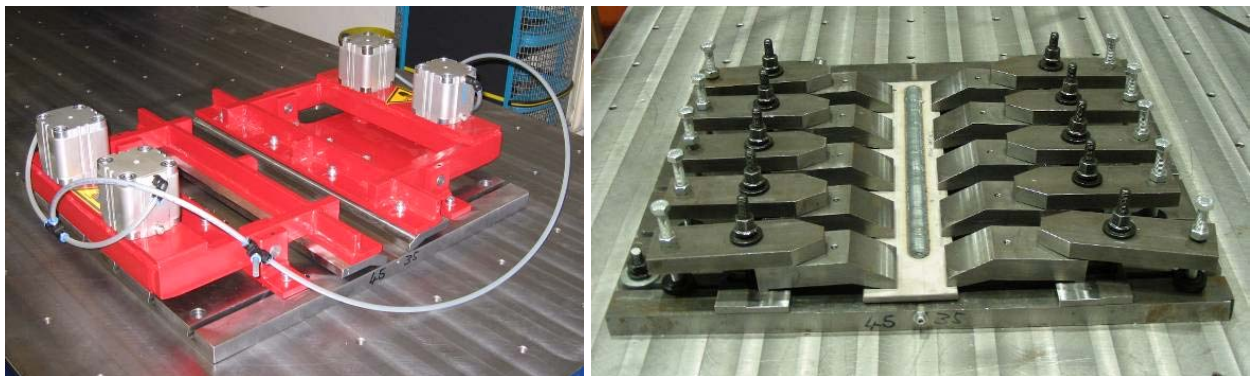
Fig. 4-12 Pneumatic (left) and mechanical (right) clamping device for friction stir welding

4.5   Material and Geometry

The austenitic stainless steel from grade DIN 1.4301 (AISI304) with a size of 500 mm x 100 mm x 4 mm was used in this work. The nominal chemical composition of DIN 1.4301 is shown in Table 4-7. The mechanical properties are given in Table 4-8.

Table 4-7 Nominal chemical composition of steel DIN 1.4301 [93]

C [%]	Si [%]	Mn [%]	P [%]	S [%]	Cr [%]	Ni [%]
<0.07	<1.00	<2.0	<0.045	<0.015	17.50-19.50	8.0-10.50

Table 4-8 Mechanical properties of steel DIN 1.4301 [93]

$R_{p0.2}$	R_m	Elongation (min.)
[MPa]	[MPa]	[%]
210	520-720	45

4.6   Experimental Procedure

Bead on plate welding of 4 mm thick steel sheets was performed. The plates were clamped on the table using a mechanical or pneumatic clamping device (Fig. 4-12). Welding was performed using a transverse speed range from 55 mm/min to 155 mm/min and spindle speeds between 400 rpm and 750 rpm. The welds were performed in force control mode. The tilt angle was varied from 1° to 3°. The plunge rate was constant (6 mm/min) for all experiments. The tool and the stirring area were protected from oxidation by an argon shield. For performing the temperature measurements with an infrared camera, no shielding has been used. A typical test setup with the mounted shielding device is shown in Fig. 4-13.

Fig. 4-13 Typical weld setup with argon shielding

To study the wear behaviour of different tool materials, two experiments were developed. The first experiment seeks to represent a friction stir spot welding process, the second experiment a linear weld.

For the spot welding experiment, the tool was plunged into the material with a defined plunge rate and spindle speed. After shoulder touchdown a dwell phase was defined and afterwards the tool was retracted.

For the linear welds, a pilot hole with a diameter of 6mm was used to reduce the wear during the plunge phase. The weld was performed with defined spindle and travel speed. All linear welds were made in force control mode. Different weld lengths were used to study the tool performance.

An example of a spot and a linear weld is shown in Fig. 4-14.
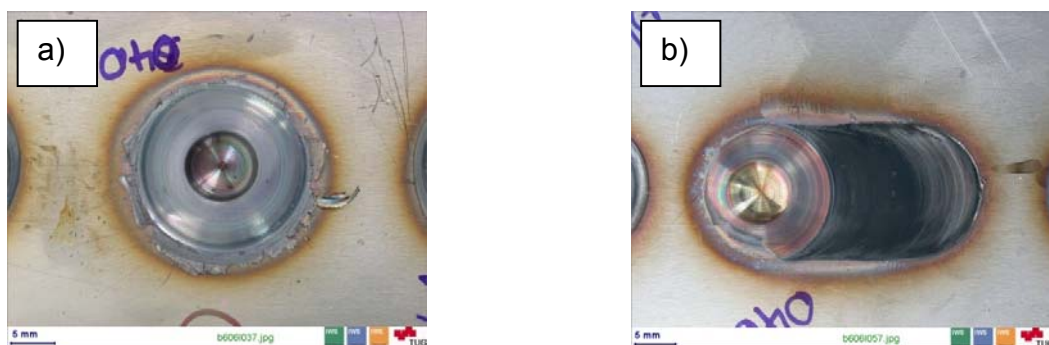
Fig. 4-14 a) Spot weld and b) 20mm long linear weld experiment in steel DIN 1.4301

Tool wear and deformation was examined using stereo microscopy, scanning electron microscopy and picture analysis software.

4.6.1 Tool geometry

The tool geometry for the experiments was as follow. The used tools had a concave shoulder, a shoulder diameter of 19 mm, medium pin diameter of 6.1 mm and pin length of 3.1 mm. Later, additional tools with three flat pin tool design were used. The details about tool geometry are shown in Fig. 4-15.
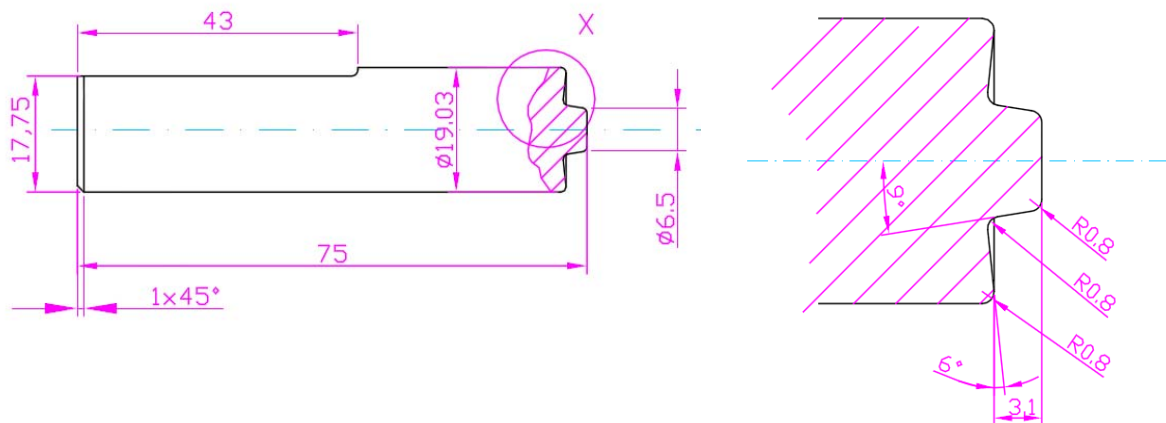
Fig. 4-15 Tool geometry for friction stir welding experiments in 4mm thick steel DIN 1.4301

4.7   Fundamental Tests

As a reference, bead on plate welding with a W25Re tool, spindle speed of 400 rpm, welding speed of 80 mm/min and tilt angle of 3° was performed and the results are shown in the following chapters.

4.7.1 Metallographic analysis

The microstructural characteristics of the specimens were examined using light optical microscopy. Metallographic samples were extracted at different positions of the weld. The polished samples for light optical microscopy were prepared using standard metallographic techniques. The cross section overview (Fig. 4-16) using light optical microscopy showed a defect free joint with an asymmetric shape. The observed microstructure is typical for austenitic stainless steel. The base metal has an annealed grain structure including a high density of twins. A slightly variation in grain size can be found from the base metal into the stir zone, the finest grains were found in the stir zone (Fig. 4-17). The height of the stir zone is 3.6 mm. In a depth of approximately 3 mm below the top surface and on the top surface, a light grey area is visible.
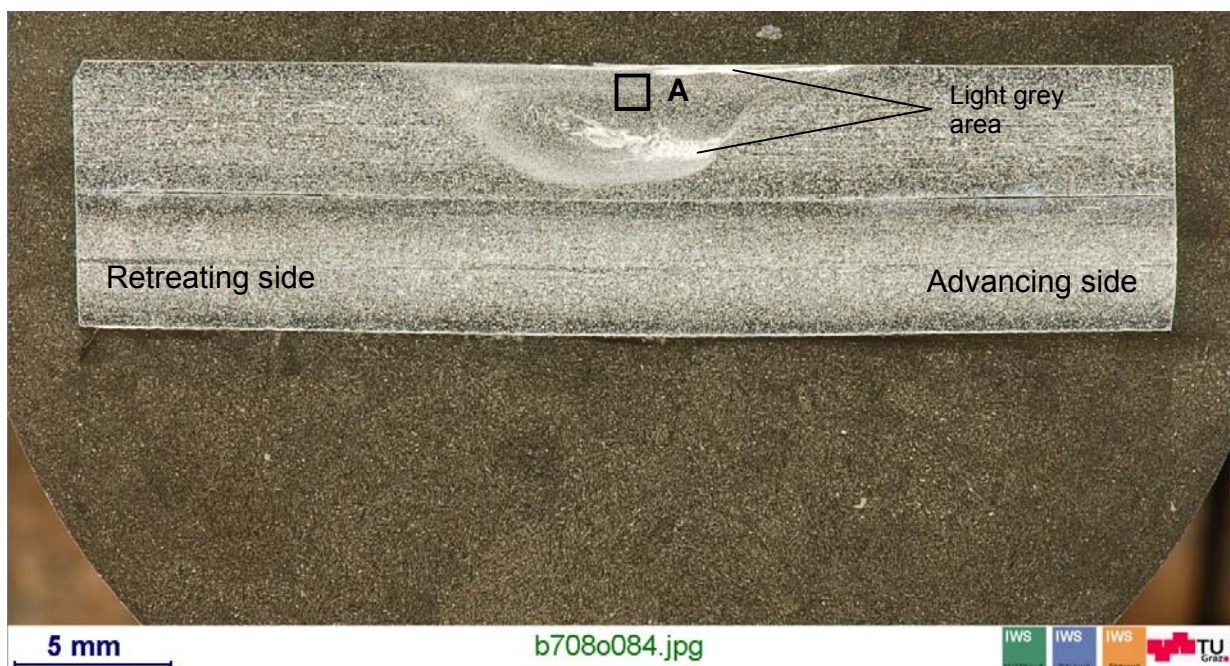
Fig. 4-16 Cross section macrograph of bead on plate welded steel DIN 1.4301 using W25Re tool material
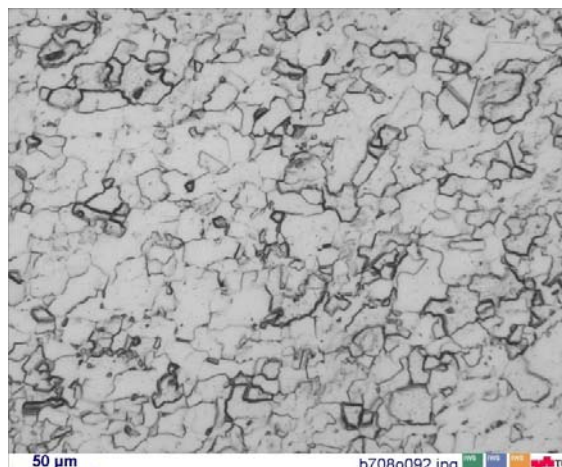
Fig. 4-17 Stir zone microstructure (Detail A of Fig. 4-16) of bead on plate welded steel
DIN 1.4301 using W25Re tool material

Using energy dispersive x-ray spectroscopy, an enrichment of tungsten with a
fraction of up to five percent was found in that light grey area. Further tungsten
enrichments were found close to the top surface. These findings suggest that tool wear
is concentrated at the pin tip and the shoulder edge. The metallographic samples of the
start zone showed an increased appearance of tungsten. This may come from a higher
tool wear, when the tool plunges into the cold material. The metallographic samples,
where a start-up hole with a diameter of 6 mm was used for plunging, showed higher
tungsten appearance than the samples at steady state but less than the ones without
keyhole.

4.7.2 Mechanical properties

Cross tensile specimens were extracted from the welded plate and the base
metal. The top and bottom surface was milled before testing to avoid notch effects. A
representative tensile sample with a thickness of 3 mm is shown in Fig 4-18. During
tensile testing, the location of fracture was in the base metal. The ultimate tensile
strength of the base metal was 683 MPa and the elongation 55%.

The hardness profile in Fig. 4-19 shows an overmatching of the weld relative to the base metal. The maximum hardness value in the weld area was 201 HV. The reason of the higher hardness is attributed to the finer grain size in the stir zone.

Fig. 4-18 Milled tensile sample with a thickness of 3 mm
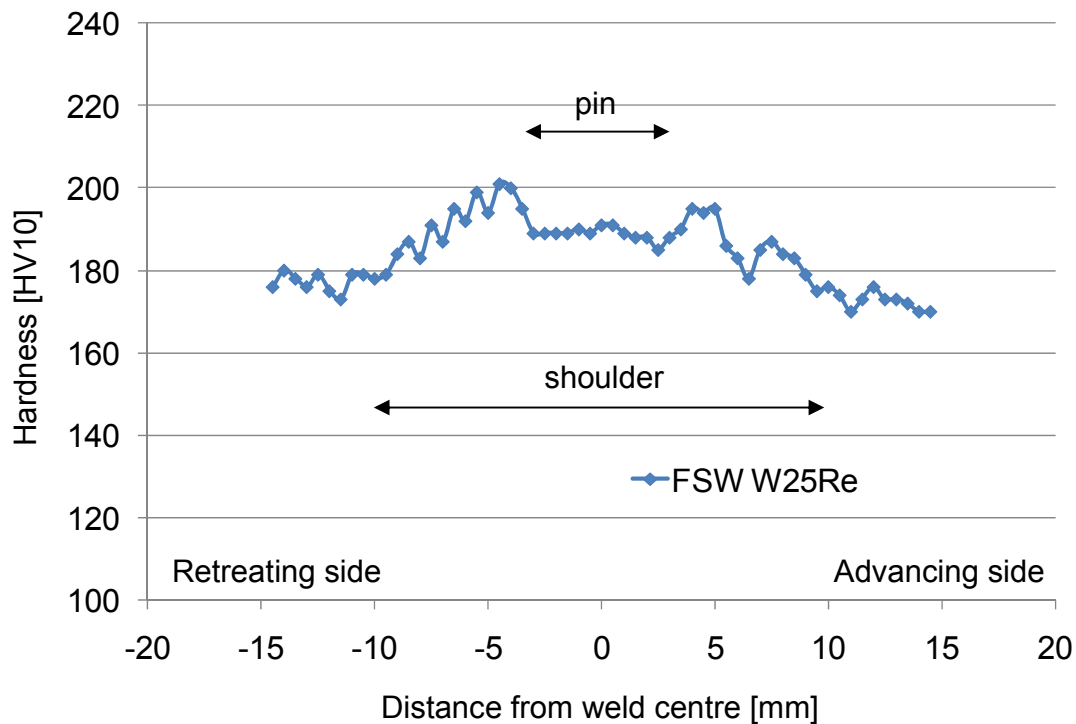
Fig. 4-19 Hardness profile for cross section of bead on plate welded steel DIN 1.4301

4.7.3 Forces and Torque

The highest forces were observed during the plunge phase. They reached nearly the maximum possible downward force of the machine (35 kN). The whole plunge phase

lasted 32 sec. Faster plunge rates were not possible due to exceeding the machine limits. During welding, the downward force was constant with a value of 19 kN. The spindle torque rose slowly during the plunge phase and rose after shoulder contact. For all welds with a plunge hole, the forces were low during the plunge phase and escalated after shoulder touchdown (Fig. 4-20).
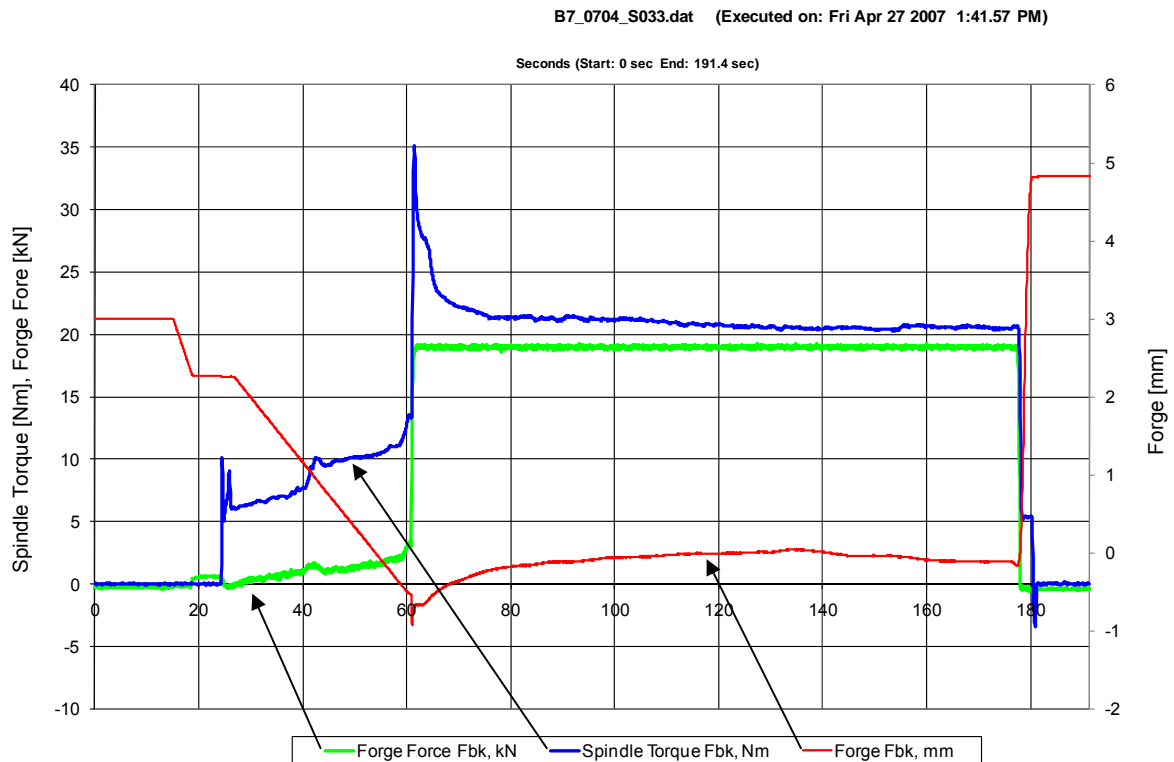
Fig. 4-20 Axial force (Forge Force), spindle torque and tool position (Forge Fbk) for a linear weld with 6mm plunge hole

4.7.3.1   The effect of welding speed on forces and torque

Increased loads in welding direction were observed at higher welding speeds. The force in welding direction was 0.55 kN for spindle speed of 400 rpm, welding speed of 80 mm/min and tilt angle of 3° and rose to a value of 1.1 kN for 155 mm/min welding speed (Fig. 4-21). The torque did not show a significant change when increasing the feed rate.
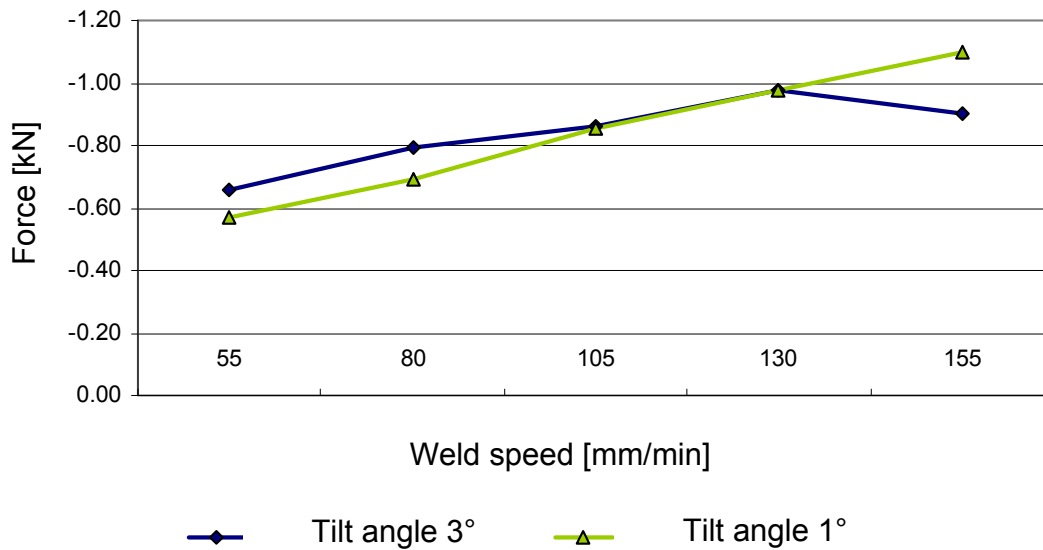
Fig. 4-21 Forces in welding direction for 1° and 3° tilt angle for 500 rpm spindle speed

4.7.3.2   The effect of spindle speed on forces and torque

When increasing the spindle speed from 400 rpm to 600 rpm a slight decrease of 0.05 kN for the force in welding direction was observed. When the torque was 27.5 Nm at 400 rpm, it decreased to a value of 22.5 Nm for 600 rpm spindle speed (Fig. 4-22).
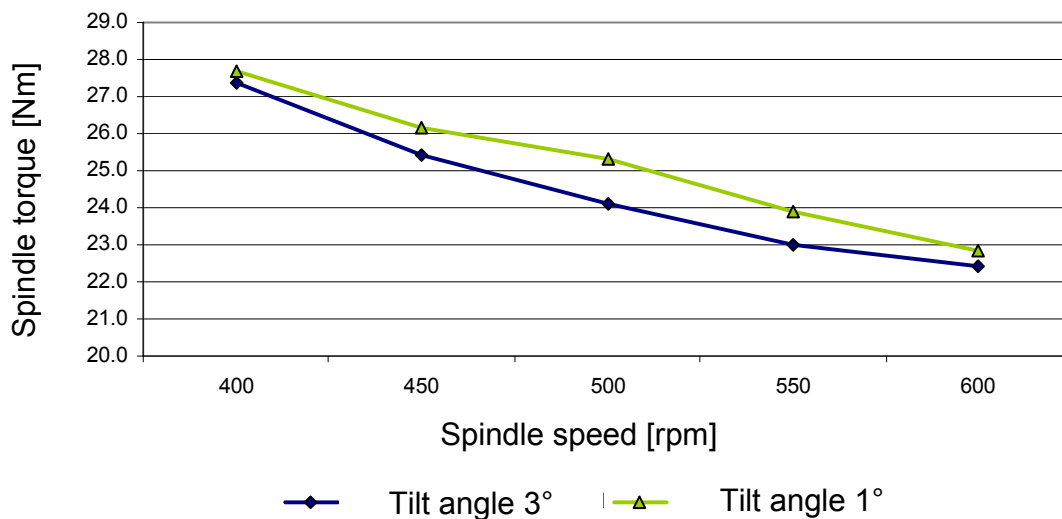
Fig. 4-22 Spindle torque for 1° and 3° tilt angle for 80mm/min travel speed

4.7.3.3   The effect of tilt angle on forces and torque

When changing the tilt angle from 3° to 1°, a little increase of torque was observed for all welding parameters. The forces in welding direction are approximately 5% lower during stirring with 1° tilt angle than with 3° as a reference.

4.7.4 Temperature

Temperature measurements were performed using thermocouples and infrared camera. The temperatures on the surface of the plates and the tools were measured using the TH3100MR infrared camera and software package IRIS. The temperature range was chosen 200°C to 2000°C with a measurement accuracy of 5°C. A representative test setup is shown in Fig. 4-23.
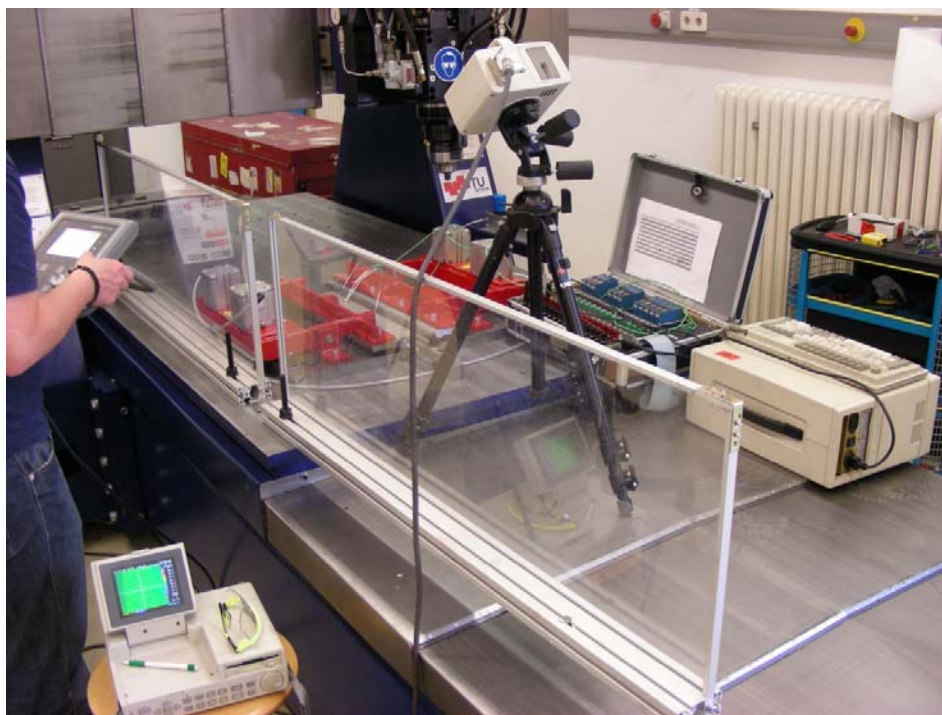
Fig. 4-23 Test setup for temperature measurements

To evaluate the temperature distribution and the correct emissivity factor, additional temperature measurements of the plate surface were performed using K-type thermocouples. The thermocouples were fixed on the plate surface with a distance of 12

mm and 15 mm to the weld centre on the advancing side using a resistance spot welding process (Fig. 4-24).
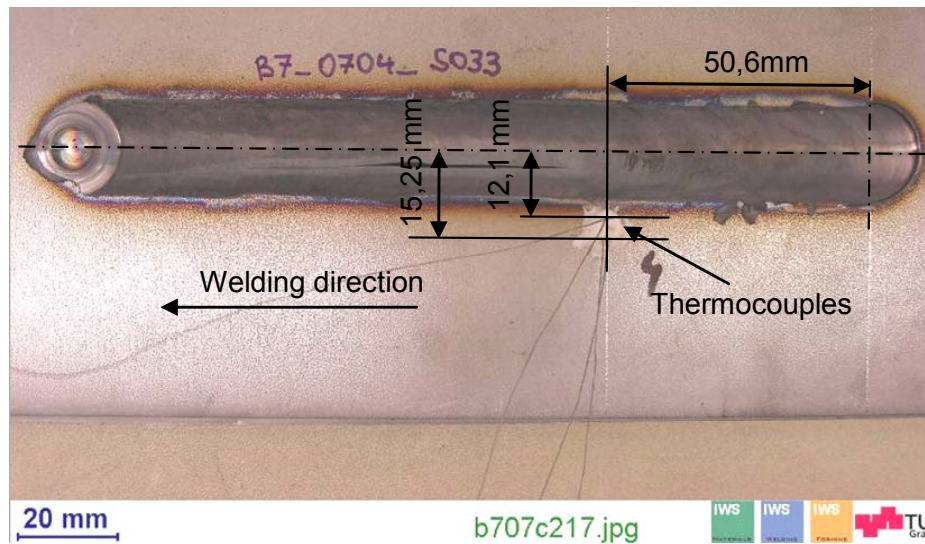
Fig. 4-24 Thermocouples on the advancing side placed 12.1 mm and 15.25 mm away from the weld center

The thermocouple, which was placed 12 mm from the weld centre recorded peak temperatures of 648°C (Fig. 4-25). Likewise results have been reported by other researchers [94].
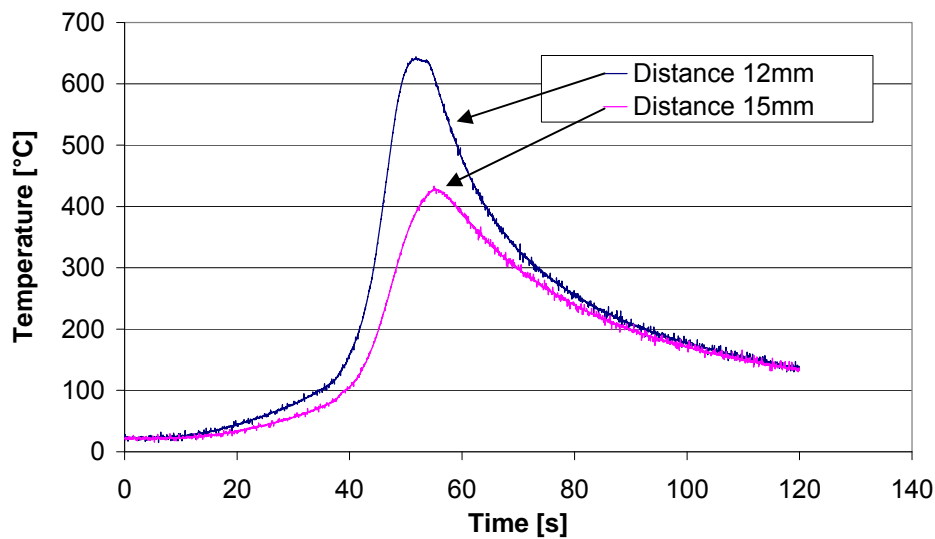
Fig. 4-25 Temperature cycle for thermocouples placed 12 mm and 15 mm from the weld centre

It was observed, that a reduction of tilt angle leads to higher peak temperatures, which can be explained by the increased heat input due to higher torque. Variation of the maximum surface temperature (measured with infrared camera) with respect to spindle speed is shown in Fig. 4-26. When increasing the spindle speed from 400 rpm to 600 rpm, the maximum temperature increased from 854°C to 911°C. The change of weld speed from 55 mm/min to 155 mm/min showed no significant change of peak temperature.
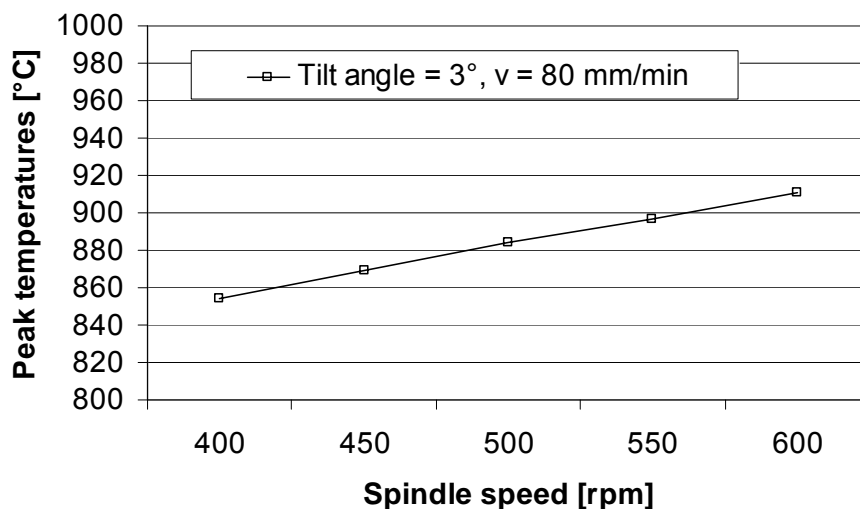
Fig. 4-26 Variation of peak surface temperatures when varying the spindle speed

Peak surface temperatures of 854°C for spindle speed of 400 rpm, welding speed of 80 mm/min and tilt angle of 3° were monitored at the shoulder area of the sheet.

4.7.5 Tool wear

Fig. 4-27 shows the areas of the tool in which significant wear occurs. For some process parameters, especially when performing hot welds, pickup of material on the tool shoulder was found (Fig. 4-27). For such cases, the analysis of tool wear using the whole geometry is not meaningful. Therefore, only the pin wear has been used for the comparison of wear.

Fig. 4-27 Tool wear and material pickup after 300 mm long bead on plate welding of 4mm thick AISI304

4.7.5.1   The effect of spindle speed and feed rate on wear

It can be observed that the welding with low spindle speed leads to less wear of the pin (Fig. 4-28). Medium spindle speed leads to an increase of wear, especially at the pin tip. With high spindle speed, further increase of pin wear was observed. With increase of welding speed, a slightly decrease of pin wear was observed.

4.7.5.2   The effect of tilt angle on wear

The results of tool wear showed less wear for stirring with 1° tilt angle than for welding with 3° tilt angle (Fig. 4-28). Most of the wear occurred at the pin tip.
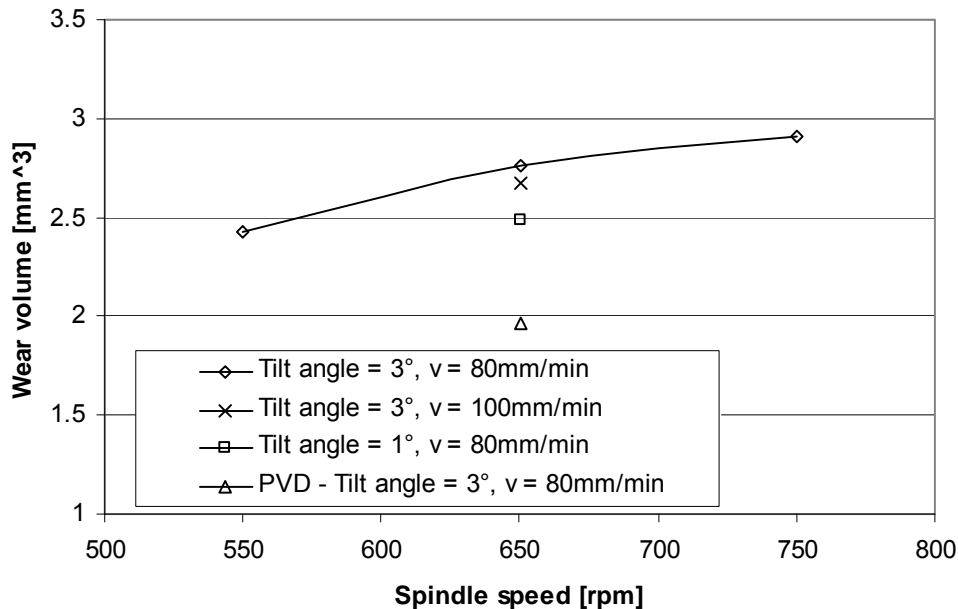
Fig. 4-28 Loss of volume due to pin wear for different welding parameters after 300 mm long bead on plate welding in 4 mm thick steel DIN 1.4301

4.8   WC-Co Tool Development

The aim of this part was to develop substrates, which can withstand the high loads and temperatures which were analyzed in the previous chapter. Therefore tools with different chemical compositions and average carbide grain sizes were defined and fabricated (Fig. 4-29). The selection was made considering the relationships discussed in chapter 4.3.2. The defined cobalt content ranged from 8 to 26 wt% and the average grain size from 0.8 µm to 9.5 µm. The selected substrates are shown in Table 4-9.
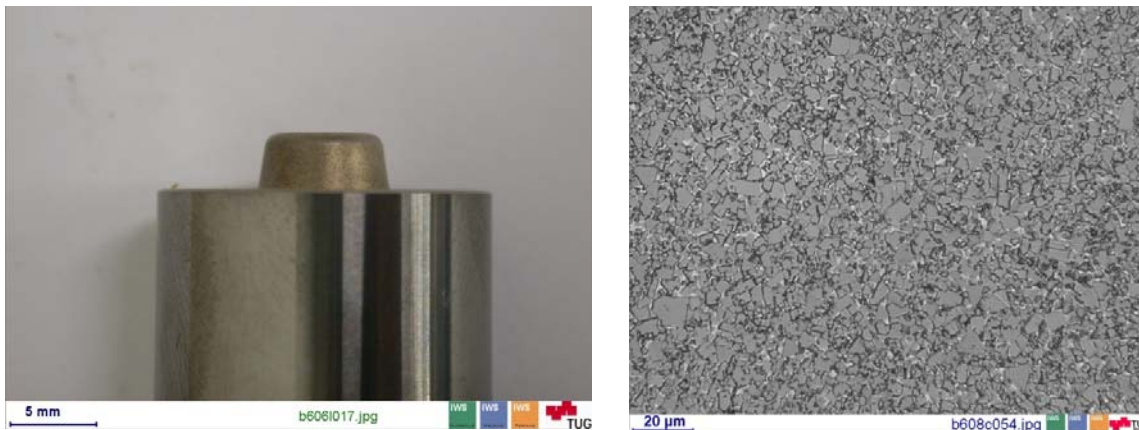
Fig. 4-29 Tool geometry and microstructure of a BB10 tool

Table 4-9 Selected compositions of WC-Co powder mixtures for the tool development

Substrate	WC [wt. %]	Co [wt. %]	TiC [wt. %]	Ta(Nb)C [wt. %]	Grain size WC [µm]	Hardness [HV30]
BB10	92	8			9,5	1275
BB40	87	13			9,5	1100
GB56	74	26			9,5	838
HB30F	90	10			0,8	1675
SB10	57.5	9,5	18	15	2,5	1575
SB40	77	11	4	8	5,3	1400

First, the tools were used for 20 mm long bead on plate welding. A hole with a diameter of 6 mm in the plate was used to reduce tool wear during the plunge phase. Subsequently, substrates that were not found relevant (e.g. due to tool fracture), were eliminated. For tools, which showed only wear, further welds with a length of 50 mm were performed. All tools which survived a length of 70 mm were of interest. These tools were then used for 150 mm and 400 mm long welds.

For the preselection following constant process parameters were used. The parameters were defined after some preliminary test welds. The higher spindle speed compared to a W25Re tool is attributed to the higher thermal conductivity of the WC-Co material (Table 4-2 and Table 4-4).

- Spindle speed: 650 rpm

- Welding speed: 80 mm/min

- Axial force: 19 kN

- Tilt angle: 3°

After welding, the tools were evaluated in terms of:

- Tool failure

- Tool wear

- Visible oxide films or annealing color on the tool

- Material pick up

- Weld quality

Each tool was documented before and after welding using the Nikon Coolpix S10VR camera. Selected tools were examined using stereo microscopy.

4.8.1 Results

In this chapter, the results of the preselection are shown and discussed. The influence of the main parameters grain size, cobalt content and addition of TiC are presented. The results of the preselection for different cobalt contents and carbide grain size are summarized in Table 4-10.

Table 4-10 Summary of tool preselection study

Average carbide grain size	Cobalt content		
	High (>20wt %)	*Medium (10 – 20wt %)*	*Low (<10wt %)*
Extra coarse	GB56 Deformation	BB40 Wear	BB10 Wear
Coarse		GB20 Deformation	WS08C00 Wear
Medium		GB30 High deformation	
Submicron / Fine		HB30F High deformation	

4.8.1.1 Influence of carbide Grain Size

The carbide grain size of the selected WC-Co tool materials ranged from submicron / fine to extra coarse. Most of the tools which were tested had a medium cobalt content. Since not all tool materials with medium cobalt content had the same chemical composition, no direct comparison can be made. But it is possible to identify a trend for the different substrates. It can be seen that the substrate HB30F with fine grain size was highly deformed after welding. When increasing the grain size, deformation decreases and for extra coarse grains (e.g. BB40), no deformation was visible. For substrates with low cobalt content, both tools did not show a deformation. A comparison of the tool probe for the substrate GB30 and BB40 after welding is shown in Fig. 4-30.
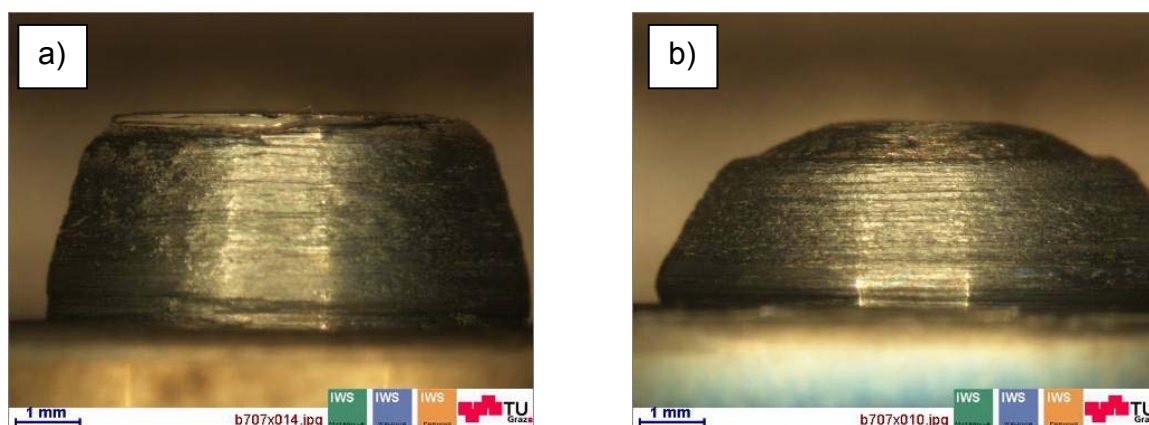
Fig. 4-30 Comparison of tool probe for substrate GB30 a) and BB40 b) after welding

4.8.1.2 Comparison Cobalt Content

To analyse the influence of the cobalt content, tools from BB10, BB40 and GB56 are analysed. The tool substrates varied only in the cobalt content, the carbide grain size was identical. Whereas the tool with high cobalt content (GB56) showed a deformation of the probe after 20mm welding, the tools with medium and low cobalt content did not deform. The probe wear was systematically lower for tools with low cobalt content (e.g. BB10). The comparison of tools with different binder content is shown in Fig. 4-31.
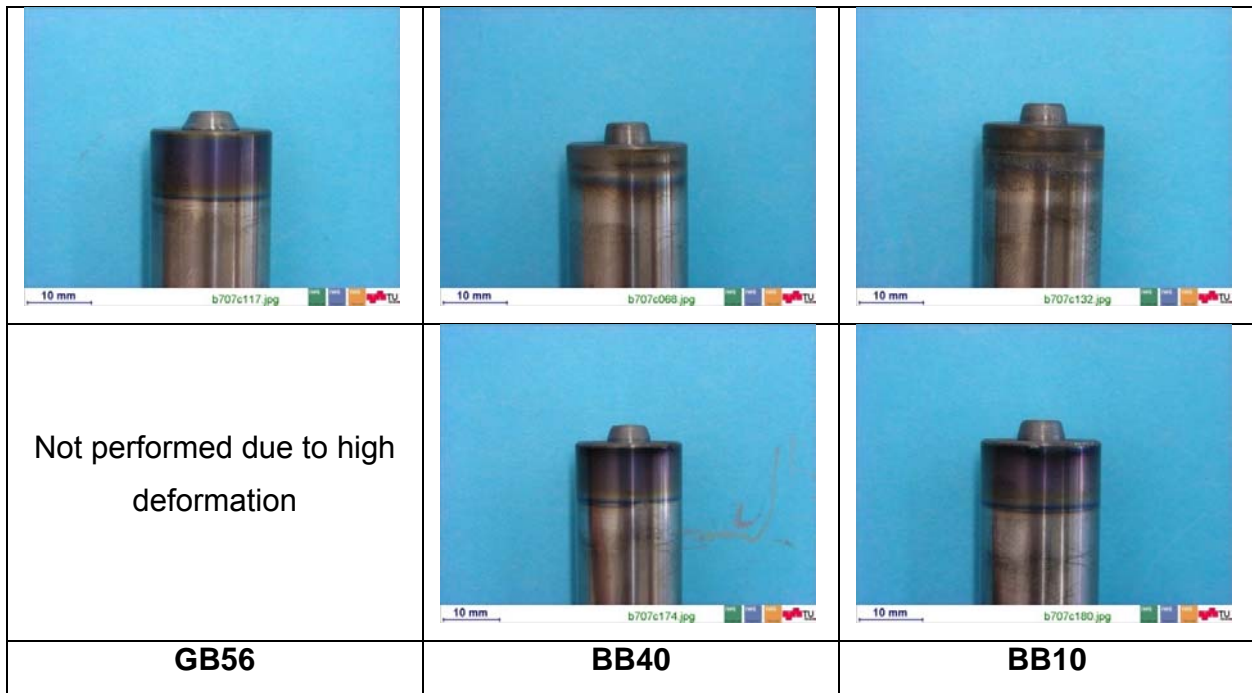
Fig. 4-31 Comparison of tool materials with different Co-Content Top) after 20mm long weld Bottom) after 150mm long weld

Due to the results of the investigation, following conclusion was made: Only substrates with **low to medium cobalt content** are applicable for friction stir welding tools.

4.8.1.3   Tool materials with TiC and Ta(Nb)C
The tool materials with the numbering SB contained 4 to 18 wt % TiC and 8 to 15 wt % Ta(Nb)C (Table 4-9). During welding, most of the tools failed due to shoulder and / or shaft fracture. An example of a tool after welding is shown in Fig. 4-32.

Fig. 4-32 Shaft and shoulder fracture of tool SB10

As discussed in chapter 4.3.2, the hardness of the substrate is increased at the expense of bending fracture strength when adding TiC. The fracture toughness of the carbide behaves in the same direction as the bending strength. The reduced fracture toughness of these substrates may cause the fracture of the tool shaft / shoulder during steel welding. Based on the results, it can be assumed that these tool materials are not suitable for friction stir welding of steel.

4.9   Optimization of Tool Substrate & Coating

From all substrates, BB10 with extra coarse grain size (9.5 µm) and low cobalt content (8 wt %) showed the best results during the first development series. Based on these results, further optimization of substrate was made (Table 4-11). Four additional substrates were defined and tested. The range of Co content was 4 wt% to 8 wt% and the grain size varied between 1.25 µm and 9.5 µm.

Table 4-11 Selected compositions of WC-Co powder mixtures for the optimization

Substrate	WC [wt. %]	Co [wt. %]	Grain size WC [µm]	Hardness [HV30]
BB10	92	8	9,5	1275
WS08C00	92	8	3	1350
BB01	94	6	5,3	1475
GB02	96	4	1,25	1750
GB10	93,5	6,5	2,5	1550

To compare the wear behavior of the different substrates, 150 mm and 400 mm long bead on plate welding was performed. The welding parameters were taken from the preselection. The tool probes after welding for the different substrates are shown in Fig. 4-33.

The tool BB01 with a cobalt content of 6 wt% and an average grain size of 5.3 µm showed the lowest wear and no deformation after 400 mm bead on plate welding. Therefore the tool BB01 was selected for further investigations.
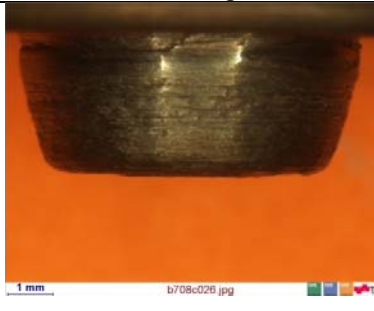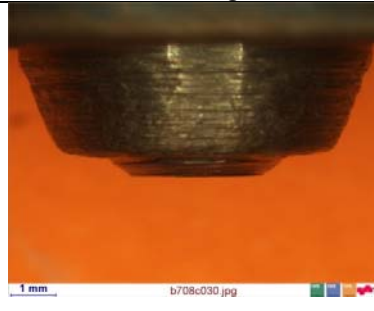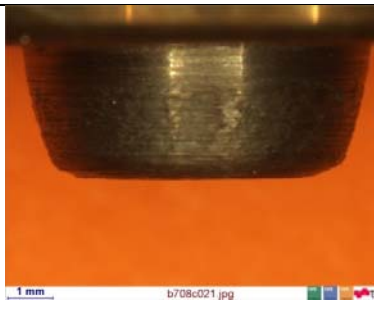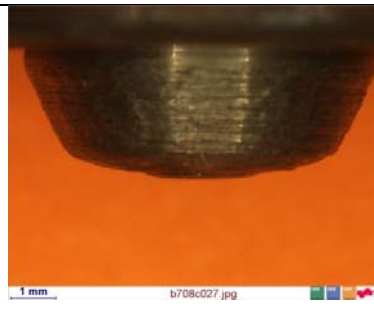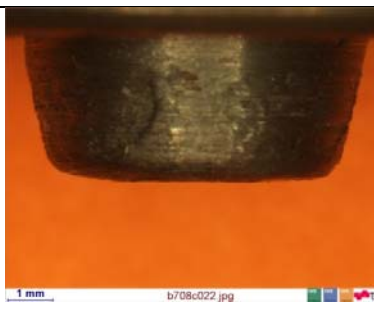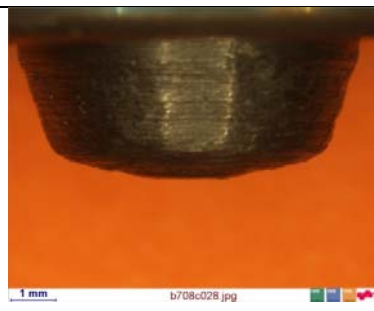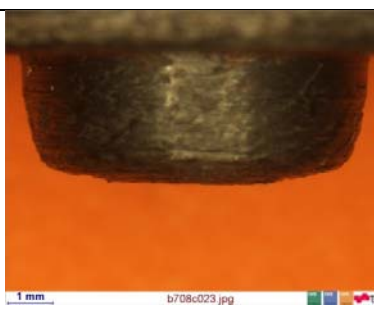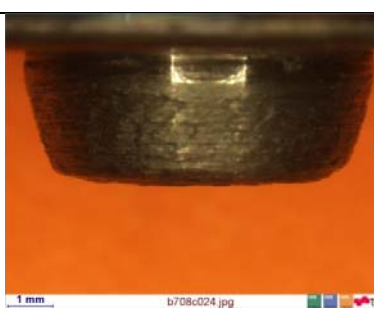
Substrate	150mm long weld	400mm long weld
BB10		
WS08C00		
BB01		
GB02		Fracture
GB10		Fracture

Fig. 4-33 Comparison of tool probe of different substrates after 150mm and 400mm long bead on plate welding

4.9.1 Microstructure

The microstructural characteristics of the specimens were examined using light optical microscopy. A representative top surface of a 400 mm long bead on plate weld is shown in Fig. 4-34. For the sample preparation, the same procedure as discussed in chapter 4.7.1 was used. The analysis using light optical microscopy showed a defect free stirring area with an asymmetric shape. The depth of the stir zone is 3.7 mm. In the stir zone of the joint, a light grey area is visible (Fig. 4-35). The grey area is attributed to the tool wear during welding. But no tool remnants were found during the metallographic analysis. It is supposed that a high density of coarse $M_{23}C_6$-type carbides was formed in the stir zone, which is attributed to the reaction between 304 stainless steel matrix and WC tool debris during FSW [95].

Fig. 4-34 Top surface of a 400 mm long bead on plate weld using BB01 tool

Fig. 4-35 Macrostructure of bead on plate welded steel using BB01 tool

4.9.2 Mechanical properties

Cross tensile specimens were extracted from the welded plate and the base metal. The top and bottom surface was milled before testing. The results showed no differences between welds which were made with W25Re and WC-Co tools. The location of fracture was again in the base metal. The hardness profile across the weld (Fig. 4-36) shows an overmatching of the weld relative to the base metal. A maximum hardness value in the weld area of 282 HV was found. The region of the highest hardness corresponds with the light grey area in the macrograph. The hardness peak in the stir zone is attributed to presence of $M_{23}C_6$-type carbides, which was discussed in the previous chapter.
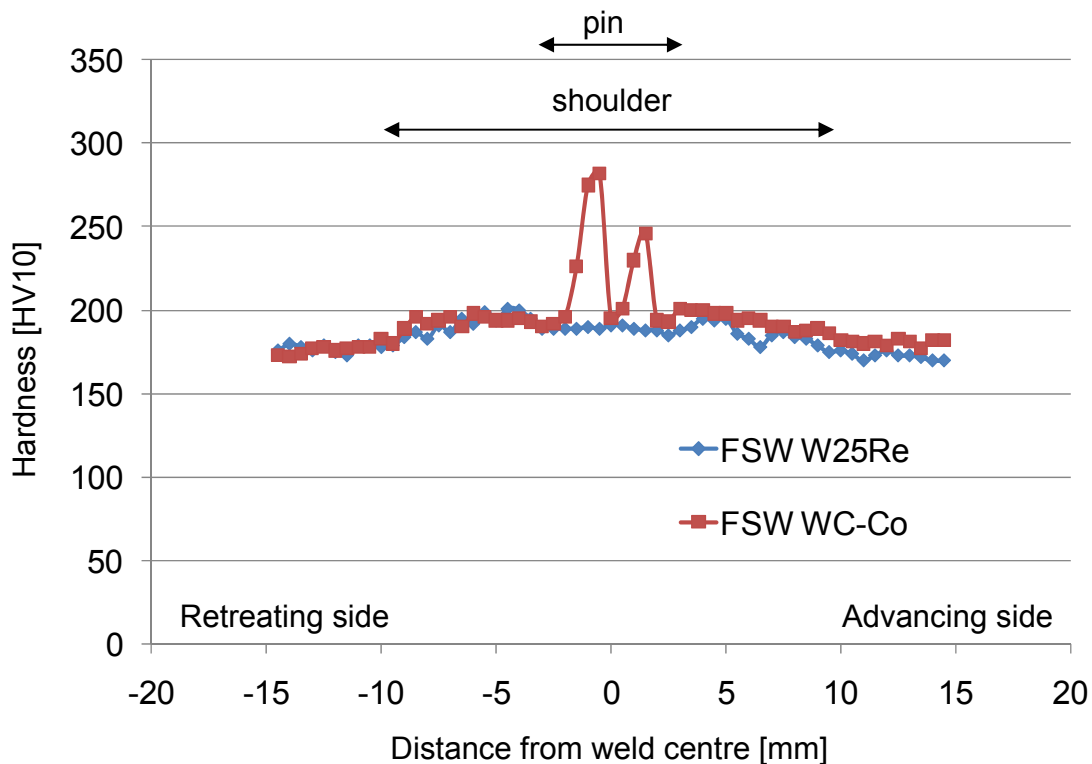
Fig. 4-36 Comparison of the hardness profile for cross section of bead on plate welded steel DIN 1.4301

4.9.3 Tool coating

Coating means the application of a thin layer with special properties (e.g. thermal barrier) onto a surface of a sintered hardmetal with the aim of further improving wear resistance. In metal-cutting applications hard coatings for tools have provided benefits in tool life and productivity.

Chemical vapour deposition (CVD) and physical vapour deposition (PVD) techniques have evolved from single layer to multilayer versions. These coatings protect the tool from high thermal exposure and abrasive wear.

To study the influence of coating for FSW tools, different coatings on the tool substrate were applied. The selection of coatings was performed together with a company partner considering the given requirements. In order to derive the heat from the tool shaft, the coating was applied on the shoulder and the pin only (Fig. 4-37). Since masking is not possible with CVD coatings, only PVD coatings were used.

Fig. 4-37 PVD coating on probe and shoulder for a WC-Co tool

For the coating of the tools, nine different types of coatings which are described in Table 4-12 were selected. Preferably coatings with one layer of AlCrN or TiAlN are used. Some of the coatings were single layer types (e.g. type 1 and 9), but also multi layer types (e.g. type 4) were considered. To ensure the required wear and heat resistance, the thickness of a single layer was in the range of 0.5 µm to 8 µm. The maximum thickness of the multilayer coating was 19 µm (Table 4-12).

Table 4-12 Composition of selected PVD coatings

Coating	Composition and single layer thickness [µm]	Coating Thickness [µm]
1	AlTiSiN	3.0
2	TiCN (7.5 µm) TiN (0.5 µm)	8.0
3	TiN/AlCrN (3.0 µm)	3.0
4	TiAlN (2.0 µm) TiN/TiAlN (3.0 µm)	5.0
5	Al2O3 (0.5 µm) TiN (0.5 µm) TiCN (1.5 µm) Al2O3 (4.0 µm) TiCN (7.0 µm) TiCN (2.0 µm) TiN (0.5 µm)	16.0
6	Al2O3 (7.0 µm) TiCN (8.0 µm) TiCN (3.0 µm) TiN (1.0 µm)	19.0
7	AlCrN (2.0 µm) TiAlN (2.0 µm) TiN/TiAlN (3.0 µm)	7.0
8	AlCrN (2.0 µm) TiCN (7.5 µm) TiN (0.5 µm)	10.0
9	AlTiN (6.0 µm)	6.0

The BB10 tools with the nine different coatings were then used for 150 mm and 300 mm long bead on plate welding. After welding, the tools were evaluated in terms of:

- Tool failure

- Tool wear

- Visible oxide films or annealing color on the tool

- Material pick up

Each tool was documented before and after welding using the Nikon Coolpix S10VR camera.

It was found, that the probe wear of the PVD coated tools was systematically lower than that of the uncoated ones (Fig. 4-38). But the results showed a complete removal of the PVD coating from the probe tip after 300 mm bead on plate welding.
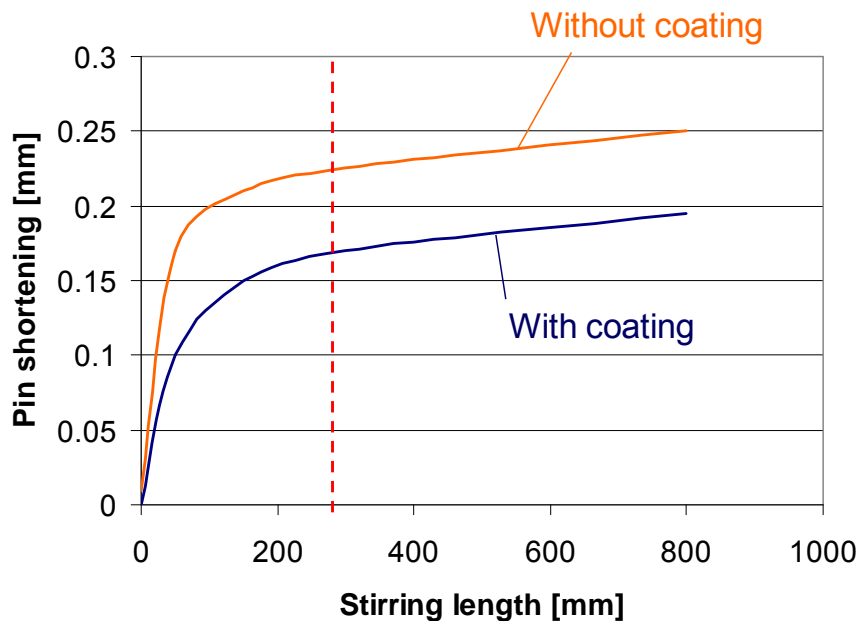
Fig. 4-38 Comparison of pin shortening for coated and uncoated BB10 tools

The comparison after welding showed that coatings with minimum one layer of AlTiN, AlCrN or doped variants, e.g. AlTiSiN, are best suitable for the given application. The comparison of probe wear after 150 mm long bead on plate welding is shown in Fig. 4-39. The tool with the coating No. 7 showed the lowest wear after 150 mm and 300 mm long bead on plate welding.
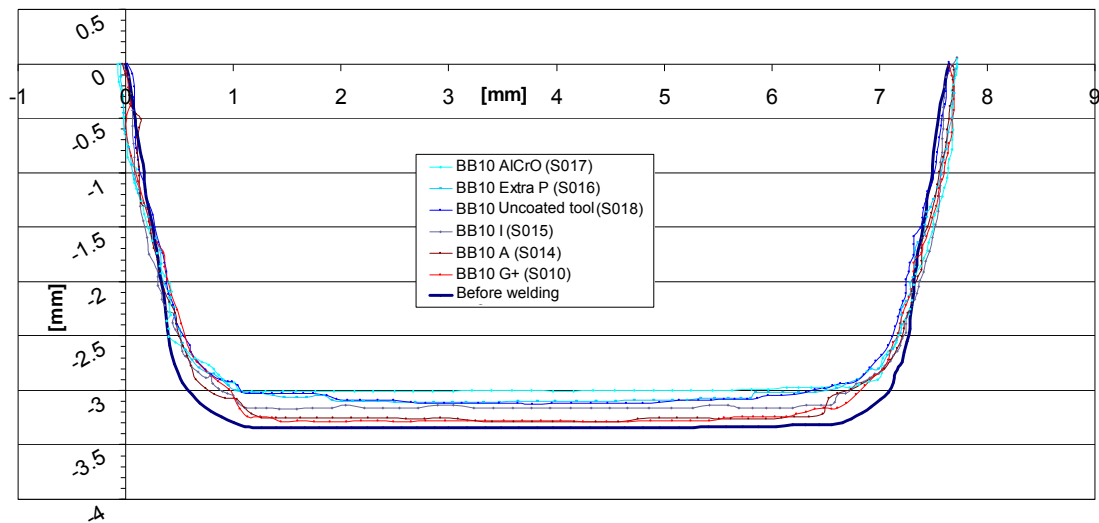
Fig. 4-39 Profile of different coated pins after 300 mm long bead on plate welding

During welding without shielding, a chemical reaction at the shoulder edge was observed for uncoated tools and designated parameters (Fig. 4-40). During welding with coated tools no chemical reaction was observed. This is maybe due to a better chemical stability of the coating.
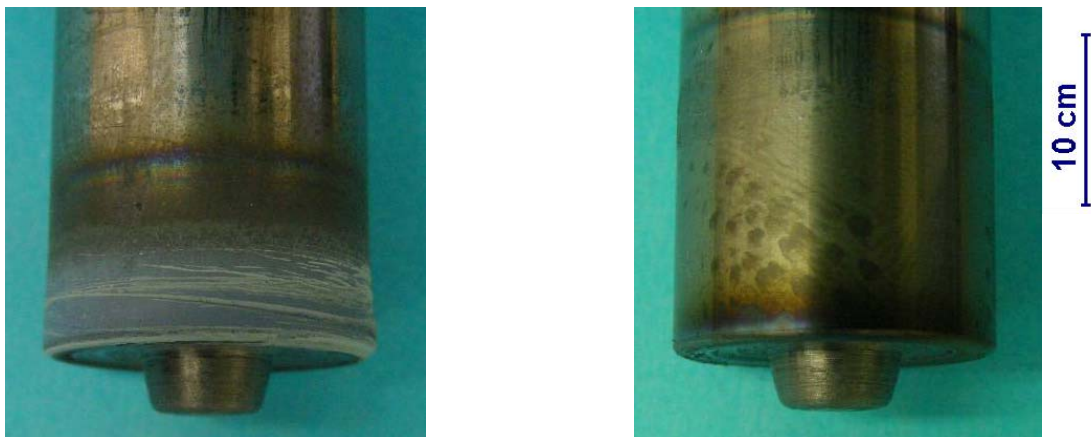
Fig. 4-40 Chemical reaction at the uncoated tool shoulder (left) and no reactions at coated shoulder (right)

Coating of tools may lead to improved service life and less reaction with the ambient medium. The application of coatings may also help reducing the wear during

plunging. But the coating will wear off during welding and contaminate the joint. Further investigations should be made to analyse the consequences of such a contamination.

4.9.4 Tool geometry

Colgrove and Shercliff have analysed the influence of pin geometry on forces and torque for FSW of aluminium alloys [96]. They reported a decrease of traversing force for a three flat pin. The three flat pin tool geometry used in this study is shown in Fig. 4-41. The substrate BB10 was used together with the coating No. 7 (Table 4-12).
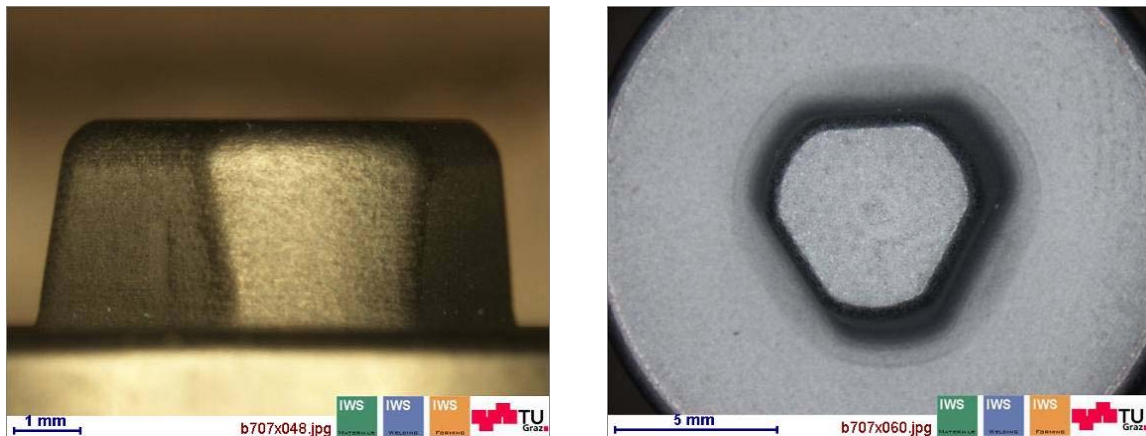
Fig. 4-41 Geometry of three flat probe

The results for bead on plate welding with this tool showed a reduction of forces in welding direction by 40% compared to a cylindrical pin (Fig. 4-42). The torque did not change significantly. Material pick-up at the probe was observed after 300 mm long bead on plate welding.
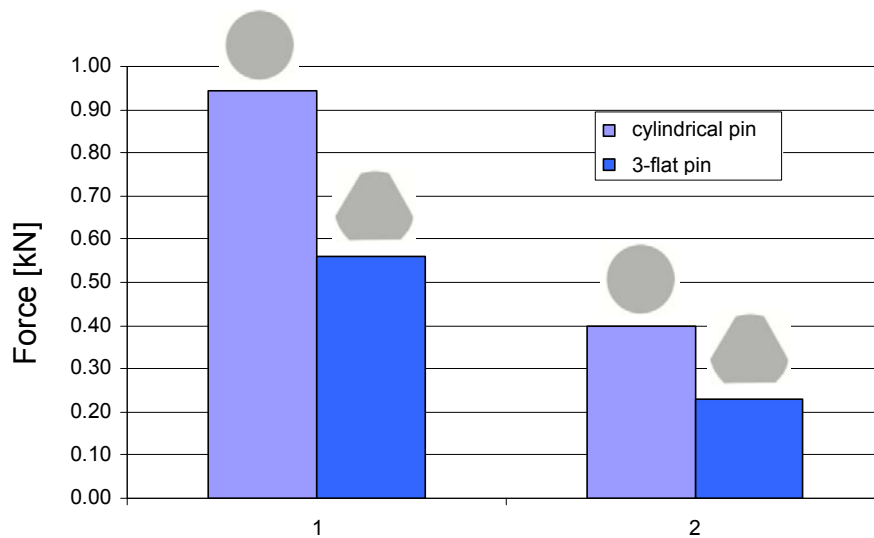
Fig. 4-42 Tool forces in (1) and across (2) welding direction

It can be seen, that a change of the geometry of the probe reduces the forces significantly. Therefore further investigations including CFD modelling should be made in future to improve / optimize the shoulder and probe design.

4.10   Material flow

The material flow in the weld is characteristic for the friction stir welding process. The properties of a weld are derived from it. Its complexity makes it a subject of many experimental studies and simulations, as shown in chapter 3.4.

One common type of examination is the marker method which was also used in this work. Therefore a metal marker which has similar mechanical and physical properties, but different density than the base material is inserted. This marker is placed prior to welding as wire, foil or particles, and stirred by FSW. During the process, the marker material deforms and flows as if it is part of the workpiece material itself; however, the presence of a foreign material could result in an inexpedient effect on the properties that control the flow, e.g. the contact condition and flow properties of the base

material [97]. A subsequent 3D computer tomography analysis highlights the distribution of markers and makes the flow behavior of the material visible. Additional metallographic analysis provides information about the resulting microstructure and size of the different zones (e.g. stir zone, thermo-mechanically affected zone, …).

The aim of the investigations in this work was the analysis of the material flow for the developed WC-Co tool. Since the tool has no extra features (like threads on the probe), the resulting material flow is of particular interest. Most of the material flow studies in literature were performed with a threaded probe design, but only little information is available for simple cylindrical or tapered design.

In recent studies, the position of the marker material was selected in the stir zone, especially in the area where the probe passes the material. In this study, the position of the marker material was in both in the TMAZ and SZ, inside and outside of the probe volume, see Figure 4-43.
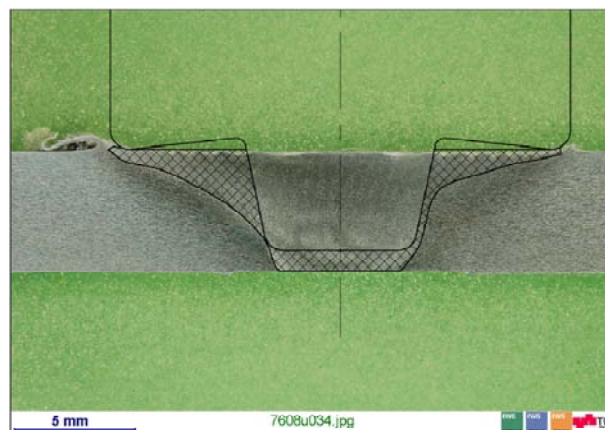
Fig. 4-43: Stirzone and volume of the tool probe

4.10.1 Experimental

In this work, bead on plate welding was performed for 5 mm thick plates of aluminium alloy EN AW 7085-T76. High strength aluminium alloy was used instead of steel in order to analyse the samples with computer tomography. The density of steel is too high for the used 3D-CT and therefore no analysis of steel samples was possible. The size of the plate was 100 mm x 400 mm. The alloy is a further development of the commonly used alloy EN AW 7075. To improve the quench sensitivity for greater plate

thicknesses, the elements Cr and Mn were reduced and Zr was added in the alloys 7050 and 7010. Further optimization of Mg and Zn led to the alloy 7085, which has a comparable toughness, good resistance to stress corrosion cracking and an improved ultimate tensile strength (~15% higher) compared to the 7050 alloy [98]. The nominal chemical composition of EN AW7085 and comparable 7075 is given in Table 4-12.

Table 4-13 Chemical composition (wt%), EN AW7075 [99], EN AW7085 [100]

Material	Si	Fe	Cu	Mn	Mg	Cr	Zn	Ti	Zr	Other
7075	0.4	0.5	1.2-2.0	0.3	2.1-2.9	0.18-0.28	5.1-6.1	0.2		rest
7085	0.06	0.08	1.3-2	0.04	1.2-1.8	0.04	7-8	0.06	0.08-0.15	rest

A WC-Co tool BB10 with a shoulder diameter of 19 mm, a concavity of 6° and a tapered probe with 3.1 mm length was used. The geometry of the tool is shown in Fig. 4-15. The parameters were defined after some preliminary test welds. The selected spindle speed is 400 rpm and the welding speed is 400 mm/min. The tool was tilted 3° in welding direction.

As marker material, a copper wire with a diameter of 1.0 mm was used. Holes at different positions were drilled into the material, into which the copper wire was inserted, see Figure 4-44 a). An example of the position of the marker P002A presented before welding is shown in Figure 4-44 b).
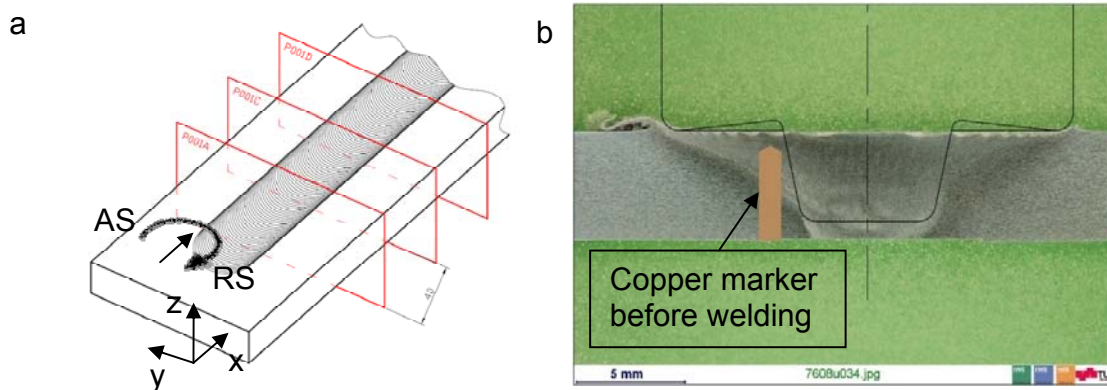
Fig. 4-44 a) Schematic view of the copper markers positions in the aluminium plate
b) Cross section with copper marker P002_A before welding

To analyze the material flow of the tool shoulder, four copper markers with a depth of 1.5 mm from the top surface and a distance of 8.5 mm and 6.5 mm from the weld center on both advancing and retreating side were defined (see Fig. 4-45).
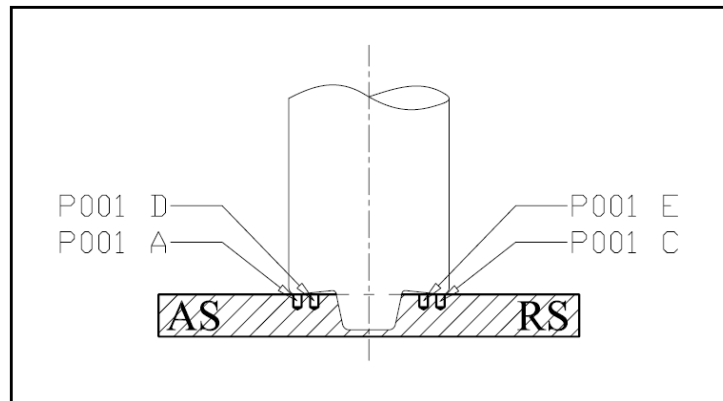
Fig. 4-45 Copper marker at the shoulder area

The area of the probe was also analyzed using four copper markers. They were placed at a depth of 4 mm and 2 mm from the bottom surface at a distance of 4.5 mm and 4 mm on both sides of the weld center (see Fig. 4-46).
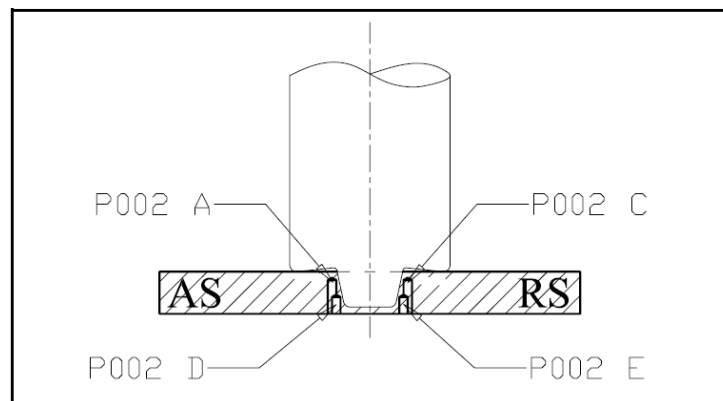
Fig. 4-46 Copper marker around the probe

Another four markers were placed below the pin, two with 1.5 mm depth and 2 mm from the bottom surface beyond the weld center (P001G and P001F) and two on the weld center 1.5 mm (P002F) and 2.5 mm deep (P002G) from the bottom surface (see Fig. 4-47).
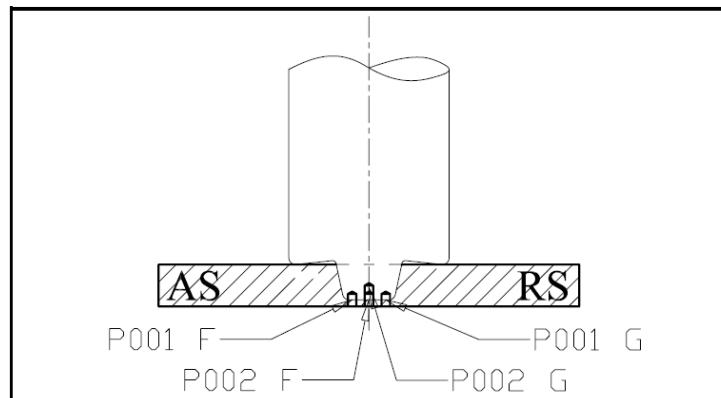
Fig. 4-47 Marker below the probe

The interest of this study is the resulting material flow and characterization of the zones for defined process parameters and the developed tool geometry. Therefore the tool moved through the whole plate and stirred all marker materials. After bead on plate welding, samples with a size of 30 x 20 x 5 mm were extracted (see Fig. 4-48) from the fully welded region. The samples were then investigated using 3D CT and metallographic analysis.
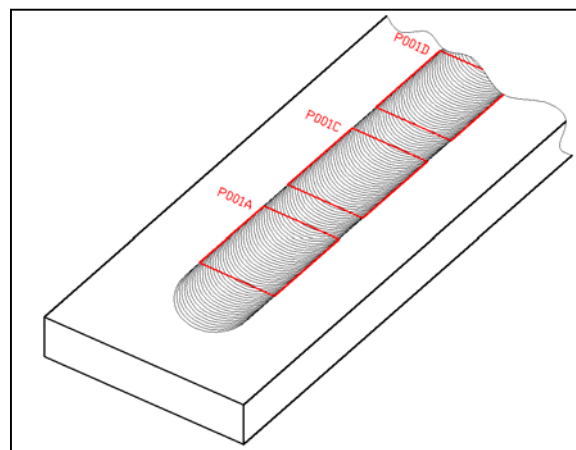
Fig. 4-48 Schematic view of the sample and extracted specimens

Table 4-14 summarizes the position of the marker material and the analysis method for the performed experiments.

Table 4-14 Overview of markers and performed investigations

Marker	Position	Length [mm]	3D CT	Metallography
P001 A	Tool shoulder, top surface	1.5	x	
P001 C	Tool shoulder, top surface	1.5	x	
P001 D	Tool shoulder, top surface	1.5	x	
P001 E	Tool shoulder, top surface	1.5	x	
P001 F	Probe tip, bottom surface	1.5	x	
P001 G	Probe tip, bottom surface	1.5	x	
P002 A	Probe, bottom surface	4.0	x	x
P002 C	Probe, bottom surface	4.0	x	x
P002 D	Probe, bottom surface	2.0	x	
P002 E	Probe, bottom surface	2.0	x	
P002 F	Probe, bottom surface	1.5	x	
P002 G	Probe, bottom surface	2.5	x	x

4.10.2 Computer tomography

Computer tomography is a non destructive testing method which can provide volume information of a test specimen. During a computed tomography examination, the specimen is irradiated from a cone beam X-ray source while gradually rotated. An array detector with a scintillator captures the weakened X-ray beam as a two-dimensional picture. With the also collected probe angle information, a computer cluster generates from all two dimensional pictures a three-dimensional computer image, see Fig. 4-49. 3D gray-scale data consisting of voxels (= volume pixels) is generated and its resolution is proportional to the edge of the sample [101].

Since this measurement system is based on the weakening of the X-ray, the contrast is dependent from the density difference and the resolution is dependent by radiography and the performance of the radiation source.
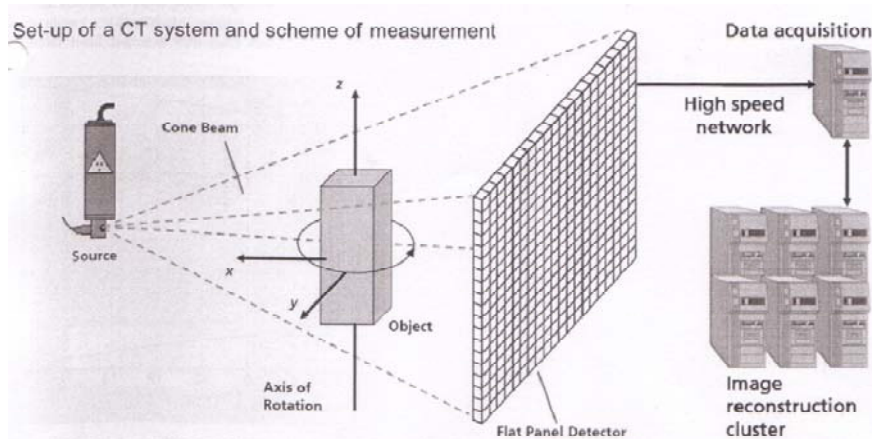
Fig. 4-49 Set-up of a CT system and measurement [101]

For the investigations in this work, the industrial 3D cone-beam computed tomography HWM RayScan 250XE, Hans Wälischmiller GmbH at the Upper Austria University of Applied Sciences Research & Development GmbH Wels was used.

4.10.3 Results and discussion

4.10.3.1 Shoulder area

The copper markers in the outer area below the shoulder show a stretched deformation in the direction of the shoulder rotation. On the advancing side the marker material is bent in feed direction and on the retreating side against the feed direction, see examples P001E in Fig. 4-50 a). The markers did not move in the area of displacement zone of the probe and have retained much of its metallic continuity.
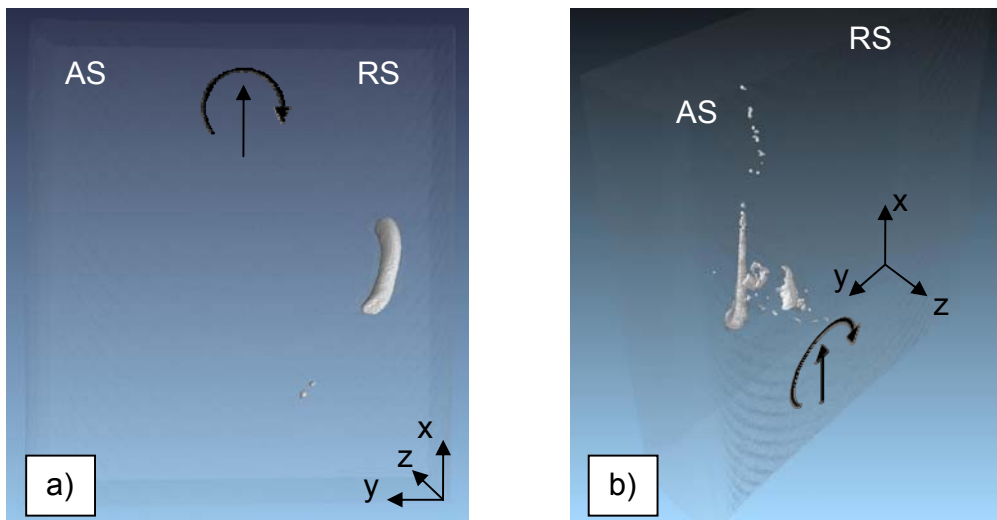
Fig. 4-50 3D CT image of copper marker P001E a) and P001D b) after welding

The marker P001D, see Figure 4-50 b), at the advancing side near the probe was split into smaller fragments. The major resulting part was bent in the direction of rotation and did not move in the middle of the stir zone. The remaining marker material was deposited in larger and smaller parts just below the shoulder a little closer to the midline. There was only little vertical movement of the resulting marker material. Therefore it is supposed that for the given tool geometry, the shoulder influences the upper region of the weld, but no downward material transport takes place.

4.10.3.2 Around Probe

The markers in the area around the probe behave very similar. The markers on the advancing and on the retreating side did not move in the displacement zone of the probe. They have been deformed in accordance with the direction of rotation and have maintained their bulk metallic continuity; only very few particles have been resolved. Fig. 4-51 a) and 4-52 a) show 3-dimensional images from the CT analysis, the macrographs Fig. 4-51 b) and 4-52 b) show the location of the copper markers together with the microstructure in the different regions.

In both cases, the copper markers are located in the thermo-mechanically affected zone and not in the displacement zone of the pin. It can be clearly seen that the originally vertically positioned marker is significantly stretched in the TMAZ. In the same way, the grain structure of the base material is deformed in this area of the weld. The

marker on the advancing side had a lens shaped section whereas the marker on the retreating side was more circular.
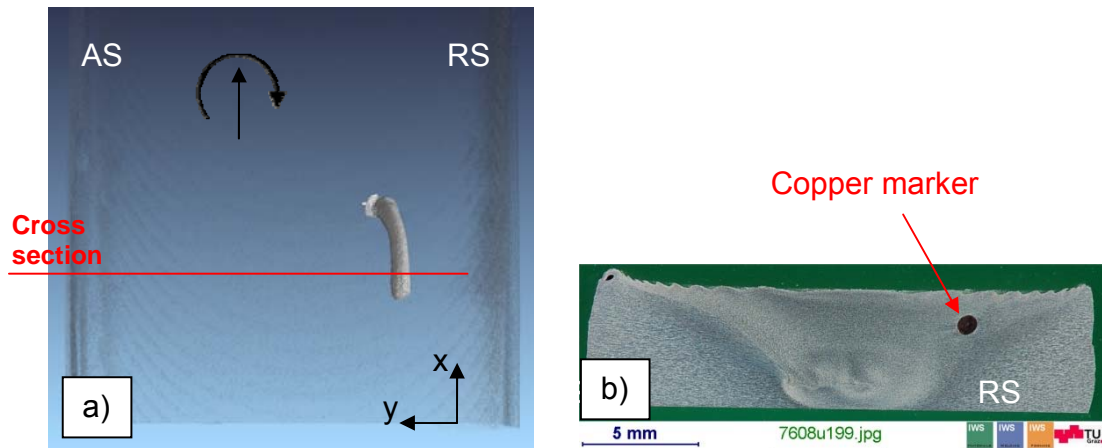
Fig. 4-51 3D CT image of copper marker P002C after welding a) and macrograph of cross section showing marker P002C b)
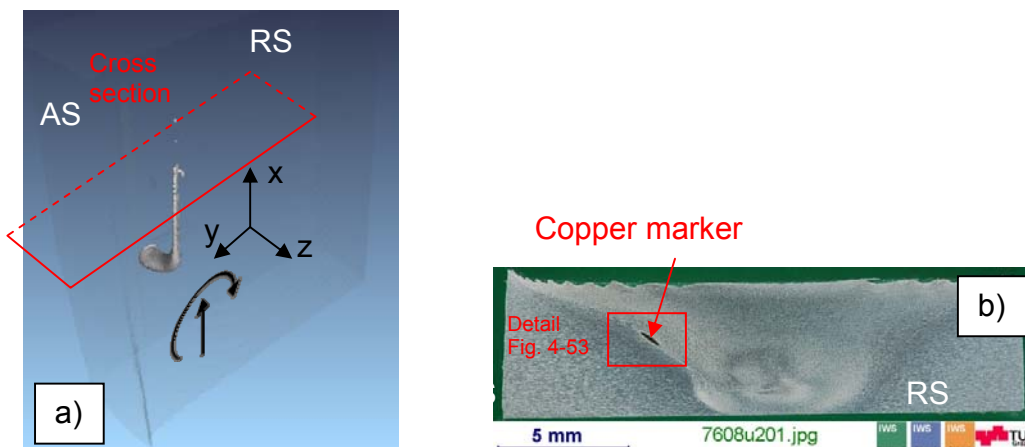
Fig. 4-52 3D CT image of copper marker P002A after welding a) and macrograph of cross section showing marker P002A b)

Fig. 4-53 Detail from Fig. 5-52: Copper marker at TMAZ, P002A

4.10.3.3 Probetip

The copper markers which were located at the probe tip have been partially positioned in the displacement area of the probe. The markers P001F on the advancing side and P001G at the retreating side show significant differences.

Probetip – Retreating Side

The marker P001G at the retreating side and P002F at the center line were stretched towards the top plate without losing their metallic continuity, see Fig. 4-54 a) and b). Before welding the length of the marker P001G was 1.5 mm, after welding it had a length of about 3.5 mm and went up to 2.9 mm across the middle of the plate thickness, see Fig. 4-55. Therefore it is assumed that an upward material flow took place and stretched the marker material. It should be noted that this flow was generated without special features e.g. threats on the probe.
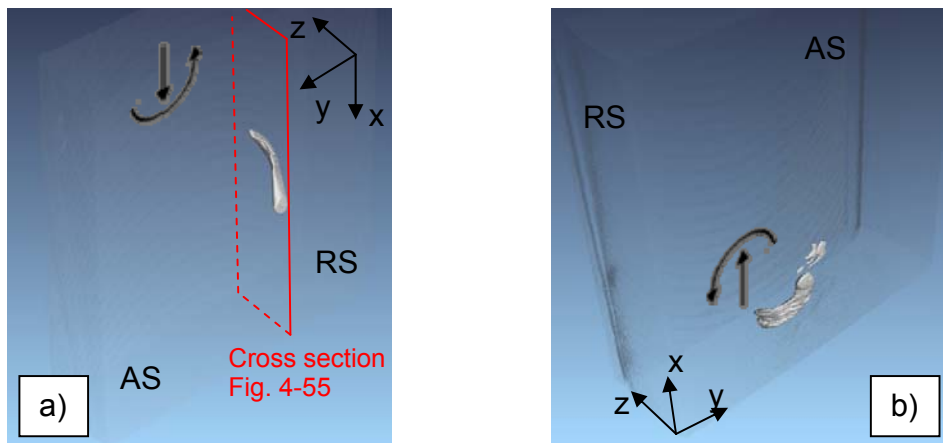
Fig. 4-54 3D CT image of copper marker P001G a) and P001F after welding b)
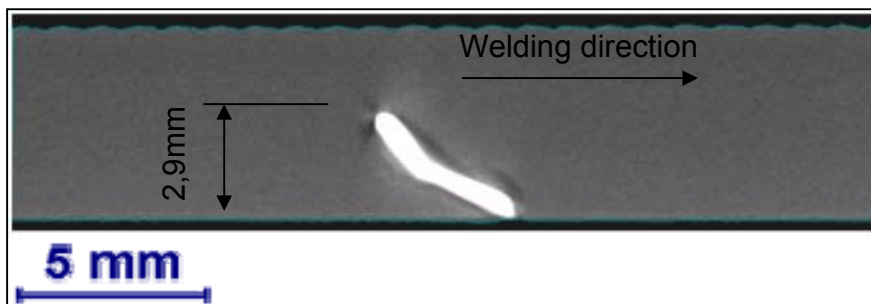
Fig. 4-55 2D CT image of copper marker P001G

Probetip - Advancing Side

The markers P001F at the advancing side and P002G at the center line in the plane between the bottom side of the probe and base material were stirred into small particles. These particles are distributed in a circular arc shape in the stir zone. Fig. 4-56 a) and b) show two-dimensional CT images in the top view.
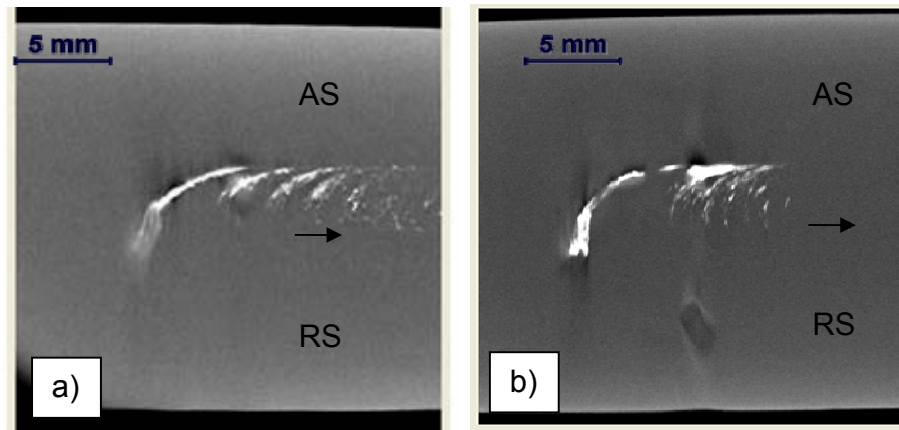
Fig. 4-56 2D CT image of copper marker P001F a) and P002G b)

Since the probe has no features (e.g. threads), this periodic deposition of marker material indicates a change in the contact condition i.e. sliding, sticking or partial sliding/sticking. This phenomenon is described as a dynamic balance between the hardening and the heat softening of the matrix, which in turn could lead to a collapse of the shear layer, in which case the rotation layer is deposited [97].

It can be clearly seen that the marker will lose its metallic continuity and spread far beyond the original position (Fig. 4-57). Furthermore, the marker material below the probe remains in this level without any vertical movement. These results are in agreement with the flow model of Arbegast, who defines the zone at the probe tip as vortex swirl zone [102].
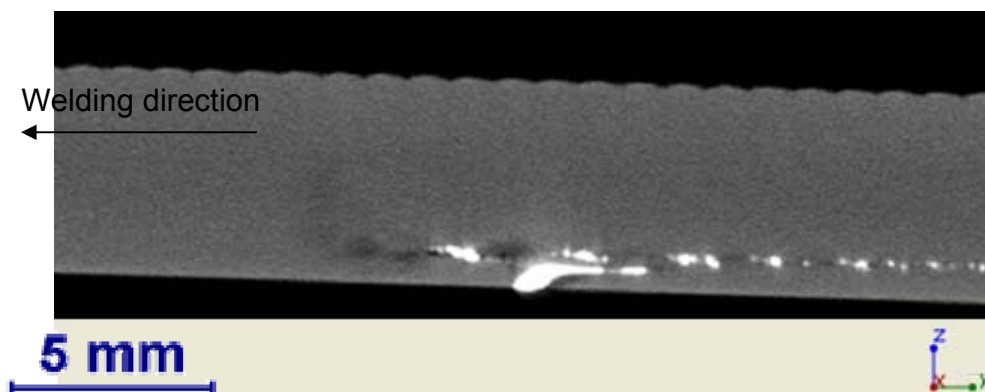
Fig. 4-57 2D CT image of copper marker P001F

Pintip - center

Apart of the marker P002G is pulled up along the retreating side of the probe and transported back towards the advancing side. A spiral distribution of the marker material was observed, as shown in Fig. 4-58.

Onion ring structures in the stirring zone are shown by the copper markers in Fig. 4-58 without a defined onion ring structure in the macrograph. These results suggest that the visible onion ring structure is a cross section of spiral structures.
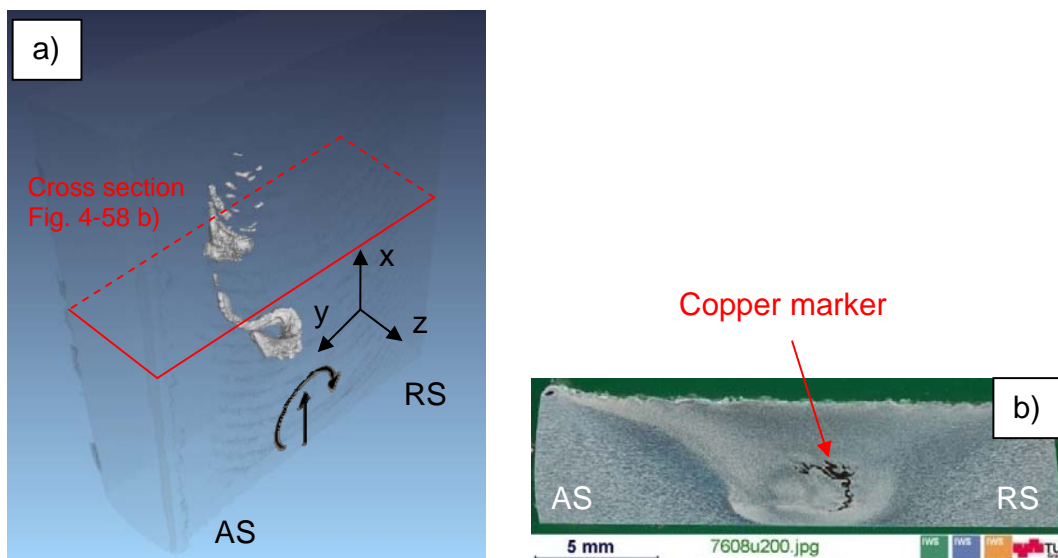
Fig. 4-58 3D CT image of copper marker P002G after welding a) and macrograph of cross section showing marker P002G b)

4.11   Tool Life

4.11.1 Linear welds

The tool life is an important factor when welding steel or other high strength alloys. To analyse the tool life of the developed WC-Co tool, different tests were conducted. First 800 mm long bead on plate welding was performed. The tool life of the coated BB01 tool was compared with a W25Re tool. Fig. 4-59 shows the pin shortening for both tools. It can be seen, that the shortening was less for the W25Re tool.
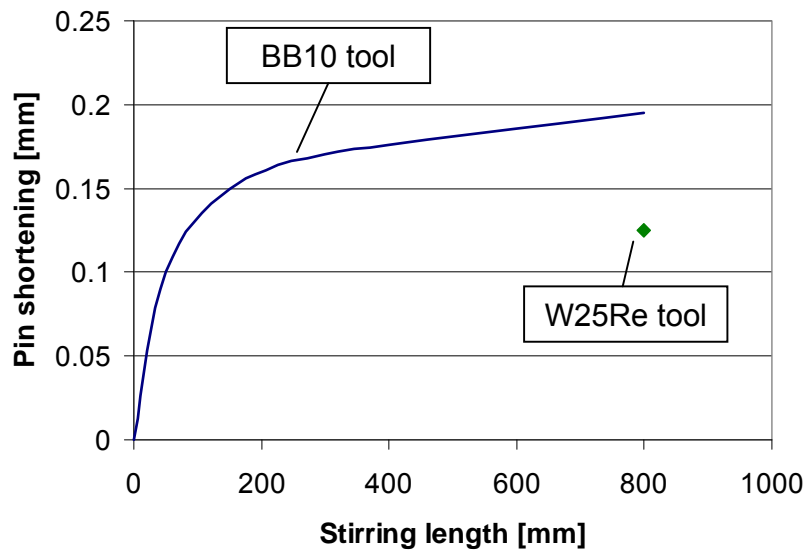
Fig. 4-59 Comparison of pin shortening for a W25Re and BB10 WC-Co tool

The goal of the second experiment was to evaluate the tool life of the BB01 tool for different plate thicknesses. The life of the tool during friction stir welding of steel DIN 1.4301 is shown in Table 4-15.

Table 4-15 Tool life during friction stir welding for BB01 tool material, welded material DIN 1.4301 and different sheet thicknesses

Plate thickness [mm]	Pin length [mm]	Plunges [number of]	Tool life [m]
1	0.8	25	10*
2	1.6	15	7.5
4	3.2	8	2.9

* Test stopped after 10m, end of tool life not reached

4.11.2 Tool life spot welds

The final tool concept for friction stir spot welding is shown in Fig. 4-60. A tool holder from a molybdenum alloy with a special geometry is used (see Appendix A). The

WC-Co tool insert with a length of about 25 mm is fixed in the tool holder. Only the WC-Co insert has to be changed at the end of the tool life.
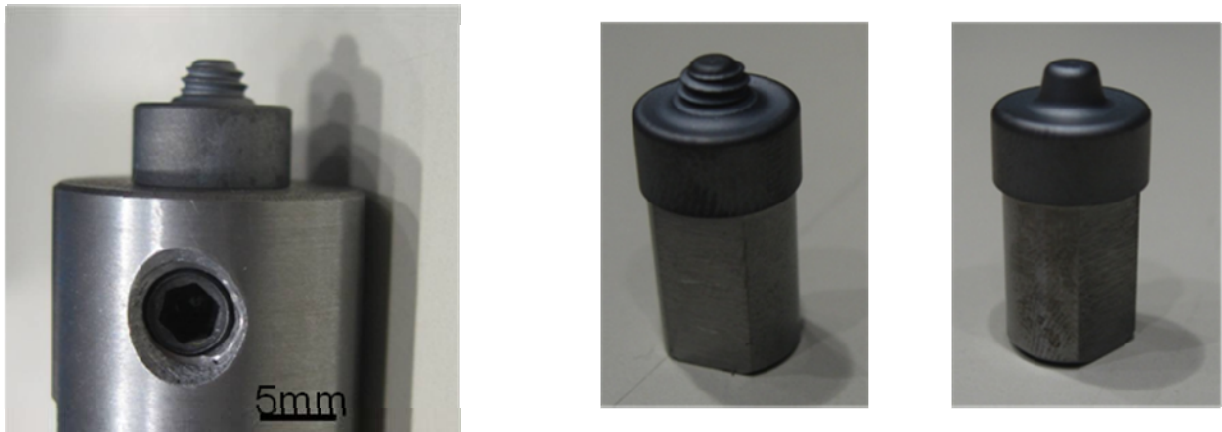
Fig. 4-60 Tool concept for FSSW of steel; tool holder with WC-Co insert (left); WC-Co inserts with different geometries (middle and right)

A representative appearance of the top surface for friction stir spot welded TRIP steel HCT 690 T Z100 is shown in Fig. 4-61. The mechanical properties and chemical composition of HCT 690 T Z100 is given in Table 4-16 and 4-17.

Sheet thickness	Yield strength [MPa]		Ultimate tensile strength [MPa]
	Min	Max	Min
≤ 3.00	410	510	700

Table 4-16 Mechanical properties of HCT 690 T Z100 steel sheets

C max	Si max	Mn max	P max	S max	Al max	V max
0.32	2.20	2.50	0.12	0.01	2.00	0.20

Table 4-17 Nominal chemical composition of HCT 690 T Z100 [wt%]

The weld time for FSSW of steel sheets was reduced to < 5 sec. A typical macrograph is shown in Fig. 4-62. Only little wear and no change of the tensile shear strength was observed after one hundred of spot welds in HCT 690 T Z100 steel. When using a W25Re tool, the probe was worn off after 25 spot welds.

Fig. 4-61 Appearance of top surface for friction stir spot weld in TRIP steel HCT 690 T Z100

Fig. 4-62 Macrograph of friction stir spot weld in TRIP steel HCT 690 T Z100

To perform further studies in a production environment, application tests at different companies were carried out. Most of these companies had experience with friction stir (spot) welding using other tool materials like W25Re (Tungsten-rhenium).

One example was friction stir spot welding of aluminium-steel sheets for an automotive application at Renault. The results were compared with a standard W25Re tool. By the use of the developed WC-Co tool it was possible to increase the tool life from 450 spots (W25Re) to > 2000 spots (WC-Co) [103].

4.12 Theoretical Analysis & Discussion: Tool Wear and Failure Mechanism

In this chapter, the wear and failure mechanisms for tools, which were observed in the previous chapter, were evaluated and discussed. The tool life ends when so much wear or deformation occurred that the functionality is no longer guaranteed. Another life limiting factor is the fracture of the probe and/or shoulder (Fig. 4-63).
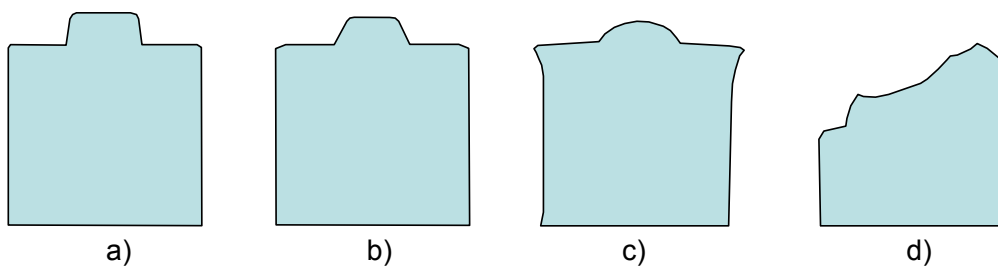
Fig. 4-63 Schematic illustration of tool wear and failure mechanism a) Original tool geometry b) Worn tool geometry c) Deformation of shoulder and pin d) Fracture

4.12.1 Wear

Wear may be defined as the surface damage or removal of material from one or both of the solid surfaces in a sliding, rolling or impact motion relative to one another. Like friction it is not an inherent material property rather it depends upon the system conditions during the operation or process. Wear rate may not essentially relate to the friction as well. Wear resistance of a material couple is generally classified in tribological studies as a non-dimensional parameter (i.e. wear volume per unit load per unit slide distance). It occurs by mechanical and/or chemical means and is generally affected by frictional heating.

For wear during friction stir welding of steel the main mechanisms taking place may be stated as a combination of two wear types – adhesive and abrasive.

For adhesive part of wear the adhesion between two matching surfaces takes place at the asperity contacts and when sliding or slip occurs these contacts are sheared. This may result in detachment of a fragment from one surface. As the sliding

continues, the fragment which now has been attached to the other surface may get detached and transferred back to the first one, or may form debris (Fig. 4-64).
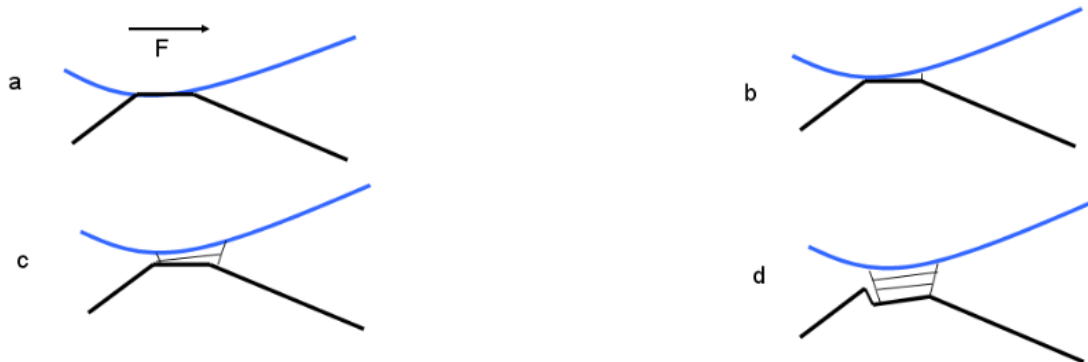
Fig. 4-64 Schematic of stepwise detachment of fragment from one of the mating surface to another through adhesion mechanism

However the work hardening and plastic deformation occurring near the interface tend to make the mechanism more towards the abrasive mechanism. In this mechanism, the asperities from one surface or hard particles slide on the other (relatively softer) surface and damage the interface by plastic deformation or fracture. There may occur two general cases – two body abrasion and three body abrasion (Fig. 4-65). In the first case, one of the surfaces usually the harder one, abrades the other (softer) one. In the second case a hard particle that is not part of any of the interacting surfaces, e.g. debris, usually caught between them, may act as abrasion agent to one or both the matching surfaces.
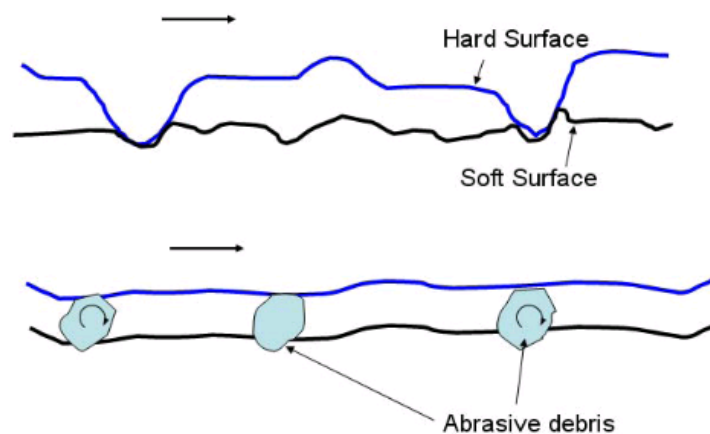
Fig. 4-65 Two-body (top) and three-body (bottom) abrasive wear mechanism

Higher hardness or strength levels of the work piece are obviously the reason for the increased wear of the tool during FSW of steels and other hard materials. Moreover the interfacial temperatures are also quite high which tends to facilitate the wear process, as mentioned earlier.

The tools which are formed by powder metallurgical methods have adverse effects on the strength of the tool due to softening at elevated temperature. This may result in generation of debris and third body abrasion will take place. Furthermore, strain hardening effects on the work piece may also play an important role during the initial plunge phase. The material flow during the plastic deformation of the work piece around the tool may increase the relative velocities at the interface hence the tool being prone to more wear, if the surface has been already damaged.

Other possible mechanisms may include fatigue effects at regions close to the shoulder; probe tip shows maximum deflections during transverse motion of the tool.

A typical appearance of a worn probe surface is shown in Fig. 4-66. The contact surface became severely worn after 800 mm long bead on plate welding. Due to the wear, a number of WC grain layers were removed and the surface results in a mix of cracked, deformed and partly removed WC grains.
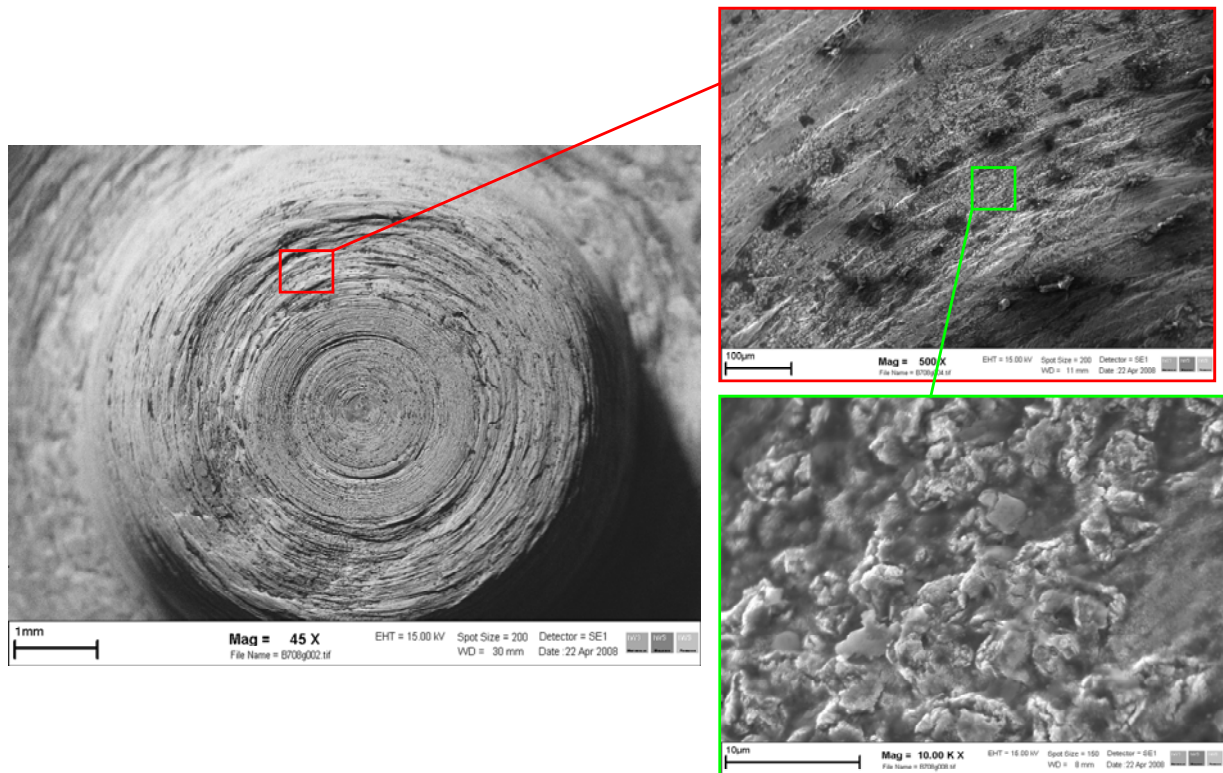
Fig. 4-66 Analysis of the worn WC-Co tool surface using scanning electron microscopy

It is assumed that at the beginning of the process, when the material is not soft enough, increased abrasive wear of the probe takes place. This assumption is assisted by the finding of higher percentage of tungsten remanents at the process start and cinch marks at the pin. During the steady state phase, adhesive and abrasive wear may take place. For the adhesive wear mechanism, thin steel surface layers on the tool shoulder were observed (Fig. 4-67). These layers would shift the contact to a similar steel/steel contact and reduces the wear of the shoulder surface. This may also reduces the shoulder wear during welding.
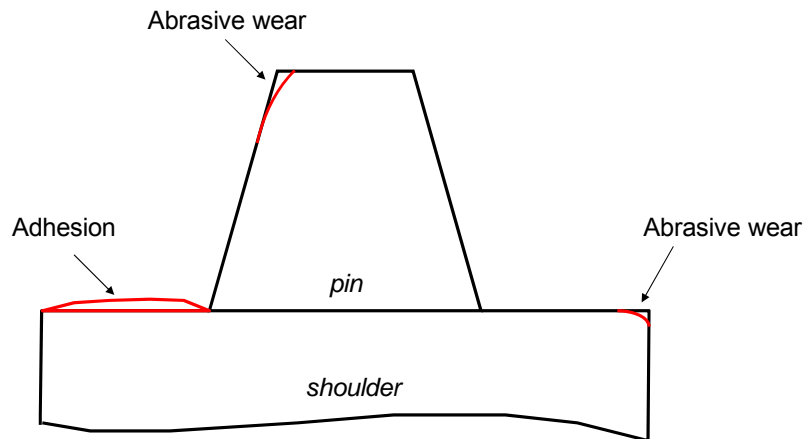
Fig. 4-67 Observed wear mechanism during friction stir welding of steel

When the temperature is too high, the binder may be weakened and a detachment of WC grains or composite scale fragments is taking place. Hence the tool wear is very high. This seems particularly critical for tools with $T_{max}/T_{service}$ around 1.

4.12.2 Deformation

The application of hardmetals as friction stir welding tools implies a high working temperature. Temperatures above 1000°C at the tool shoulder were measured by different researchers. As shown in Table 4-2, the coarse grained substrates show less deformation than fine grained substrates. Since the relationships which were discussed in chapter 4.3.2 cannot explain this behavior, it is essential to study the properties of tool materials at high temperature where plastic deformation appears. The stress-strain curves for a coarse grained and a fine grained alloy at different temperatures are shown in Fig. 4-68 [104]. It can be seen, that the relationships which were discussed in chapter 4.3.2 apply only to room temperature and can even reverse with increasing temperature.
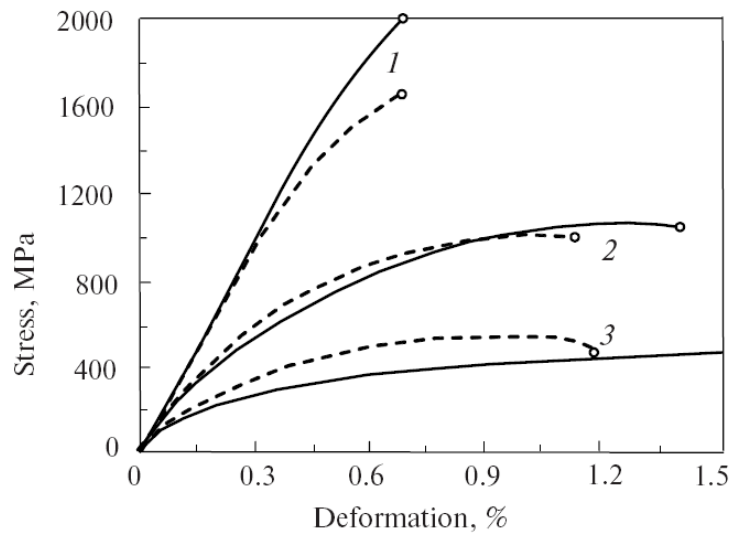
Fig. 4-68 Stress-strain curves for a coarse-grained (- - -) and a fine-grained (----) alloy of the WC-17Co type at T = 700°C (1), 800°C (2) and 1000°C (3) [104]

Ostberg et.al. [105] analyzed the mechanisms of plastic deformation of WC–Co and Ti(C, N)–WC–Co. He performed three-point bending measurements at different temperatures (Fig. 4-69). The WC–Co deforms mainly elastically at 750°C but at 800°C the first sign of plastic deformation can be seen. At 900°C the material shows a ductile behavior and above 1000°C it is highly plastic. Above 900°C, the complete WC–Co material becomes weaker than the WC skeleton, indicating that a certain amount of grain boundary sliding (GBS), accommodated by binder phase deformation, occurs. Around 1000°C, the WC–Co starts to exhibit a highly plastic behavior together with a significant deformation of the skeleton. This suggests that deformation by GBS is accommodated by the WC grain deformation [105].
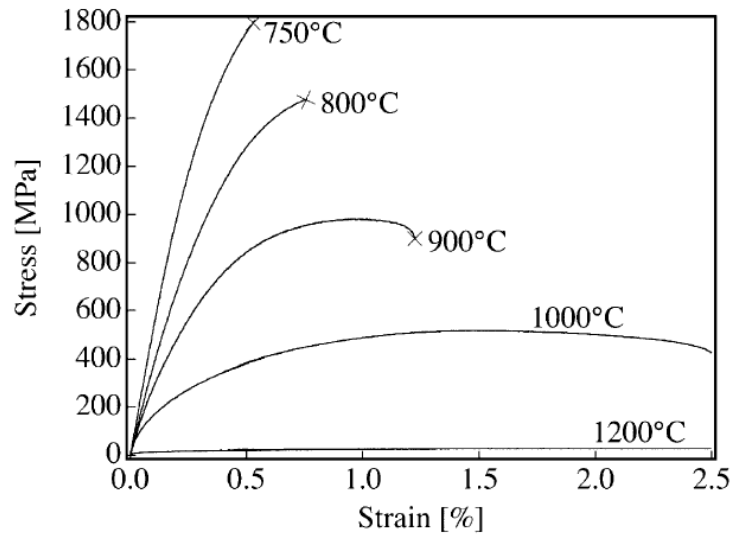
Fig. 4-69 Three-point bending measurements at different temperatures showing transition from brittle to ductile and to highly plastic behaviour for WC-Co [105]

Fig. 4-70 summarizes the main mechanism controlling the mechanical behavior of hardmetals as a function of temperature. Three temperature domains can be defined: I ± brittle; II ± bulk deformation controlled by (IIa) the binder or (IIb) the carbonitride phase; and III ± carbide grain boundary sliding. A high temperature domain (III) where the flow stress is inversely proportional to the carbide grain size starts at 827°C for WC-Co [106].
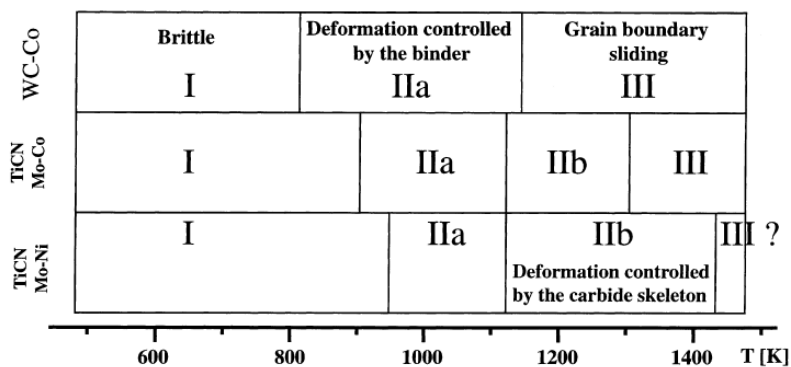
Fig. 4-70 Main mechanism controlling the mechanical behavior of hardmetals as a function of temperature [106]

A total conclusion of the authors about the effect of the studied factors on the high temperature bending strength of WC–Co hard metals is as follows: **The bending strength of hard metals increases with decrease in cobalt and carbon contents at any temperature in the range from room temperature to 1000°C**. The strength dependences on the sizes of carbide particles and grains of the γ-phase at low (below 600°C) and high temperatures are of the opposite nature. At low temperatures the alloy bending strength increases with decreasing carbide grain sizes, while at 1000°C coarse grained alloys are stronger. For both low and high carbon WC–10Co alloys, the highest strength under the above conditions is exhibited if carbide particle size ranges from 4.0 to 5.0 µm [107].

It can be seen, that GBS is the main factor influencing the deformation behavior at higher temperatures (>880°C) Fig. 4-70. Since GBS is reduced with larger grain size, the deformation at high temperatures is less for coarse grained alloys. This may explain why friction stir welding tools with coarse grained substrates have less deformation and wear than medium or fine grained alloys.

4.12.3 Fracture

Beside the tool fracture due to poor fracture toughness of the material, which was also discussed in chapter 4.2, further reasons for tool fracture are possible. First an overloading of the tool during the welding process may result in a fracture of the probe or shoulder. Therefore force control welding should be used to avoid overloading the tool.

Second, it is necessary to remove sources of stress concentration to protect the tool from fracture. For a better understanding of the stresses inside a tool during plunge phase and after shoulder touchdown, a 3D FEM based model, which was developed within our group, was used. To cope with high distortion of the mesh built-in ALE (Arbitrary Lagrangian Eulerian) and mesh remapping features were invoked. The calculated stresses in the tool for different plunge depths are shown in Fig. 4-71. A detailed description of the model is given in [108].
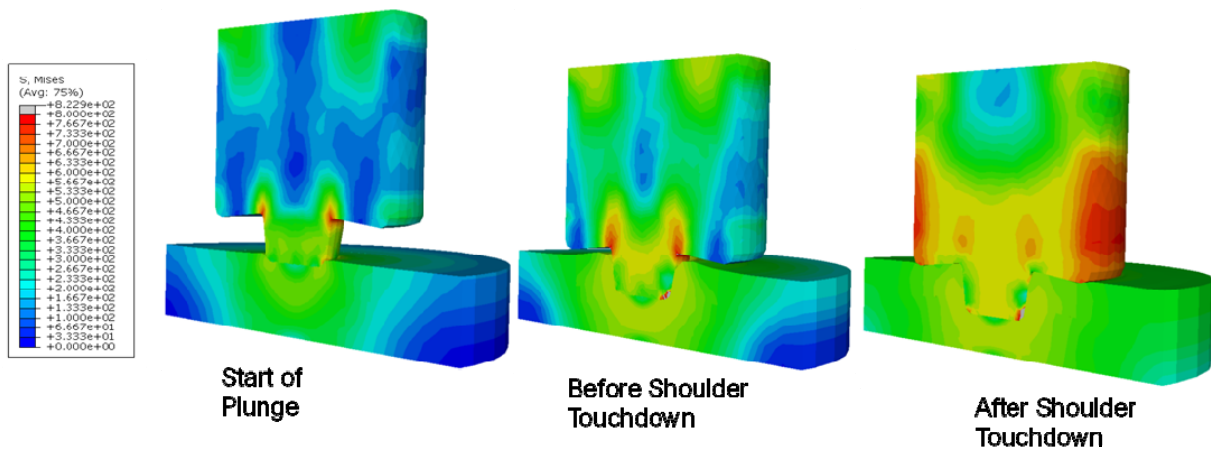
Fig. 4-71 Calculated stresses in the tool at different plunge depths, only mechanical results – thermal part not incorporated (Work-Piece: 304L, Tool: WC-Co, spindle speed: 1600 rev/min, plunge rate: 288 mm/min) [108]

It can be seen that at the beginning of the process (start of plunge) there is a stress concentration at the probe/shoulder section. The effective torque leads to a torsional stress which is highest at the outer pin area. Since the effective torque will rise during the plunge of the pin, the torsional stress will increase until shoulder touchdown. This is especially critical for small radii at the probe/shoulder section. During linear welding, an additional bending moment due to the force in welding direction will occur.

The growing of cracks inside the tool from the surface was observed in this region, see Fig. 4-72. When the cracks size becomes critical, it leads to fracture of the probe. The fracture of the tool probe was a typical failure during the tool life tests (Fig. 4-73).

Fig. 4-72 Cracks in the probe / shoulder radii of a WC-Co tool

Fig. 4-73 Pin fracture of a WC-Co tool after 50mm long bead on plate welding

Another possible reason of stress concentration is the wear or deformation which can lead to a new geometry.

When the outer part of the concave shoulder touches the surface, high stresses appear in the tool shoulder. This can lead to deformation or fracture of the shoulder (Fig. 4-74). Radial cracks in the tool shoulder were observed for high plunge rates. Further analysis of stresses and improvements of the tool geometry are not covered within this work but planned for the future.
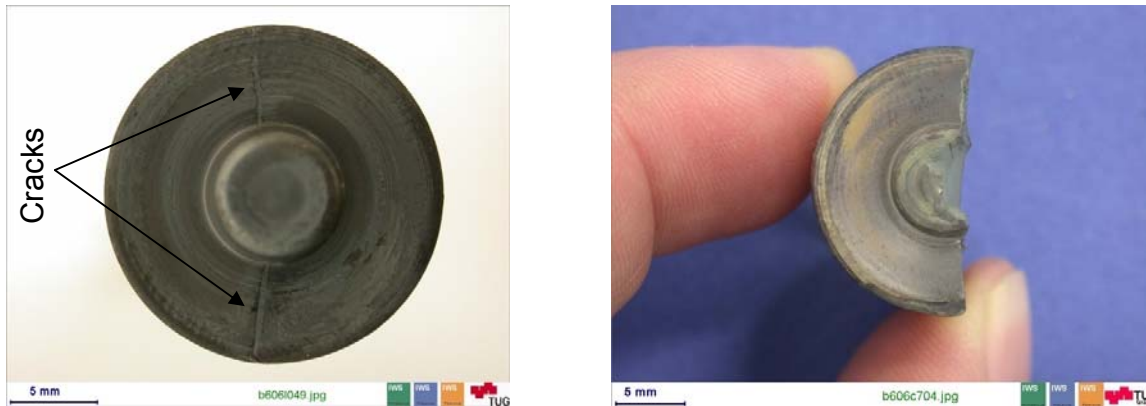
Fig. 4-74 Radial cracks in the tool shoulder after touchdown (left), tool fracture after touchdown of the shoulder (right)

4.12.4 Discussion comparison WC-Co - WRe tools

The performed work showed that both tool materials have their strength and weaknesses. The W25Re tool material has a sufficient high temperature strength and excellent fracture toughness, but shows severe wear during welding. Since the hardness at room temperature is relatively low compared to other tool materials, it rapidly wears during the plunge phase or friction stir spot welding. As further criteria, the price is quite high and therefore the industrial application is limited.

The developed WC-Co tool has a high hardness and compressive strength at room temperature. The observed wear during plunge phase and friction stir spot welding is quite low. At elevated temperatures the tools show severe wear. Due to the relationships discussed in this chapter, it is recommended to keep the process temperature below 1000°C. The best tool performance was observed when welding thin (up to 2 mm) steel sheets with low strength. For such steel sheets, the process

temperatures can be much lower than for high strength steels, where a sufficient softening is necessary.

The properties of both tool materials are summarized in Table 4-18.

Table 4-18 Comparison of properties at room and elevated temperature for W25Re and WC-Co

Property	W25Re		WC-Co	
	Room temperature	Elevated temperature	Room temperature	Elevated temperature
Hardness	+	+	+++	+
Compressive strength	+	++	+++	++
Fracture toughness	++	+++	+	+
Material availability	+		+++	
Tool flexibility	++		-	
Tool durability	+		+	
Material costs	--		+++	

4.13   Preheating

The performed work showed that the highest axial forces occur during the plunge phase. The high forces require a massive and stiff equipment, especially when welding steel. The wear of some tool materials (e.g. W25Re) is also quite high. To reduce / eliminate the problems, different methods of preheating were investigated in literature [8, 109]

In order to decrease the tool loads, tool wear and welding defects for high strength alloys, a new technique was developed [110].

The invention relates to a device (Fig. 4-75, 1) and a method for connecting at least two workpieces (7, 8) by friction welding. The device here comprises an axis (10) which can be driven in a rotating manner and on which a friction welding tool (1) is arranged, wherein the friction welding tool (1) has at least one pin-like tool (2), which can be driven in a rotating manner and is surrounded by at least one hollow cylinder (3), which can be driven in a rotating manner. The friction welding tool (1) can be moved along its axis of rotation (10) by the plastifying workpieces (7, 8), wherein the pin-like tool (2) and the hollow cylinder (3) can be moved independently of each other in the axial direction. The hollow cylinder (3) has on its side facing the at least one upper workpiece (7) a detachable friction liner (6) with a friction surface (5).

Fig. 4-75 Device for friction stir spot welding of two workpieces with a hollow cylinder having a detachable friction liner with a tool [110]

First tests showed that preheating of the workpiece up to 1000°C is possible with the device. The temperature can easily controlled by the axial force, spindle speed and size of the friction surface. The axial force during the plunge phase for a preheated workpiece (~ 800 °C) was reduced to a value of 9.8 KN (compared to 30 kN for a conventionally plunge). Since the available friction stir welding machine (description in

chaper 4.4.1) has no possibility to control the spindle speed of the wear surface and the tool independently, no further tests were performed. To further develop and study the procedure in detail, a prototype welding head is planned for the future.

5 Friction Stir Welding of 15-5PH Steel

The objective of this chapter is to provide details about the optimization of process parameters, the resulting microstructure, the influence of heat treatment on the mechanical properties and tool life during welding.

5.1   Studied Material

The precipitation hardening steel 15-5PH in solution annealed and hardened condition (Table 5-1) was selected for this study.

Table 5-1 Heat treatments and conditions of steel 15-5PH

Condition	*Heat treatment*
A	*(1) Solution annealing at 1040°C for 30min, air cooling below 30°C*
H	*(1) Solution annealing at 1040°C for 30min, air cooling below 30°C* *(2) Ageing at 540°C for 4h, air cooling*

The fabrication, range of chemical composition and properties of this steel are shown in chapter 3-6. The measured chemical composition and mechanical properties are given in Table 5-2. The thermal treatment was as follows. First a solution heat treatment at 1040°C for 30 minutes was performed, followed by air cooling (condition A) and tempering at 480°C for 1 hour (condition H). The M_S temperature for this steel is around 130°C and the M_F temperature is around 30°C. The microstructure of the base metal is martensitic with a small amount of retained austenite at room temperature.

Table 5-2 Measured chemical composition and mechanical properties of 15-5PH

Element	C	Si	P	S	Mn	Mo
wt %	0.028	0.62	0.02	0.001	0.73	0.22
Element	Al	Cr	Ni	Cu	Nb	Fe
wt %	0.39	15.38	5.08	3.27	0.28	balance

	Tensile strength [MPa]	Yield strength [MPa]	Elongation [%]
Condition A	1110	963	8
Condition H	1438	1385	9

Due to the fabrication process, the steel plates show inhomogeneities, which are represented in Fig. 5-1. The inhomogeneities have a higher chromium content of approximately 20 wt%. Further enrichment of Nb carbides is visible, these carbides are bigger than those which are found in the rest of the matrix (see Fig. 5-2). The two areas which are shown in Fig. 5-1 were analyzed using energy dispersive x-ray spectroscopy (EDXS) and the results are shown in Fig. 5-3 and Fig. 5-4.
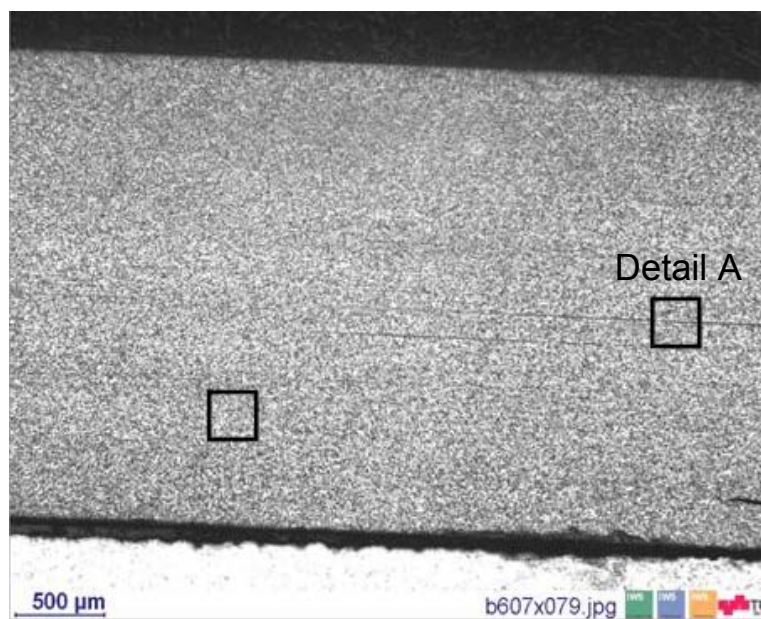
Fig. 5-1 15-5PH cross section showing base material with inhomogenities in the middle of the plate (Detail A)

Fig. 5-2 Detail A of Fig. 5-1 showing the inhomogenities
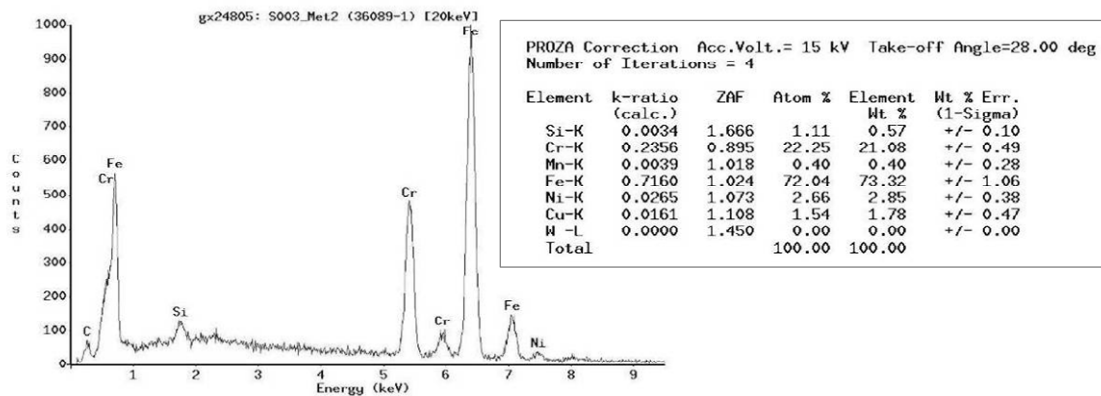
Fig. 5-3 Energy dispersive spectroscopy result for area 1 of Fig. 5-2
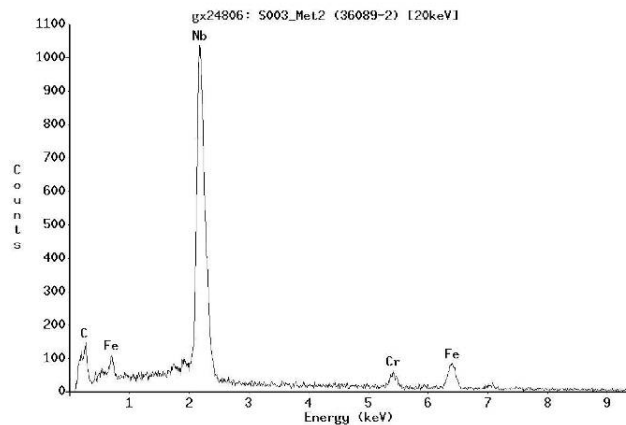
Fig. 5-4 Energy dispersive spectroscopy result for particle (area 2 of Fig. 5-2)

The dimensions of the plates were 2.6 mm thick, 500 mm long and 100 mm wide. The butt surface was milled before welding. After milling, the plates were cleaned and degreased.

5.2   Process Parameter Optimization

5.2.1 Experimental procedure

The butt welds for both condition A and H were conducted using a load controlled friction stir welding machine as described in chapter 4.4.1. Since the spindle and the bearings of the machine were exposed to high temperatures during welding, a water cooled welding head was used (Fig. 4-10). Argon shielding gas with a flow rate of 14 l/min was used during welding to protect tool and work piece from oxidation. The plates were clamped using the mechanical clamping device shown in Fig. 4-12. A typical weld setup with the argon shield and is shown in Fig. 5-5.
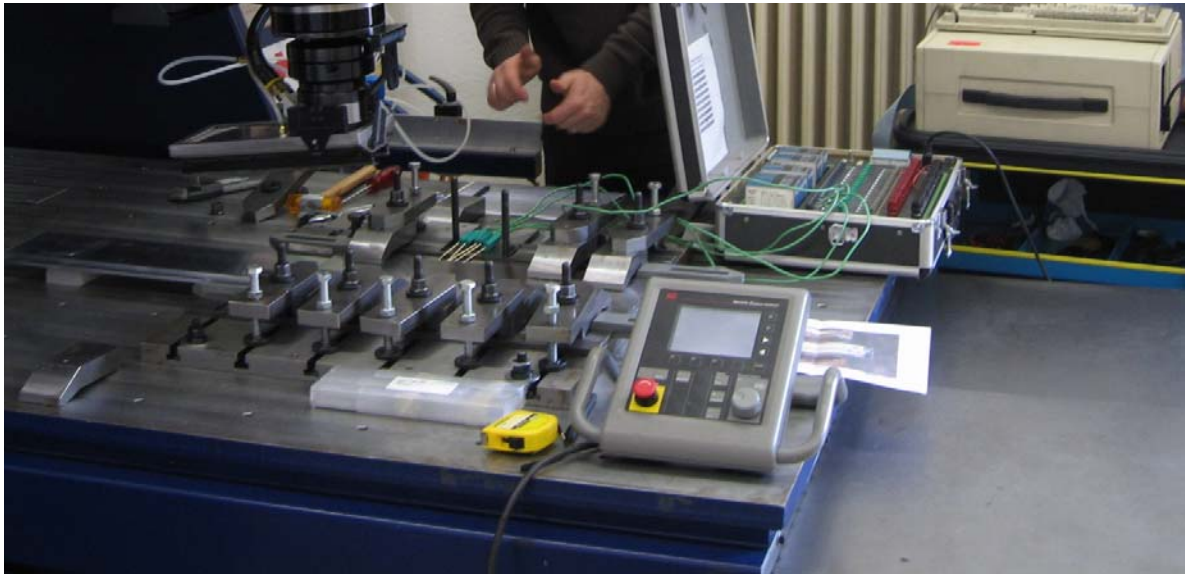
Fig. 5-5 Typical weld setup with argon shielding mounted on the weld head

In order to achieve sound welds with no defects, the welding parameters together with the tool geometry have to be optimized. The main process parameters are the spindle speed, the welding speed, the tilt angle and the axial force (load controlled welding process).

Since the tool for steel welding has no special features like threats, the main parameters are the shoulder diameter, the probe diameter and length. Two different tool materials were used for this study. One tool was made from W25Re, the other tool was WC based (BB10, see Table 4-11).

The first design which was used in this study was as follows: the tool had a concave shoulder, 16 mm shoulder diameter, 6 mm probe diameter and 2.3 mm probe length (Fig. 5-6). For the first trials, a steel backing plate was used.
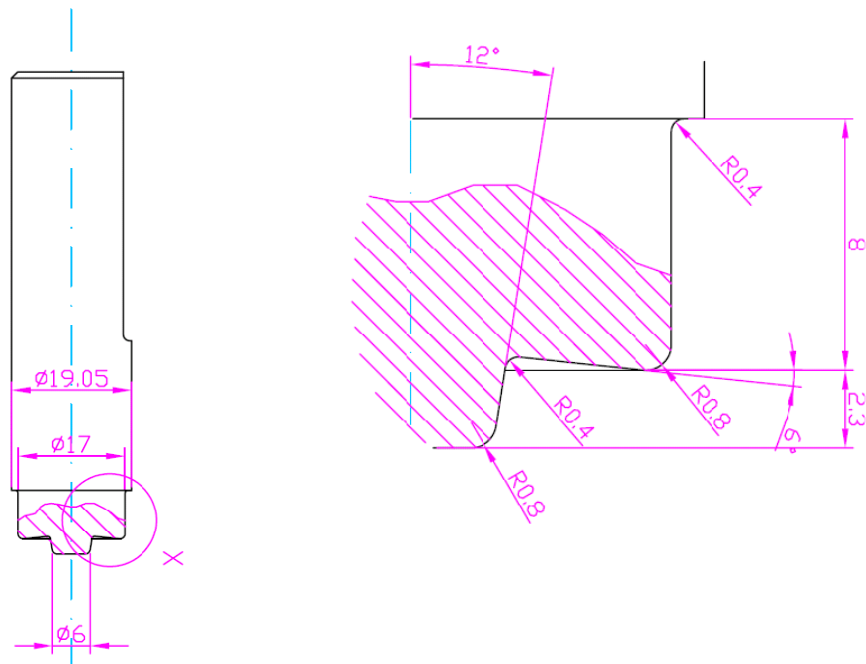
Fig. 5-6 Tool geometry for the first development study

Different combinations of welding parameters were selected for the first trials (Table 5-3). The first tests with the defined tool geometry were unsuccessful because the probe was penetrating into the backing plate. As it is shown in Fig. 5-7 and 5-8, the 15-5PH steel plates were lap welded onto the backing plate. When reducing the forge force, the plunge depth was still too high and when the force was too low, pores appeared on the advancing side of the weld.

Table 5-3 Welding parameters for the first development study using a W25Re tool

Weld No	Plunge phase		Welding phase		
	Spindle speed [rpm]	Plunge rate[mm/min]	Spindle speed [rpm]	Welding speed [mm/min]	Axial Force [kN]
1				80	19
2				80	16
3			500	90	16
4				100	16
5				120	16
6				80	14
7	800	6	450	80	16
8				80	17
9				80	14
10				80	12
11			550	100	14
12				120	15
13				120	16
14				150	16
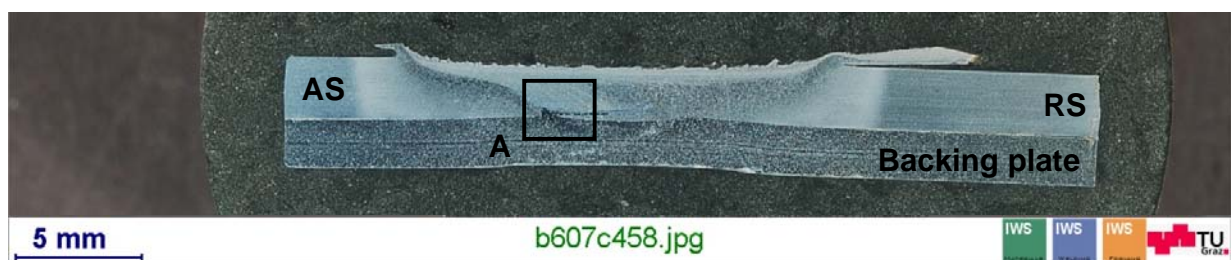
Fig. 5-7 Macrograph for unsuccessful 15-5PH butt friction stir weld

Fig. 5-8 Detail A of Fig. 5-7 showing backing plate penetration

5.3   Further Parameter Optimization

As a result of the first trials, the probe length was reduced to 2.1 mm. The other tool parameters were kept constant. For further parameter optimization, the tilt angle was kept constant at 3°. The tool rotation speed ranged from 300 rpm to 450 rpm and the welding speed ranged from 60 mm/min to 350 mm/min. A summary of the used process parameters is given in Table 5-4. All welds were made in force control mode. To avoid sticking of the material, a coated (Al_2O_3 + Ti_2O_3) steel backing plate was used. A complete welding process is shown in Figure 5-9;

i.   in the first stage of the process, the tool plunges into the cold material with a defined spindle speed of 800 rpm, a plunge rate of 6mm/min and a maximum downward force of 35 kN (machine limit). After the shoulder touchdown, a dwell time of 2 sec is defined to heat up the material at the start.

ii.   The spindle speed is reduced and the tool starts to move along the joint line with a defined axial force, welding speed and acceleration. After the defined welding length the tools stops

iii. The tool is retracted from the material and the tool rotation is stopped, the shielding remains on the plate and argon gas flows through it for further 20 sec

iv. The weld head together with the shielding is removed from the weld area

Table 5-4 Summary of process parameters which resulted in a defect free weld

Weld Nr.	Spindle speed [rpm]	Weld speed [mm/min]	Tilt angle [°]	Tool material
S001		60	3°	WRe
S002		100	3°	WRe
S003	300	150	3°	WRe
S004		200	3°	WRe
S005		100	1°	WRe
S006		80	3°	WRe
S007		100	3°	WRe
S008	450	150	3°	WRe
S009		350	3°	WRe
S010		100	3°	WC
S011		350	3°	WC
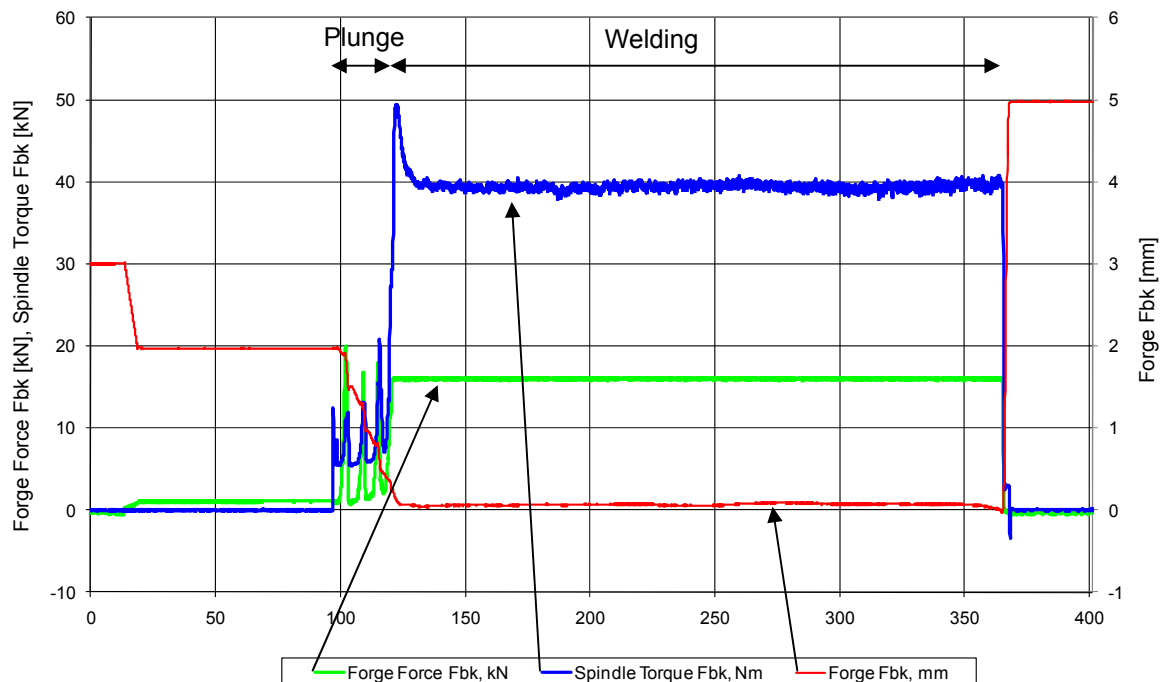
Fig. 5-9 Process parameter plot for a complete weld in force control mode

It can be seen from Fig. 5-9 that the plunge rate of the tool was not constant. With a constant plunge rate, the machine stopped due to exceeding the machine limits (axial force > 35 kN). To avoid this problem, the rotating tool was pushed into the material with a plunge rate of 6 mm/min until the axial force rose above 20 kN. Then the plunge rate of the tool was reduced for a short time. This procedure was repeated until the shoulder was touching the top surface of the plates.

5.4   Optimized Friction Stir Welds

By performing numerous experiments, the welding parameters for the butt weld of 15-5PH steel were optimized. The optimized parameters by which a defect free weld was obtained are shown in Table 5-5. The development was done using both tool materials. It was observed, that the BB10 tool needs a higher spindle speed than the W25Re tool. The parameter window for W25Re was relatively large, whereas only one parameter set gave satisfactory results when using the BB10 tool.

Table 5-5 Summary of process parameters with which a defect free weld was obtained

Weld Nr.	Spindle speed [rpm]	Weld speed [mm/min]	Tilt angle [°]	Tool material
S001	300	60	3°	WRe
S002	300	100	3°	WRe
S003	300	150	3°	WRe
S006	450	80	3°	WRe
S007	450	100	3°	WRe
S008	450	150	3°	WRe
S010	450	100	3°	WC

A representative weld appearance for a defined parameter set is shown in Fig. 5-10. The bright areas with a distance of approximately 20 mm to the weld are attributed to the moving of the shielding gas device during welding. The load controlled welding process gave an equally weld appearance with only little flash. At the areas which remained blue after welding, the shielding did not fully cover the plates.

Fig. 5-10 Weld appearance of 15-5PH butt weld

The mechanical properties and resulting microstructure are discussed in the following chapter.

5.4.1 Weld shape and plate distortion

The welding with a 3° tilted tool resulted in a plate thinning (undercut) at the top of the weld. The measured value of 0.29 mm (Fig. 5-11) was not adequate for the planned application. In conformance with the specifications of company partner, the thinning in the weld center should not exceed 0.1 mm.
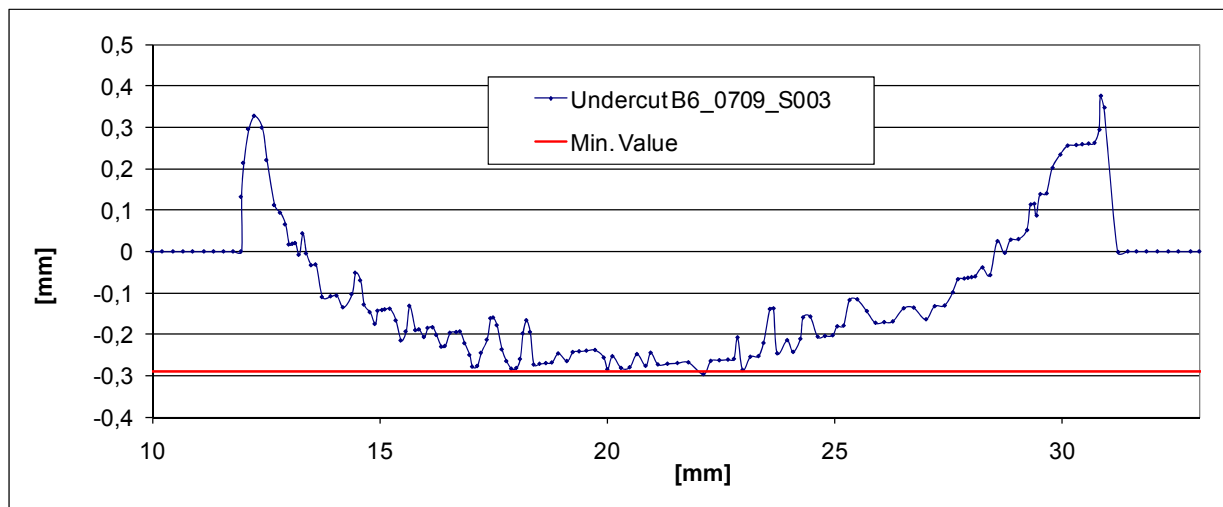
Fig. 5-11 Undercut for butt friction stir weld of steel 15-5PH with 3° tool tilt angle

To reduce the value of undercut, two methods are possible. First the shoulder diameter of the tool can be reduced, second the tilt angle of the tool can be reduced. Since the change of the tool geometry may also lead to a change in process parameters, the tilt angle was reduced in this work. Values of 0.5° and 1.0° were selected. With 0.5° tilt angle, no defect free weld was possible, but with 1°, a sound weld was generated (Fig. 5-12). The thinning for the 1° tilted tool is 0.09 mm which is an acceptable value.

Fig. 5-12 Macrograph of transverse section of butt friction stir weld of steel 15-5PH with 1° tool tilt angle

The angular distortion of the welded plate was 1.2° which is less than the 2.8° for conventionally fusion welded plates (experiments performed at the company partner).

5.4.2 Temperature measurements

Due to the friction stir welding process, the distinct zones of the weld will experience different temperature histories. The evolution of microstructure and mechanical properties depend on the distance of the considered zone with respect to the weld center. Temperature measurements in the heat affected zone (HAZ) are also essential to study the aging of the copper precipitates which will influence the softening of the material (chapter 3.6).

K type thermocouples were placed on the top surface of the plate, and on the bottom side of the plate. The thermocouples were fixed on the plates using a spot welding process. Fig. 5-13 shows a representative temperature distribution on the retreating side for thermocouples placed 10 mm, 12 mm and 14 mm away from the weld center line. The maximum temperatures in the stir zone are even higher. The 15-5PH steel has a low carbon content, and therefore the Ac_1 temperature is quite high. The strength of the steel is also high and it is known that stronger materials produce more heat during friction stir welding. Therefore it is expected, that the whole SZ becomes fully austenitic during welding. But temperature measurements in the stir zone are difficult because the material flow during welding will move and sometimes destroy the thermocouples. To get as close as possible to the temperatures in the stir zone, an additional thermocouple was placed on the bottom side of the plate at the tool axis. The backing place was prepared using drilling and milling processes to move out the thermocouple.

The measured temperatures on the top plate rise with increasing heat input, the highest maximum temperatures were found for 450 rpm spindle speed and 80 mm/min travel speed. The temperatures on the advancing side are a little bit higher than on the retreating side (Fig. 5-14).
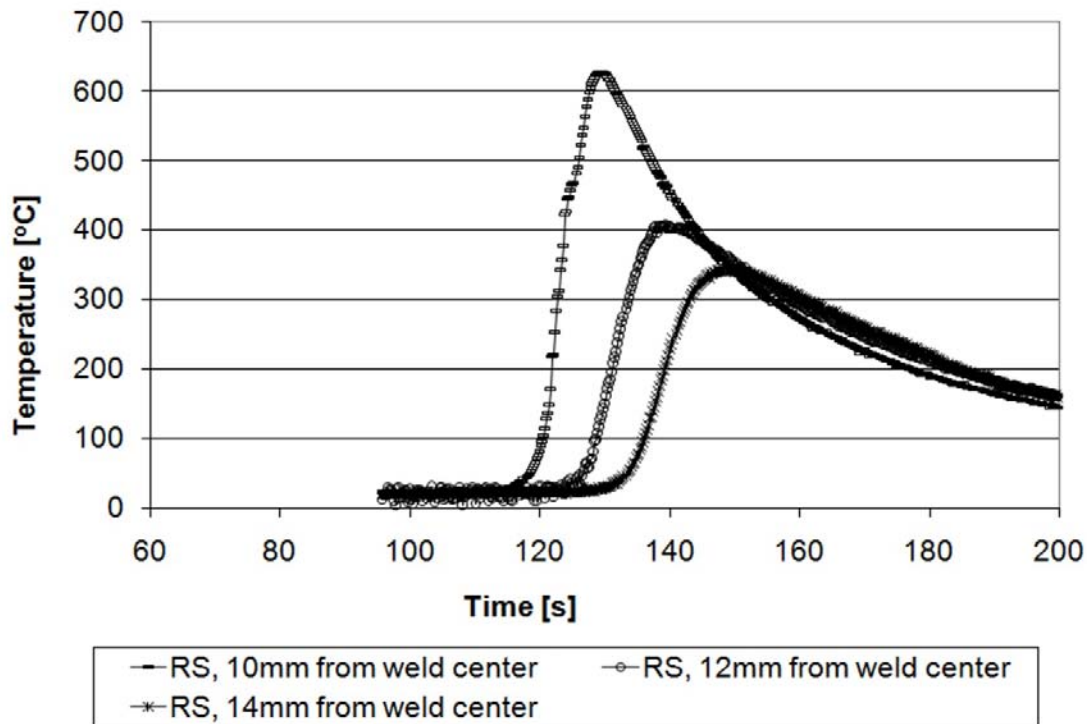
Fig. 5-13 Temperature distribution on RS for spindle speed 450 rev/min and weld speed 150 mm/min

Copper precipitation in the material 15-5PH starts at a temperature of about 450°C (see chapter 3-6). The maximum temperatures of the thermocouples placed 14 mm from the weld center are all below 450°C. Therefore no overaging and softening of the material (condition H) is expected. Process parameters with high energy input show a temperature of > 450° at the thermocouples which were placed 12 mm away from the weld center (Fig. 5-14).
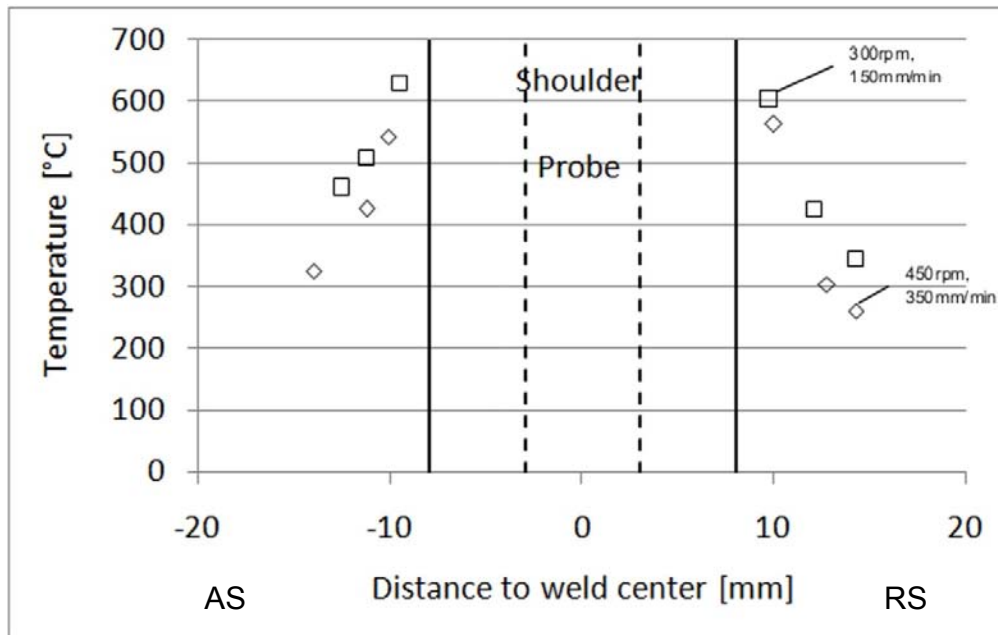
Fig. 5-14 Maximum temperatures for different positions and welding parameters

For low energy input welds, the maximum temperature was observed slightly below 450°C. For high energy input, softening due to overaging in the region of 12 mm from the weld center is expected whereas for low energy input welds, no significant influence shall occur. The temperatures 10 mm apart from the weld center exceeded 450°C for all welds. Therefore overaging is expected with less softening for low heat input welds.

The thermocouple which was placed on the bottom side of the plate was destroyed due to the material flow during welding. But a peak temperature of 1037°C was observed before the loss of the signal. Therefore, peak temperatures above 1100°C are expected in the weld centre.

For welds in condition A, no significant change of the maximum temperatures with respect to welding parameters was observed. It is expected, that the temperatures are high enough to age the material which was welded in condition A.

5.4.3 Mechanical properties

A typical hardness profile for the transverse direction of a friction stir welded joint in condition H is shown in Fig. 5-15. The hardness drops in the heat affected zone and slightly increases in the stir zone. The drop is more pronounced for welds with higher heat input. The used welding parameters have less or no influence on the hardness in the stir zone (see Fig. 5-15).

For welds in condition H the hardness profile shows an aging peak in the HAZ/TMAZ which is about 320HV and slightly below the hardness of the base metal in condition A. The parameter set with the lowest heat input has a highest minimum hardness and the smallest width of the transition zone. These results are in good agreement with the temperature measurements.
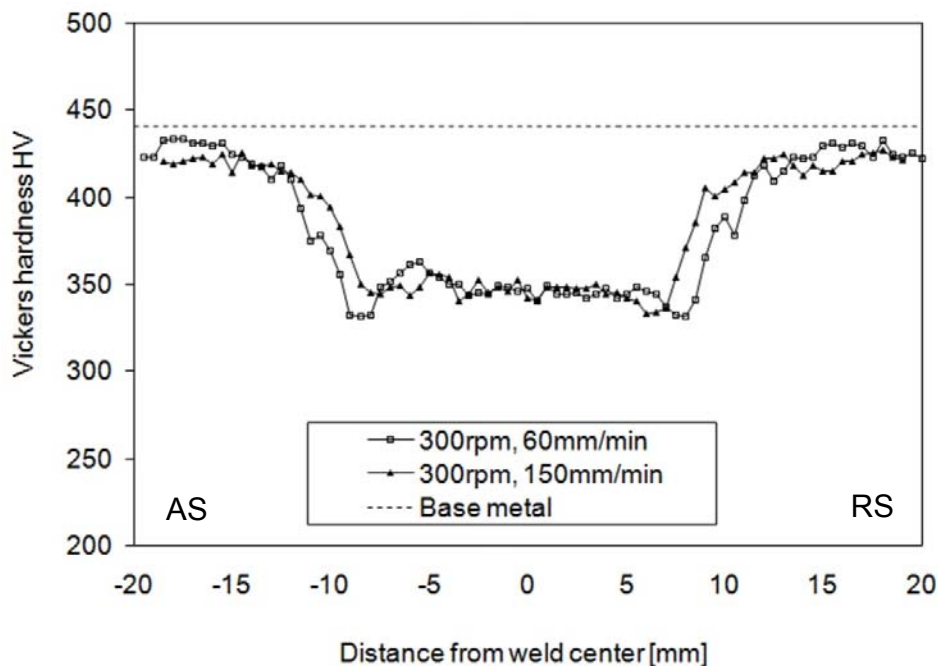
Fig. 5-15 Vickers hardness profiles for friction stir welds of 15-5PH condition H for two different welding parameters

When welding in the condition A, the hardness of the stir zone is slightly below the hardness of the base material in condition A. In the HAZ region an aging of the material takes place and the hardness increases. A post weld heat treatment (PWHT) of

520°C for 1h hardens the stir zone, TMAZ/HAZ and base material after welding (see Fig. 5-16). Only a slight overaging occurs in the HAZ that was heated into the aging temperature during welding.
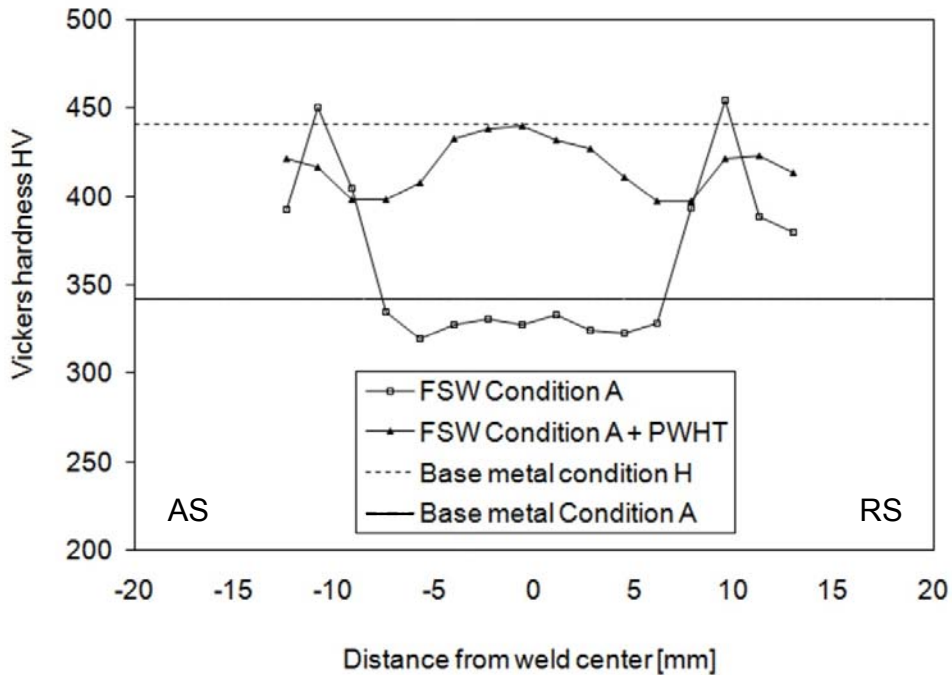
Fig. 5-16 Vickers hardness profiles for friction stir welds of 15-5PH condition A

During tensile testing, the specimens which were welded in condition A, fractured in the stir zone. The joint efficiency compared to the base metal in condition A was around 95%. However, a significant reduction of elongation from 8% to 3% was observed. By applying a post weld heat treatment of 520°C for 1h, joint efficiencies of 98% (compared to condition H) were obtained (Table 5-6).

The joint efficiency of the specimens which were welded in condition H was around 80%, which is comparable to other welding processes [111]. The elongation was lower than in the base metal but similar to the welds in condition A. The location of the fracture was at the stir zone/TMAZ zone for the specimens which were welded in condition H and condition A + PWHT. Generally it was found that increasing heat input will lower the strength of the joint which is in agreement with the hardness measurements.

Table 5-6 Summary of mechanical properties for friction stir welded 15-5PH butt joints

	Tensile strength [MPa]	Elongation [%]
Condition A	1050	3.2
Condition A + PWHT	1405	3.3
Condition H	1140	3.6

After tensile testing, fractography using SEM was performed for all specimens. A typical fracture surface for welds in condition A is shown in Fig. 5-17 (a). The surface has a dimpled structure. The dimples for the condition H and A+PWHT are relatively small, whereas the analysis for the welds in condition A shows larger dimples (Fig. 5-17).
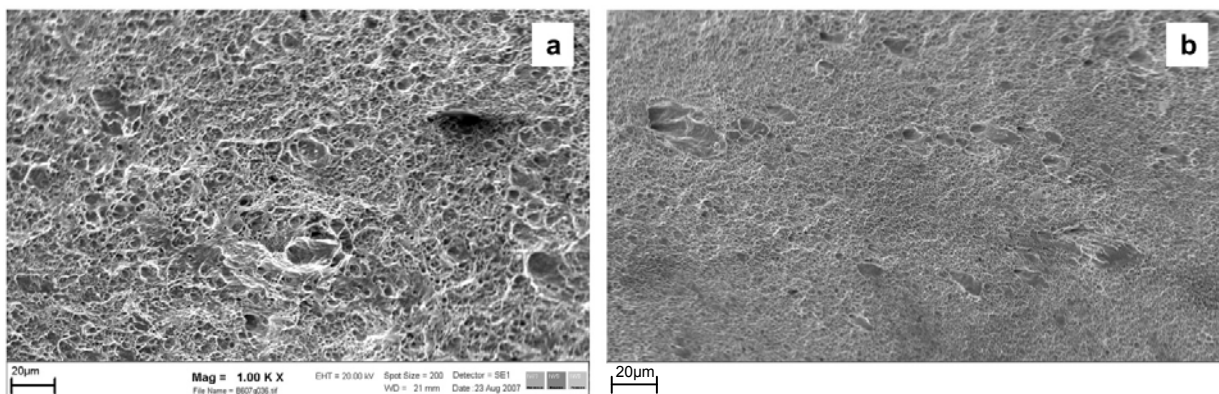
Fig. 5-17 Fracture surface of friction stir welded 15-5PH steel samples a condition A; b condition H

At the bottom of the cavities, small particles are visible. By a detailed analysis of these particles, carbide particles like NbC were found (see Fig. 5-18). For all conditions the observed fracture mode was micro-ductile.
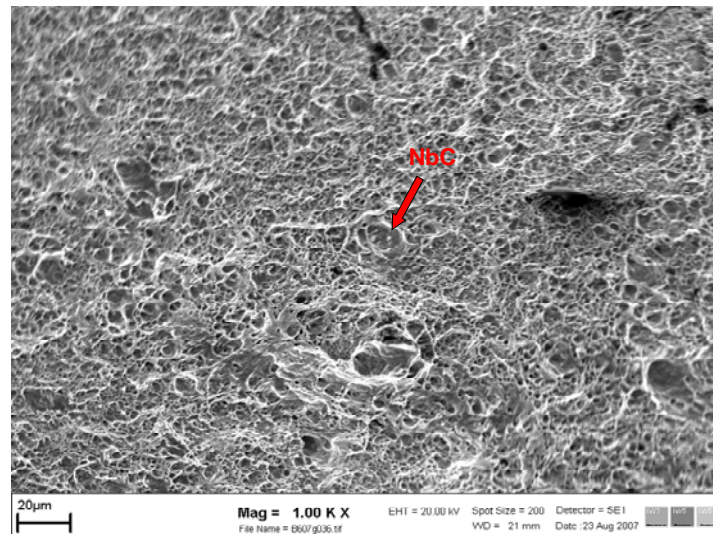
Fig. 5-18 Fracture surface of friction stir welded 15-5PH steel samples condition A showing Nb carbides

5.4.4 Microstructure

The characteristics of the friction stir weld were investigated using light optical microscopy (LOM), scanning electron microscopy (SEM) and transmission electron microscopy (TEM). The specimens were cut at at different sections of the steady state process. The samples for LOM and SEM were prepared using standard metallographic techniques. The SEM analysis was performed using the Gemini DSM986 device. For the TEM observations, thin foils perpendicular to the welding direction were extracted from the stir zone and heat affected zone. This sample preparation was done using focus ion beam (FIB) technique. The TEM and EFTEM analysis were done using a Philips CM20 at Research Institute for Electron Microscopy and Fine Structure Research (FELMI) at Graz University of Technology.

Fig. 5-19 shows a typical macrostructure of the transverse section of the friction stir weld. The left and right side of the cross section are related to the advancing (AS) and retreating side (RS) of the weld. There are no macroscopic defects visible. The optimized tool with a 2.1 mm long pin was sufficient to produce a fully consolidative weld in the 2.6 mm thick steel. On the top surface the size of the stir zone corresponds with the shoulder diameter of the tool. On both sides of the stir zone, a HAZ extends with a

range of 1 mm – 1.5 mm. At the highest weld speed of 350 mm/min, small pores appeared on the advancing side.

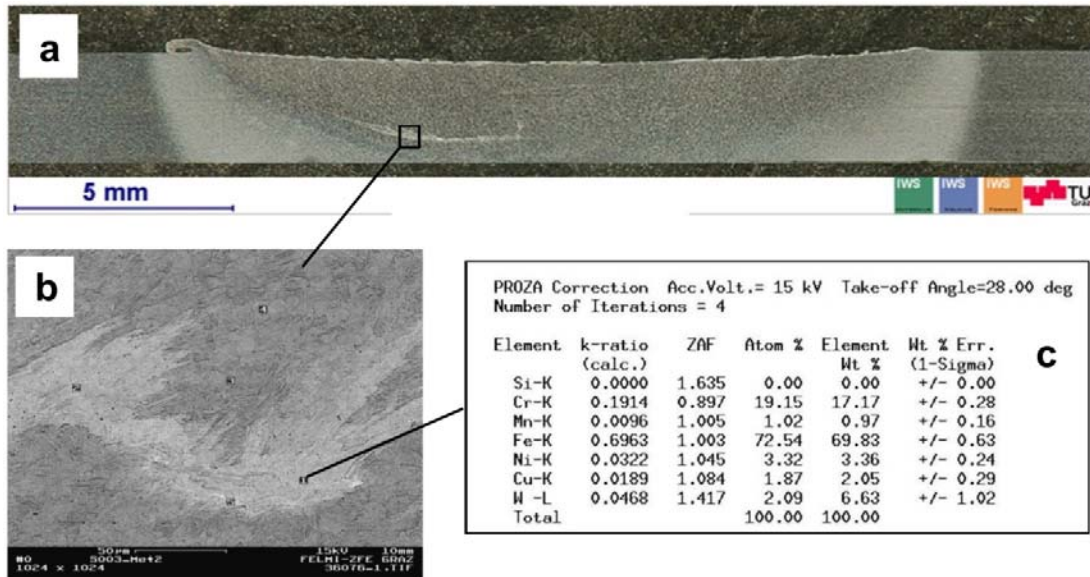

Fig. 5-19 Macrograph of transverse section of butt friction stir weld of steel 15-5PH under hardened condition

Due to the fact that during friction stir welding there is no global melting, the typical solidification with dentritic, elongated arms [112] does not appear. The macrograph indicates that the whole friction stir weld area is martensitic. No big differences of the structure between the different zones can be observed in the macrograph.

For a more detailed investigation, SEM analysis was performed for the distinct regions. Characteristic pictures of HAZ, TMAZ and SZ are shown in Fig. 5-20. The whole weld area is martensitic after cooling down to room temperature but a variation in grain size depending on the different zones can be observed. Starting from the base metal into the HAZ, the grain size first decreases (fine grained HAZ). Below Ac_1, the material remains martensitic with an aging of the copper precipitates may take place. Close to the stir zone the grain size increases and is than very uniform in the SZ. These results were verified by EBSD grain mappings of selected regions. The grain coarsening is more pronounced for welds with high heat input. The investigations for the grain size distribution in the SZ show a slightly decrease of the grain size from the top to the bottom (see Fig. 5-21). These findings suggest that higher temperatures will occur at the top, close to the tool shoulder. These results were found for all conditions.
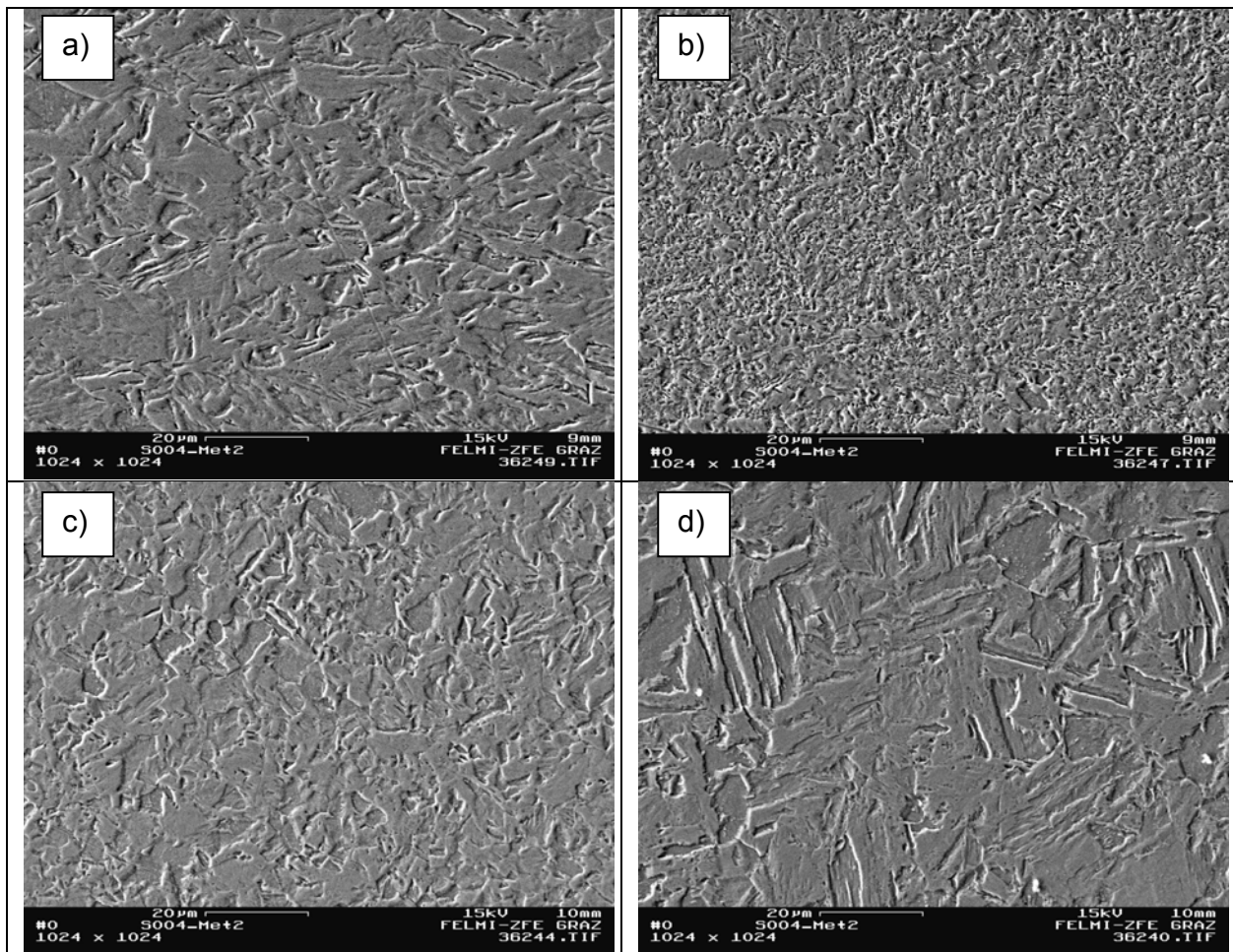
Fig. 5-20 SEM micrographs for locations: BM (a), fine grained HAZ (b), coarse grained HAZ (c) and SZ (d) of the butt friction stir weld of steel 15-5PH in hardened condition
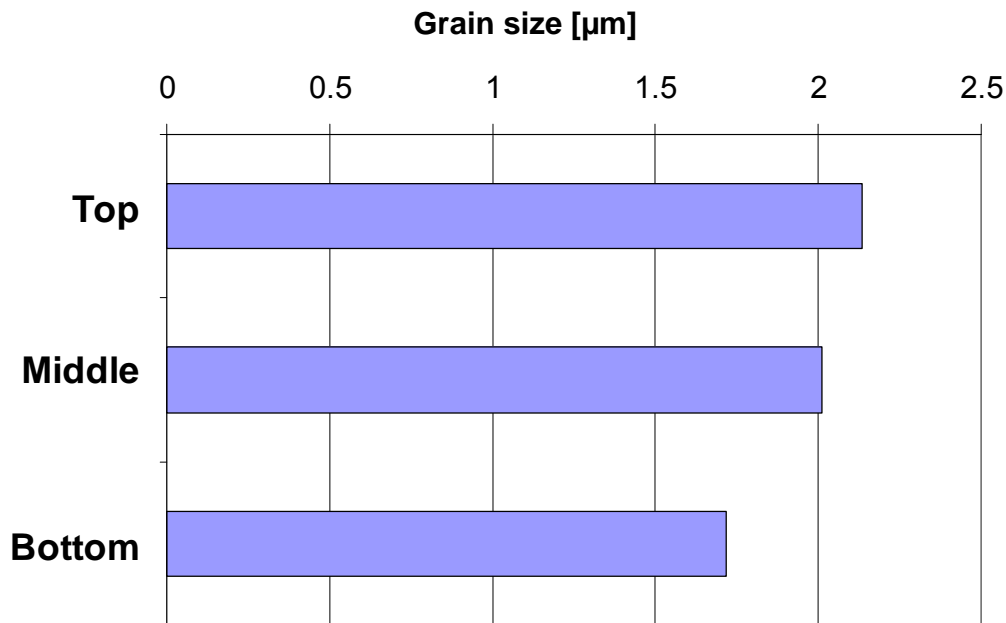
Grain size [µm]

Fig. 5-21 Change of grain size at the weld centre from plate top to plate bottom

The analysis using SEM gave additional information on the weld microstructure, but no boundary between SZ and TMAZ / HAZ was observed. Therefore EBSD analysis was performed for these areas. Fig. 5-22 shows the EBSD orientation image for the stir zone and the heat affected zone. The images for different positions in the stir zone showed that the microstructure is relatively uniform throughout the cross section of the SZ but the texture became relatively diffuse. This may come from the deformation during the stirring process and phase transformation. It can be seen, that large clusters with similar orientation exist in the stir zone, wheras the areas with similar orientation are considerably smaller in the HAZ. The reason of this behaviour is the recrystallised stir zone and the non-recrystallised HAZ. Since not a complete mapping was performed for the whole transition region, an edge between the SZ and TMAZ / HAZ is not visible. But due to the fact, that the distance between the Fig. 5-22 (a) and 5-22 (b) is pretty small, a sharp edge is expected.
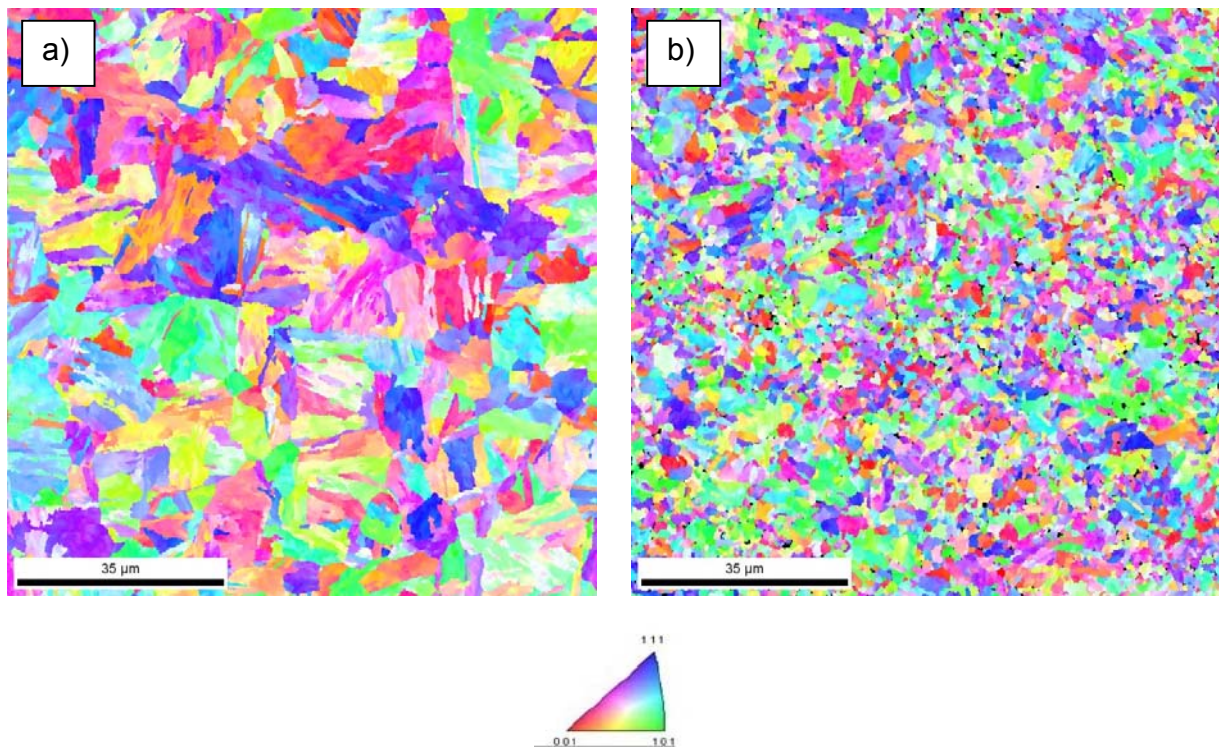
Fig. 5-22 High resolution orientation image map of advancing side of the weld in Figure 5-19, SZ (a), HAZ (b)

In the base metal, a small percentage of austenite, called retained austenite, exists [107]. A small percentage austenite was also found in the HAZ, but no austenite was found in the SZ. The SZ is probably completely transformed into martensite when cooling down from the austenitic region. The lack of austenite in the SZ may explain the reduced elongation during tensile testing as shown in chapter 5.4.3.
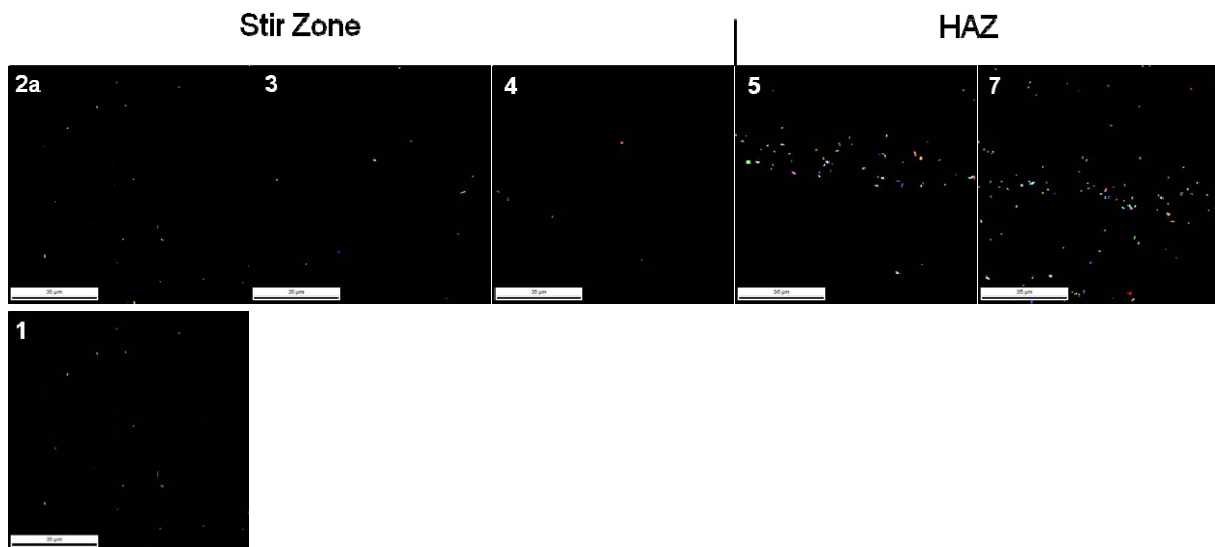
Fig. 5-23 Presence of austenite for different regions; no austenite in the SZ; few percent austenite in the HAZ, the small dots respresent austenite

To verify these results, EFTEM analysis was performed for the stir zone and heat affected zone. The retained austenite can be identified by its typical high nickel content. It was possible to identify retained austenite in the HAZ. However, no austenite was found in the stir zone. Figure 5-24 shows a TEM bright field image of the stir zone.
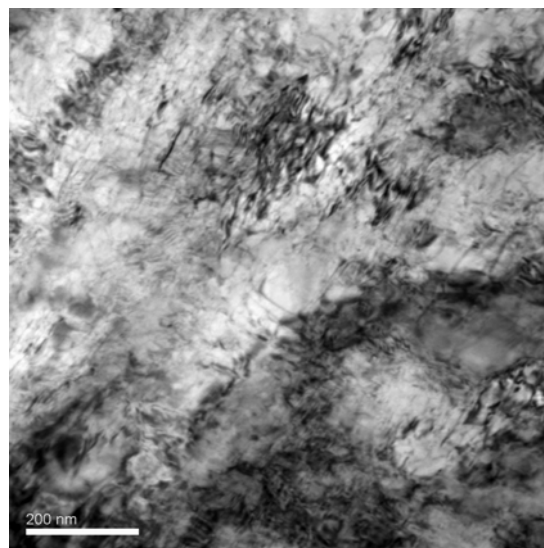
Fig. 5-24 Transmission electron microscopic brigth field image of friction stir welded 15-5PH steel showing SZ

In all regions, finely dispersed niobium carbides were found. The niobium is incorporated because of its high affinity to carbon and prevents the precipitation of chromium carbides leading to a reduced corrosion resistance. The size of the niobium carbides in the stir zone is smaller than in the heat affected zone. Figure 5-25 (a) shows a TEM image of the heat affected zone. The presence of niobium carbides with a globular shape and a size of about 100nm in the HAZ is shown in Fig. 5-25 (b). The niobium carbides were also found during fractography (see Fig. 5-18).
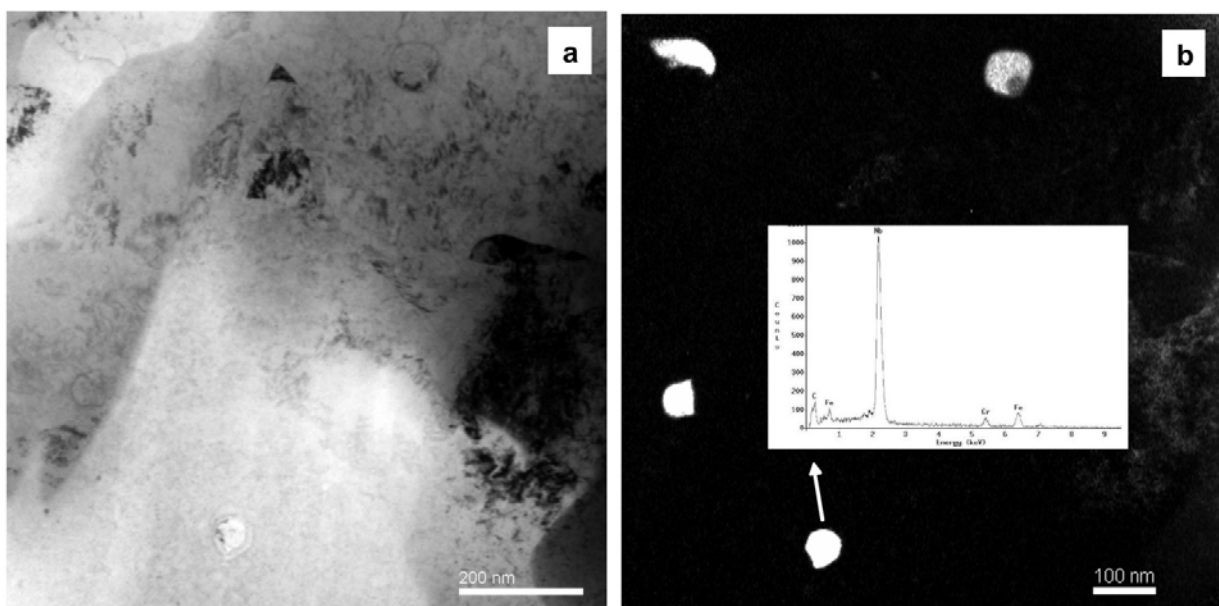
Fig. 5-25 Image (TEM) of friction stir welded 15-5PH steel showing HAZ, condition A a bright field image b corresponding dark field image using Nb M jump ratio – white and energy dispersive spectroscopy result for one particle
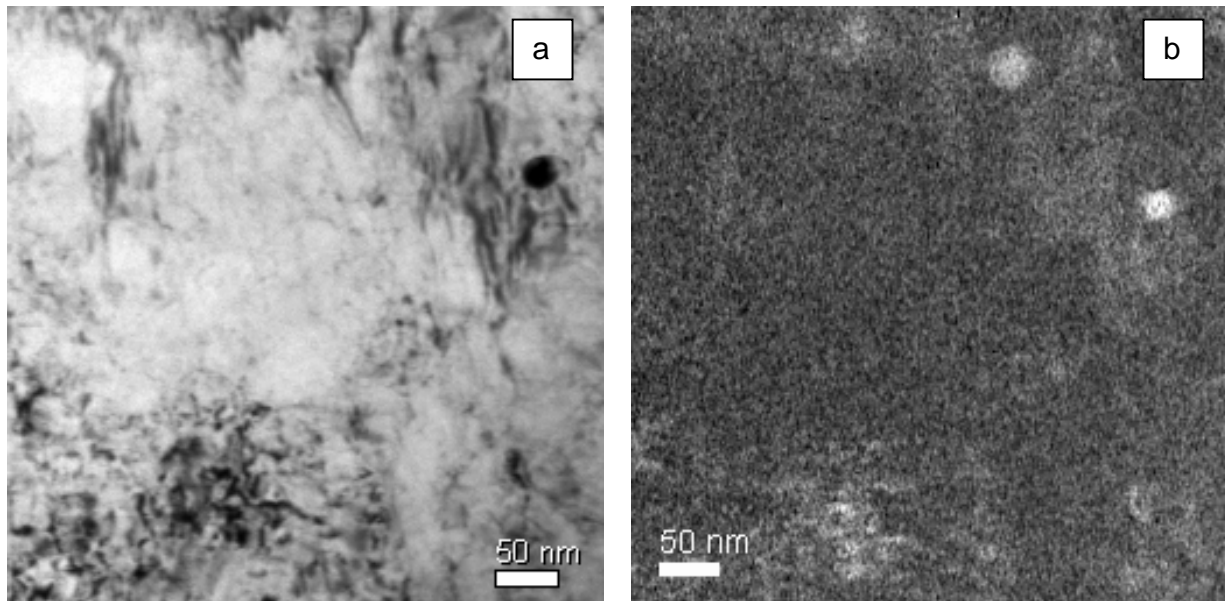
Fig. 5-26 Image (TEM) of friction stir welded 15-5PH steel showing SZ, condition A a bright field image b corresponding dark field image using Nb M jump ratio

5.4.5 Copper precipitation

The Vickers measurements show the change of the hardness in the HAZ which is expected due to the copper precipitation mechanism. The effect of different temperatures on the microstructure and mechanical properties of PH15-5 was studied in detail by Bajguirani [113]. The steel structure contains fine, coherent with matrix, bcc copper rich precipitates. High aging temperatures, causes consequential loss of coherency between steel matrix and copper precipitates lattices, growth of the precipitates and their lattice type transition to fcc. The presence of copper precipitates in the outer HAZ was revealed using TEM and ETEM and is shown in Fig. 5-27. The precipitates are roughly spherical with a size of about 10 nm and they are homogenous distributed in this area. With increasing temperatures, the copper precipitates grow. But it is known that a large fraction of coarse precipitates leads to a reduction in strength. This may explain the loss of strength in the HAZ due to overaging.
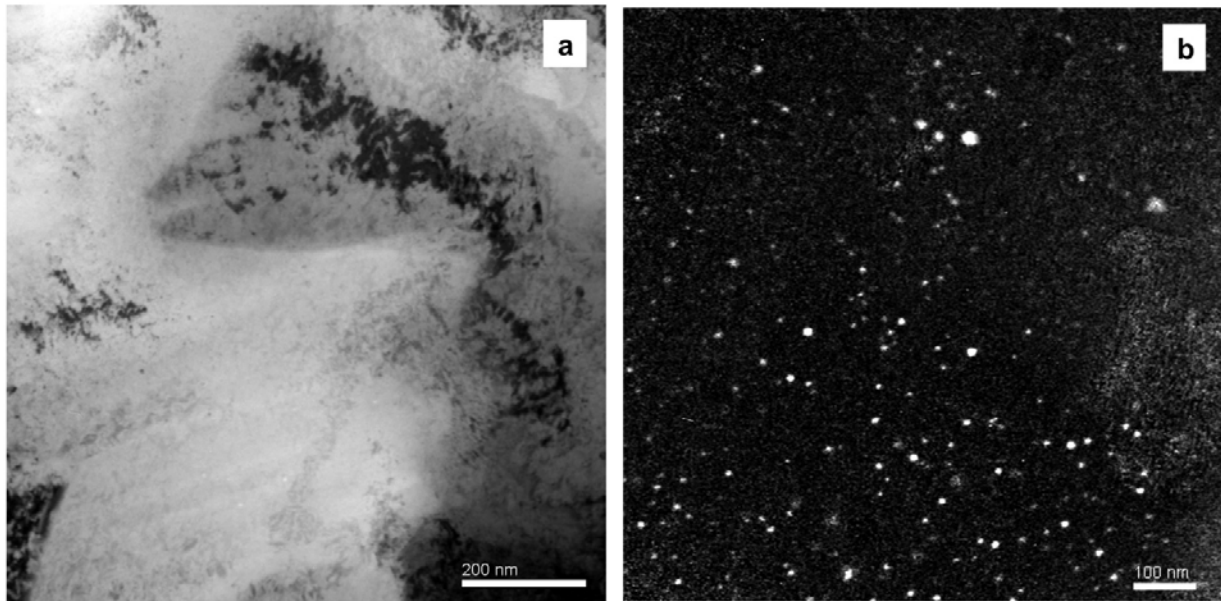
Fig. 5-27 Image (TEM) of friction stir welded 15-5PH steel showing HAZ, condition A a bright field image b corresponding dark field image using Cu L jump ratio (right)

For the samples of the stir zone, no presence of copper precipitates was recognized. Since the temperature in the stir zone is expected to be higher than 1000°C, a complete dissolution of copper precipitates may take place. To support this result, samples of welds in condition H were put into a heat furnance and tempering at 480°C for 1 hour was conducted. The tempering should lead to a re-precipitation of Cu particles in the martensite phase. A hardness profile was performed and it can be seen, that the whole stir zone was hardened relatively uniform with a maximum hardness of 430 HV10. Other zones, where copper precipitation took place during welding were further overaged and the hardness is reduced. The size of the zone where the high hardness was observed indicates, where a dissolution of copper precipitates took place. Additionally the the temperatures in this area must exceed the dissolution temperature of copper precipitates.

5.4.6 Tool life and wear

It is well recognized that friction stir welding of steel will lead to tool wear and the life of the tool is limited. Since the maximum weld length for the given application is between 2.0 m and 2.4 m (specification given by the company partner), the welding length with one tool must exceed this width. Also the quality and properties of the weld must be constant. Due to the limitation of the plate length, six welds with each 450 mm were performed using a W25Re tool. Micrographs at different regions were obtained using optical microscopy (OM) and scanning electron microscopy (SEM). As shown in Fig. 5-28 (a), a light grey area is visible on the top surface and on the advancing side, close to the bottom surface. An EDXS analysis (Fig. 5-28 (c)) showed an enrichment of tungsten up to 7 wt % in this area. The presence of tungsten is due to the wear of the tool during friction stir welding. These results are in accordance with the tool wear which was primarily at the probe tip and at the shoulder edge (see Fig. 5-29). Details about the wear of a tool during friction stir welding of steel are discussed in chapter 4-12.

Fig. 5-28 a macrograph of transverse section of butt friction stir weld of steel 15-5PH under hardened condition, b details of tungsten remanents on AS and c results of spot analysis
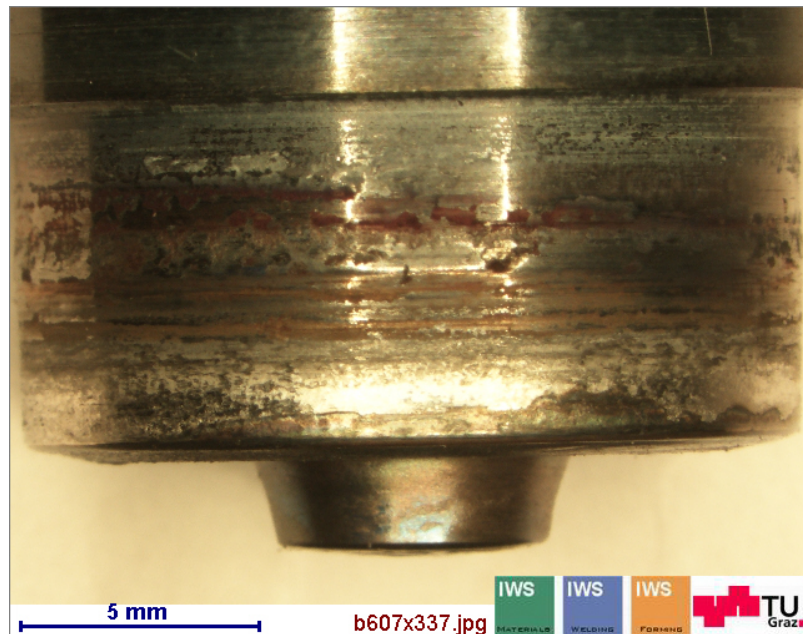
Fig. 5-29 W25Re tool profile after 2250 mm welding

Tensile test specimens were extracted after 500 mm, 1000 mm and 2250 mm. Fig. 5-30 shows the ultimate tensile strength in relation to the weld length. It should be also noted that the weld was performed using six plunge phases which also increase the wear, especially of the probe. It can be seen that the ultimate tensile strength does not change significantly during the weld length. Therefore a W25Re tool should be applicable to weld also the maximum width of the belt. A similar investigation was made using the WC-Co tool BB10 (chemical composition shown in Table 4-11). The tool also survived the whole weld length and no influence on the ultimate tensile test of the joint was observed.
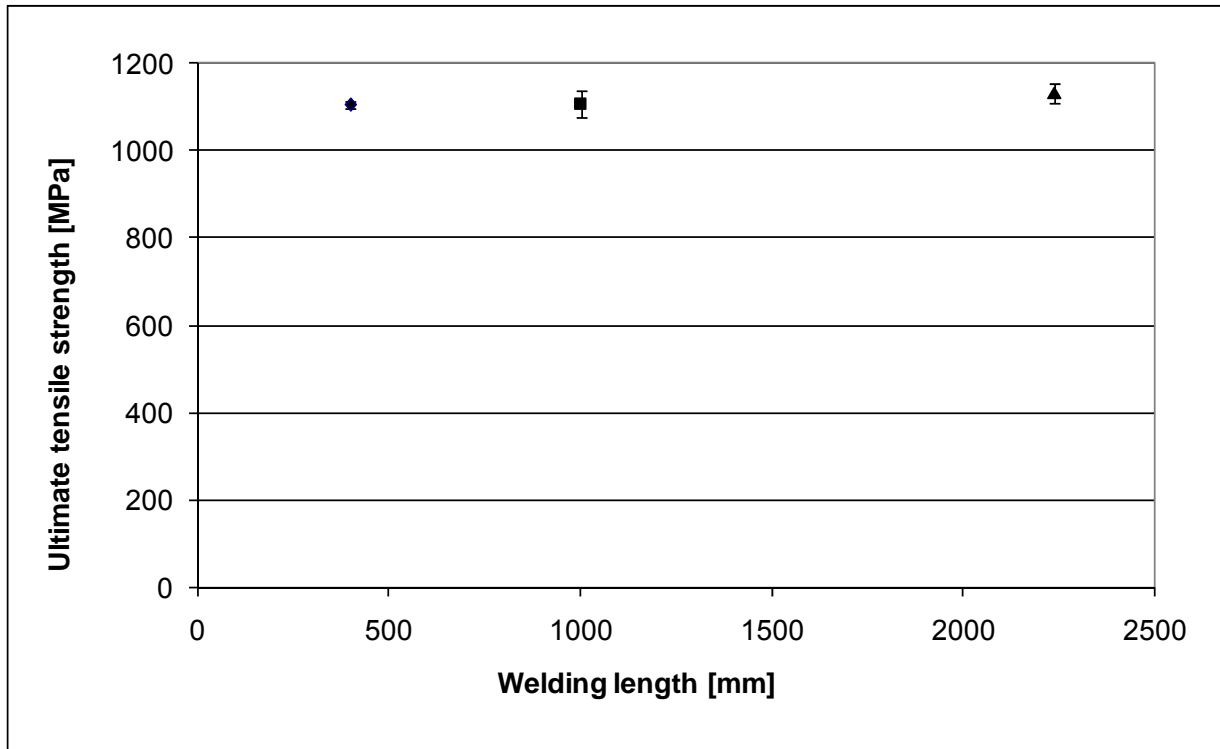
Fig. 5-30 Ultimate tensile strength in relation to the welding length for the W25Re tool

5.4.7 Fatigue Test

The determined weld quality is based on metallographic analysis, hardness measurements, tensile and fatigue tests. The results of the fatigue test for the 15-5PH butt weld in condition H are shown here.

Since the weld is planned for an endless belt for an industrial application, the cross weld must resist the different stresses during rotating.

Fatigue test results under bending stresses with a rate of load cycles n = 1500 / min and R = -1 for flat specimens are shown in Fig. 5-31. Reference data from the company partner for a TIG welded joint and base material is plotted for comparison. The average fatigue life for FSW and TIG weld specimens were 164 900 and 157 500, respectively. FSW welds showed higher average life, but also a higher scatter in this limited amount of test data (Fig. 5-31).
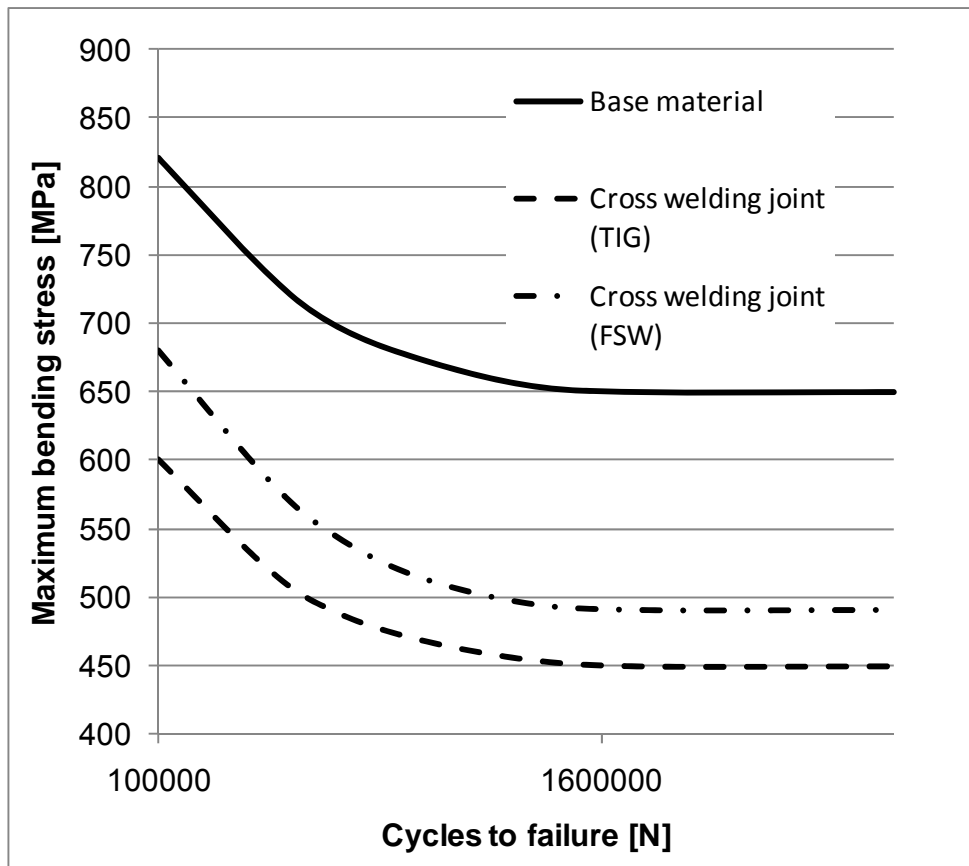
Fig. 5-31 Fatigue test results for parent material and TIG / FSW (W25Re tool) cross welded joints

6 Summary & Conclusions

Within this study, tool and process parameters for friction stir welding of steels were developed.

First a systematic selection of potential tool materials was carried out considering the defined requirements. In order to achieve a deeper understanding of the process and the tool demands during friction stir welding of steel, the development of bead on plate welding process for a 4 mm thick austenitic stainless steel was performed. The influence of welding parameters on forces, spindle torque and temperatures were investigated. The selected tool material WC-Co was developed together with a tool coating and suitable process parameters. Tool wear and weld quality of the developed tool and a reference W25Re tool were analyzed and compared. Moreover, the effect of tool geometry on forces was investigated. Additionally, the wear and failure mechanism of a tool during friction stir welding of steel were analyzed and discussed.

Following conclusions can be made:

- Bead on plate welding for 4 mm thick steel DIN 1.4301 has been successfully performed using tungsten-rhenium and tungsten-carbide based tools.
- The tool loads, temperatures and wear behaviour of uncoated and PVD coated tools were analysed under realistic process parameters.
    - o Higher feed rates increase the forces in welding direction but reduce the tool wear. The increase of the spindle speed has a converse effect.
    - o The pin wear of the coated tools was systematically lower than for uncoated tools.
    - o The force in welding direction and the spindle torque for tools with coatings showed no significant change.
- WC based tool material with coarse grained carbide and low cobalt content gave the best results during the development.
- The life limiting factors for friction stir welding tools were identified and analysed, which are wear (mainly abrasion and adhesion), deformation and brittle fracture.

- The tool life of WC-Co tools decreases with pin length, the best results were achieved for 1mm thick steel plates. The tool life during linear welding was comparable with a W25Re tool. During friction stir spot welding, the developed WC-Co tool has a considerably better tool life.

In this study, friction stir welding of the precipitation hardening steel 15-5 PH was performed and the resulting microstructure and mechanical properties were investigated for different welding parameters. The used tool materials W25Re and WC-Co were capable to produce sound welds. The tool design with a reduced pin length of 2.1 mm resulted in a fully consolidative weld.

Following conclusions can be made:

- A rise of the heat input resulted in higher maximum temperatures. The highest temperatures were observed on the advancing side.

- The weld area is fully martensitic with a small amount of retained austenite in the HAZ and TMAZ. On the advancing side of the stir zone and on the top surface, a contamination with tool material (tungsten) was observed. The existence of niobium carbides and copper precipitates was analysed for the different distinct regions.

- A loss of strengthening due to overaging in the HAZ and TMAZ was observed. The amount of overaging was reduced by using welding paramters with lower heat input. As expected, the best results gave the welds in condition A (solution annealed) with an additional post weld heat treatment.

- The fatigue properties of FSW welded joints were better than that of conventionally TIG welded joints.

- Both tool materials were capable of welding 2250 mm without a change of mechanical properties which is sufficient for the given application.

7 Bibliography

[1] W.M. Thomas, E.D. Nicholas, J.C. Needham, M.G. Murch, P. Templesmith, C.J. Dawes, G.B. Patent Application No. 9125978.8 (December 1991).

[2] C. Dawes, W. Thomas, TWI Bulletin, 6, November/December 1995, p. 124.

[3] R. S. Mishra, Introduction, Friction Stir Welding and Processing, R. S. Mishra, M. W. Mahoney, Ed., ASM International, 2007.

[4] ISO/DIS 25239-1, Friction stir welding - Aluminium - Part 1: Vocabulary

[5] W. J. Arbegast, A flow-partitioned deformation zone model for defect formation during friction stir welding, Scripta Materialia, Volume 58, Issue 5, Viewpoint set no. 43 'Friction stir processing', March 2008, p 372-376.

[6] C. B. Fuller, Friction Stir Tooling: Tool Materials and Designs, Friction Stir Welding and Processing, Mishra R S, Mahoney M W, Ed., ASM International, 2007.

[7] C. J. Dawes and W. M. Thomas, Weld. J., Vol 75, 1996, p 41.

[8] R. S. Mishra and Z. Y. Ma, Friction stir welding and processing, Materials Science and Engineering, 2006, p 1-78.

[9] L. E. Murr, Y. Li, R.D. Flores and E.A.Trillo, Mater. Res. Innov., Vol 2, 1998, p 150.

[10] Y. Li, E.A.Trillo and L.E. Murr, J. Mater. Sci. Lett., Vol 19, 2000, p 1047.

[11] Y. Li, L.E. Murr and J.C. McClure, Mater. Sci. Eng. A, Vol. 271, 1999, p 213.

[12] W. M. Thomas and E.D. Nicholas, Friction stir welding for the transportation industries, Materials & Design, Vol. 18, 1997, p 269-273.

[13] W. J. Arbegast, Friction Stir Welding: After a decade of development, Friction Stir Welding and Processing IV, 2007, The Minerals, Metals & Materials Society (TMS).

[14] W. Thomas, I. Norris, D. Staines and E. Watts, Com-stir[TM] - Compound motion for friction stir welding and machining, Connect, no.124, May - June 2003, p 8.

[15] W. Thomas, D. Staines, E.D. Nicholas and P. Evans, Reversal Stir Welding – ReStir[TM] Preliminary trials, http://www.twi.co.uk/j32k/getFile/spwmtjan2003.pdf, [10.01.2006].

[16] W. Thomas, D. Staines, E.R. Watts and I.M. Norris, The simultaneous use of two or more friction stir welding tools, www.twi.co.uk/j32k/getFile/spwmtjan2005.pdf, [10.01.2006].

[17] S. Kallee, W. M. Thomas, Forschungsaktivitäten in der Verfahrens- und Werkzeugentwicklung, Proceedings „FSW-Technologietage", 2005, (Ranshofen, Austria), p 24-25.

[18] E. R. Watts, D. G. Staines, W. M. Thomas and E. D. Nicholas, Dual-rotation Stir Welding - Preliminary trials, http://www.twi.co.uk/j32k/getFile/sperwapr2004.pdf, [10.01.2006].

[19] S. Sheikhi, Varianten des Rührreibschweißens, Proceedings „Lehrgang Reibrührschweißen", (Geesthacht, Germany), 2005.

[20] W. Thomas, P. Fielding, P. Threadgill and D. Staines, Skew-stir^{TM} variation on a theme, Connect, no.113, July - August 2001, p 3.

[21] A. Gerlich, G. A. Cingara, T. H. North, Stir Zone Microstructure and Strain Rate during Al 7075-T6 Friction Stir Spot Welding, Metal. Trans., (2006).

[22] J.A. Schneider, A.C. Nunes, Jr., Characterization of Plastic Flow and Resulting Micro textures in a Friction Stir Weld, Metallurgical and Materials Transactions B, Vol 35B, (2004), p 777-783.

[23] Nandan, R., DebRoy, T., Bhadeshia, H.K.D.H., Recent Advances in Friction Stir Welding– Process, Weldment Structure and Properties, Progress in Materials Science, (2008), p 1-33.

[24] S. Khosa, T. Weinberger, N. Enzinger, FEA of material flow pattern in FSSW of Al 6082-T6 using different process parameters and tool geometries, Proceedings of the 5th International Conference on Heat Transfer, Fluid Mechanics and Thermodynamics, (Sun City, South Africa), 2007.

[25] T. Pan, A. Joaquin, D. E. Wilkosz, L. Reatherford, J. M. Nicholson, Z. Feng, M. L. Santella, Spot Friction Welding for Sheet Aluminium Joining, Proceedings of 5th International Friction Stir Welding Symposium, (Metz, France), 2004.

[26] T. Iwashita, US Patent Application No. 6,601,751 B2; August 2003.

[27] Z. Feng, M. L. Santella, S. A. David, R. J. Steel, S. M. Packer, T. Pan, M. Kuo, R. S. Bhatnagar, Friction Stir Spot Welding of Advanced High- Strength Steels – A Feasibility Study, SAE International, 2005.

[28] C. G. Rohdes, M. W. Mahoney, W. H. Bingel, R.A. Spurling and C.C. Bampton, Scr. Mater., Vol 36, 1997, p 69.

[29] G. Liu, L.E. Murr, C.S. Niou, J.C. McClure and F.R. Vega, Scr. Mater., Vol 37, 1997, p 355.

[30] K. V. Jata, and S. L. Semiatin, Scr. Mater., Vol. 43, 2000, p 743.

[31] S. Benavides, Y. Li, L.E. Murr, D. Brown and J.C. McClure, Scr. Mater., Vol 41, 1999, p 809.

[32] P. L. Threadgill, TWI Bull., March 1997.

[33] S. M. Packer, R. J. Steel, T. Nelson, C. D. Sorensen and M. W. Mahoney, "Tool Geometries and Process parameters Required to Friction Stir Weld High Melting Temperature Materials", 2005-AWS-20.

[34] J.A. Schneider, Temperature Distribution and Resulting Metal Flow, Friction Stir Welding and Processing, Editors: Mishra R S, Mahoney M W, ASM International, 2007.

[35] K.N. Krishnan, On the Formation of Onion Rings in Friction Stir Welds, Mater. Sci. Eng. A, Vol 327, 2002, p 246 – 251.

[36] G. Biallas, R. Braun, C. Dalle Donne, G. Staniek, and W.A. Kaysser, Mechanical Properties and Corrosion Behavior of Friction Stir Welded 2024-T3, First Int. Conf. on FSW, June 1999 (Thousand Oaks, CA).

[37] Y.S. Sato, H. Kokawa, K. Ikeda, M. Enomoto, S. Jogon, and T. Hashimoto, Microtexture in the Friction-Stir Weld of an Aluminium Alloy, Metall. Mater. Trans. A, Vol 32, 2001, p 941 – 948.

[38] D.P. Field, T.W. Nelson, Y. Hovanski, and K.V. Jata, Heterogeneity of Cristallographic Texture in Friction Stir Welds of Aluminium, Metall. Mater. Trans. A, Vol 32, 2001, p 2869-2877.

[39] J.A. Schneider and A.C. Nunes, Jr., Characterization of Plastic Flow and Resulting Microtextures in a Friction Stir Weld, Metall. Mater. Trans. B, Vol 35, 2004, p 777-783.

[40] Y. Li, L.E. Murr, and J.C. McClure, Solid State Flow Visualization in the Friction Stir of 2024 Al to 6061 Al, Scr. Mater., Vol. 40 (No 9), 1999, p 1041-1046.

[41] L.E. Murr, Y. Li, R.D. Flores, E.A. Trillo, and J.C. McClure, Intercalation Vortices and Related Microstructural Features in the Friction Stir Welding of Dissimilar Metals, Mater. Res. Innovat., Vol 2, 1998, p 150 – 163.

[42] K. Colligan, Material Flow Behavior during Friction Stir Welding of Aluminium, Weld. Res. Suppl., July 1999, p 229s-237s.

[43] T.U. Seidel and A.P. Reynolds, Visualization of the Material Flow in AA2195 Friction-Stir Welds Using a Marker Insert Technique, Metall. Mater. Trans. A, Vol 32, 2001, p 2879-2884.

[44] M. Guerra, C. Schmidt, J.C. McClure, L.E. Murr, and A.C. Nunes, Jr., Flow Patterns during Friction Stir Welding, Mater. Charact., Vol 49, 2003, p 95-101.

[45] B. London, M. Mahoney, W. Bingel, M. Calabrese, R.H. Bossi, and D. Waldron, Material Flow in Friction Stir Welding Monitored with Al-SiC and Al-W Composite Markers, Proc. Symp. On FSW and Processing II, K.W. Jata, M.W. Mahoney, R.S. Mishra, S.L. Semiatin, and T. Lienert, Ed., TMS, 2003, p 3-12.

[46] A.C. Nunes, Jr., Wiping Metal Transfer in Friction Stir Welding, Aluminium 2001: Proc. 2001 TMS Annual Meeting Automotive Alloys and Joining Aluminium Symp., G. Kaufmann, J. Green, and S. Das, Ed., TMS, p 235-248.

[47] W.J. Arbegast, Modeling Friction Stir Joining as a Metal Working Process, Hot Deformation of Aluminium Alloys, Z. Jin, Ed., TMS, 2003.

[48] A.P. Reynolds, Visualization of Material Flow in Autogenous Friction Stir Welds, Sci. Technol. Weld. Join., Vol 5 (No. 2), 2000, p 120-124.

[49] R. S. Mishra and Z. Y. Ma, Friction stir welding and processing, Materials Science and Engineering, 2006, p 51-53.

[50] W. M. Thomas, P. L. Threadgill, E. D. Nicholas, Feasibility of friction stir welding steel, Science and Technology of Welding and Joining, Vol. 4 No. 6, 1999.

[51] A. P. Reynolds, T. Wei, T. Gnaupel-Herold, H. Prask, Structure, properties, and residual stress of 304L stainless steel friction stir welds, Scripta Materialia, Vol. 48, 2003, p 1289–1294

[52] Beyer M, Rührreibschweißen (FSW) von Stählen, „GKSS Lehrgang" Rührreibschweißen. 2005, (Geesthacht, Germany).

[53] R. Nandan, T. DebRoy, H.K.D.H. Bhadeshia, Recent Advances in Friction Stir Welding – Process, Weldment Structure and Properties, Progress in Materials Science, (2008), p37-38.

[54] W. Schatt and K. P. Wieters, Powder Metallurgy - Processing and Materials, 1997: Liveseys Ltd. p. 43f; 121f; 411f; 447-469.

[55] "Tungsten alloys", trade literature, Plansee GmbH, Germany, 2008.

[56] M. W. Mahoney, C. B. Fuller, W. H. Bingel and M. Calabrese, "Friction Stir Processing of Cast NiAl Bronze," Thermec 2006, July 4-8, 2006 (Vancouver, Canada), TMS.

[57] T.W. Nelson, C. D. Sorensen, R. J. Steel and S. M. Packer, Improved Polycrystalline Cubic Boron Nitride Tooling for Friction Stir Welding High Temperature Alloys, Proceedings of the 6th International Symposium on Friction Stir Welding, 2006, (St. Sauveur, Canada), TWI, paper on CD.

[58] M. Collier, R. Steel, T. Nelson, C. Sorensen and S. Packer, Grade development of Polycristalline Cubic Boron Nitride for Friction Stir Processing of Ferrous Alloys, Proceedings of the fourth International Conference on Friction Stir Welding, May 14-16, 2003 (Park City, UT), TWI, paper on CD.

[59] M. W. Mahoney, R. J. Steel, T. Nelson, S. M. Packer, and C. D. Sorensen, Friction Stir Welding of HSLA-65 Steel with Low/No Distortion, Proceedings of the Seventh International Conference on Friction Stir Welding, May 20-22, 2008 (Awaji, Japan), TWI, paper on CD.

[60] S.H.C. Park: Ph.D. thesis, Tohoku University, 2005.

[61] A. Fischer, C. Zietsch, Tool Failure Analysis and Criteria for the Selection of Friction Stir Tool Materials, Proceedings of International Seminar on Friction Stir Welding Steels, Geesthacht, Germany, 2007.

[62] C.D. Sorensen, et.al. 2007, "Friction Stir Processing of D2 Tool Steel For Enhanced Blade Performance", Friction Stir Welding And Processing IV, TMS Annual Meeting, Orlando, FL., ISBN 978-0-87339-661-5.

[63] W. J. Kyffin, G. L. Threadgill, H. Lalvani, B. P. Wynne, Progress in FSSW of DP800 high strength automotive steel, Proceedings of the 6th International Symposium on Friction Stir Welding, 2006, (St. Sauveur, Canada), TWI, paper on CD.

[64] R. P. Martinho, F. J. G. Silva, A. P. M. Baptista, Wear behaviour of uncoated and diamond coated Si_3N_4 tools under severe turning conditions, 16th International Conference on Wear of Materials, September 2007, p 1417-1422.

[65] C. D. Sorensen, T. W. Nelson, Friction Stir Welding of Ferrous and Nickel Alloys, Friction Stir Welding and Processing, Editors: R. S. Mishra, M. W. Mahoney, ASM International, 2007.

[66] A. P. Reynolds, M. Posada, J. DeLoach, M. J. Skinner and T. J. Lienert, FSW of Austenitic Stainless Steels, Proceedings of the Third International Symposium on Friction Stir Welding, Sept. 2001 (Kobe, Japan), TWI, paper on CD.

[67] M. Posada, J. DeLoach, A. P. Reynolds, and J. P. Halpin, Mechanical Property and Microstructural Evaluation of Friction Stir Welded Al-6XN, Trends in Welding Research, Proceedings of the Sixth International Conference, April 15-19, 2002, (Pine Mountain, GA) ASM International, p 307-311.

[68] S.H.C. Park, Y.S. Sato, H. Kokawa, K. Okamoto, S. Hirano, and M. Inagaki, Rapid Formation of the Sigma Phase in 304 Stainless Steel during Friction Stir Welding, Scr. Mater., Vol 49 (No. 12), Dec. 2003, p 1175-1180.

[69] C. D. Sorensen and T.W. Nelson, Sigma Phase Formation in Friction Stirring of Iron-Nickel-Chromium Alloys, Trends in Welding Research, Proceedings of the Seventh International Conference, ASM International.

[70] C.B. Owen, "Two-Dimensional Friction Stir Welding Model with Experimental Validation", M.S. thesis, Brigham Young University, Provo, UT, 2006.

[71] T.D. Clark, "An Analysis of Microstructur and Corrosion Resistance in Underwater Friction Stir Welded 304L Stainless Steel", M.S. thesis, Brigham Young University, Provo, UT.

[72] Precipitation Hardening Stainless Steel- Alloys, properties, Fabrication Process < http://www.azom.com/details.asp?ArticleID=2819 > [18/07/2008].

[73] 15-5PH stainless steel [18/07/2008]

http://www.aksteel.com/pdf/markets_products/stainless/precipitation/15-5_PH_Data_Sheet.pdf .

[74] 17-4PH stainless steel [18/07/2008]

http://www.aksteel.com/pdf/markets_products/stainless/precipitation/17-4_PH_Data_Sheet.pdf .

[75] Lecture 15: Duplex and Other Steels Mmat 380 [18/07/2008].

[76] W.M. Garrison, Jr., J.A. Brooks, Mater. Sci. Eng. A149 (1991) 65.

[77] K.C. Antony. J. Metals 15 (1963), p. 922.

[78] P.W. Hochanadel, C.V. Robino, G.R. Edwards and M.J. Cieslak. Mater. Trans. A 25A (1994), p. 789.

[79] D. Kotecki, F. Armao, Stainless steel properties-how to weld them where to use them, Copyright © 2003 by The Lincoln Electric Company.

[80] J. C. Lippold, D. J. Kotecki, Welding metallurgy and weldability of stainless steel, 2005, ISBN 0-471-47379-0.

[81] W. Gan, T. Li, S. Khurana, Tool mushrooming in Friction Stir Welding of L80 Steel, Friction Stir Welding and Processing IV, TMS, 2007, p 279 – 283.

[82] T. W. Nelson, C.D. Sorensen, R. J. Steel and S. M. Packer, Improved Polycrystalline Cubic Boron Nitride Tooling for Friction Stir Welding High Temperature Alloys, 7th International Symposium 'Friction Stir Welding', 2008, Paper on CD

[83] C. B. Fuller, Friction Stir Tooling: Tool Materials and Designs, Friction Stir Welding and Processing, R. S. Mishra, M.W. Mahoney, Ed., ASM International, 2007.

[84] Trade literature, Megastir, US, 2008.

[85] Trade literature, Plansee GmbH, Germany, 2008.

[86] J. Pirso, M. Viljus, S. Letunovitš, Friction and dry sliding wear behaviour of cermets, Wear, Volume 260, Issues 7-8, 7 April 2006, p 815-824.

[87] J. Pirso, S. Letunovitš, Friction and wear behaviour of cemented carbides, Wear, Volume 257, Issues 3-4, August 2004, p 257-265.

[88] H. J. Liu, H. Fujii, and K. Nogi, Wear behavior of Hard Alloy Tools in the Friction Stir Welding of AC4A + 30 vol.% SiCp Aluminium Matrix Composite, Proceedings of the Fifth International Conference on Friction Stir Welding, Sept. 14-16, 2004, Metz (France), TWI, paper on CD.

[89] T. Weinberger, C. Kolbeck, Properties of WC-Co, unpublished research, 2007.

[90] W. Schatt, K. P. Wieters, Powder metallurgy, Processing and Materials.1997 ISBN 1 899072 05 5.

[91] Z. Z. Fang, Correlation of transverse rupture strength of WC–Co with hardness, International Journal of Refractory Metals & Hard Materials, 2005, Vol 23, p 119-127.

[92] Cooperation, MTS Systems, I-Stir MRH PDS Friction Stir Welder. User´s Manual. 100-161-389A, 2006.

[93] DIN EN 10088-1 Deutsches Institut für Normung, Nichtrostende Stähle Teil 1: Verzeichnis der nichtrostenden Stähle Deutsche Fassung 2005, p 30.

[94] A. P. Reynolds, T. Wei, T. Gnaupel-Herold, H. Prask, Structure, properties, and residual stress of 304L stainless steel friction stir welds, Scripta Materialia, Vol. 48,

2003, p 1289–1294.

[95] Y. S. Sato, M. Muraguchi and H. Kokawa, Reaction in 304 austenitic stainless steel during friction stir welding using WC-based alloy tool, IIW Doc. IX-2272-08, 2008.

[96] P. A. Colegrove and H. R. Shercliff, Modelling the Friction Stir Welding of Aerospace Alloys, Proceedings of the 5th International Symposium on Friction Stir Welding, 2004, Metz, France, paper on CD.

[97] H.N.B. Schmidt et al., Material flow in butt friction stir welds in AA2024-T3, Acta Materialia 54, (2006), p 1199–1209

[98] D. J. Chakrabarti, J. Liu, R. R. Sawtell, G. B. Venema. New Generation High Strength High Damage Tolerance 7085 Thick Alloy, Materials Form, Volume 28, 2004.

[99] Association, The Aluminum. International Alloy Designations and Chemical Composition Limits for Wrought Aluminum and Wrought Aluminum Alloys, 2004.

[100] H. Luonga, M. R. Hill, The effects of laser peening on high-cycle fatigue in 7085-T7651 aluminum alloy, Materials Science and Engineering A, p 477, 2008.

[101] S. Kasperl, J. Hiller, M. Krumm, Computed Tomography Metrology in Industrial Research and Development, MP Materials Testing, 6, 2009, Bd. 51.

[102] W.J. Arbegast, Modeling Friction Stir Joining as a Metalworking Process, The Minerals, Metals. and materials Society, Hot Deformation of Aluminium Alloys III, 2003.

[103] B. Criqui, Robust joining processes for series production today and tomorrow, Lightweight Vehicle Structure Conference, 2009, p 165.

[104] D. Mari, et al., Experimental Strategy to Study the Mechanical Behavior of Hard Metals for Cutting Tools., Int. J. Refract. Hard Met., 1999, vol. 17, pp. 209–225.

[105] G. Ostberg, et al., Mechanisms of Plastic Deformation of WC–Co and Ti(C, N)–WC–Co, Int. J. Refract. Hard Met., 2006, Vol. 24, pp. 135–144.

[106] D. Mari, et al., International Journal of Refractory Metals & Hard Materials, 17 (1999) p 209 - 225.

[107] N.V. Novikov, V.P. Bondarenko, V.T. Golovchan, HighTemperature Mechanical Properties of WC–Co Hard Metals (Review), Journal of Superhard Materials, 2007, Vol. 29, No. 5, p 261–280.

[108] S. U. Khosa, T. Weinberger, N. Enzinger, A Novel Approach for Modeling of Friction Stir Spot Welding Process considering Deformable Tool, Proceedings of 9th

International Seminar Numerical Analysis for Weldability, accepted for publication, Seggau, Austria, 2009.

[109] H. Fujii, T. Tatsuno, T. Tsumura, R. Ueji, K. Nakata, K. Nogi, Laser Assisted Hybrid Friction Stir Welding of Carbon Steel, 7th International Symposium 'Friction Stir Welding', 2008, Paper on CD

[110] T. Weinberger, Device and Method for the Friction Stir Spot Welding of Two Workpieces with a Hollow Cylinder having a Detachable Friction Liner and with a Tool, Patent Application WO/2009/126981, 22.10.2009

[111] J. R. Davis, ASM Specialty Handbook: Stainless Steels, ASM International, 1994.

[112] E. Herny et. al., Local Mechanical and Microstructural characterization of electron beam welded 15-5PH stainless steel, available online http://www.msm.cam.ac.uk/phase-trans/2005/LINK/137.pdf, [10.5.2008].

[113] H.R. Habibi Bajguirani, The effect of ageing upon the microstructure and mechanical properties of type 15-5 PH stainless steel, Materials Science and Engineering A338, (2002), p 142-159.

A Tool Drawings

1.1. Tool drawing for friction stir welding of 4 mm thick steel sheets
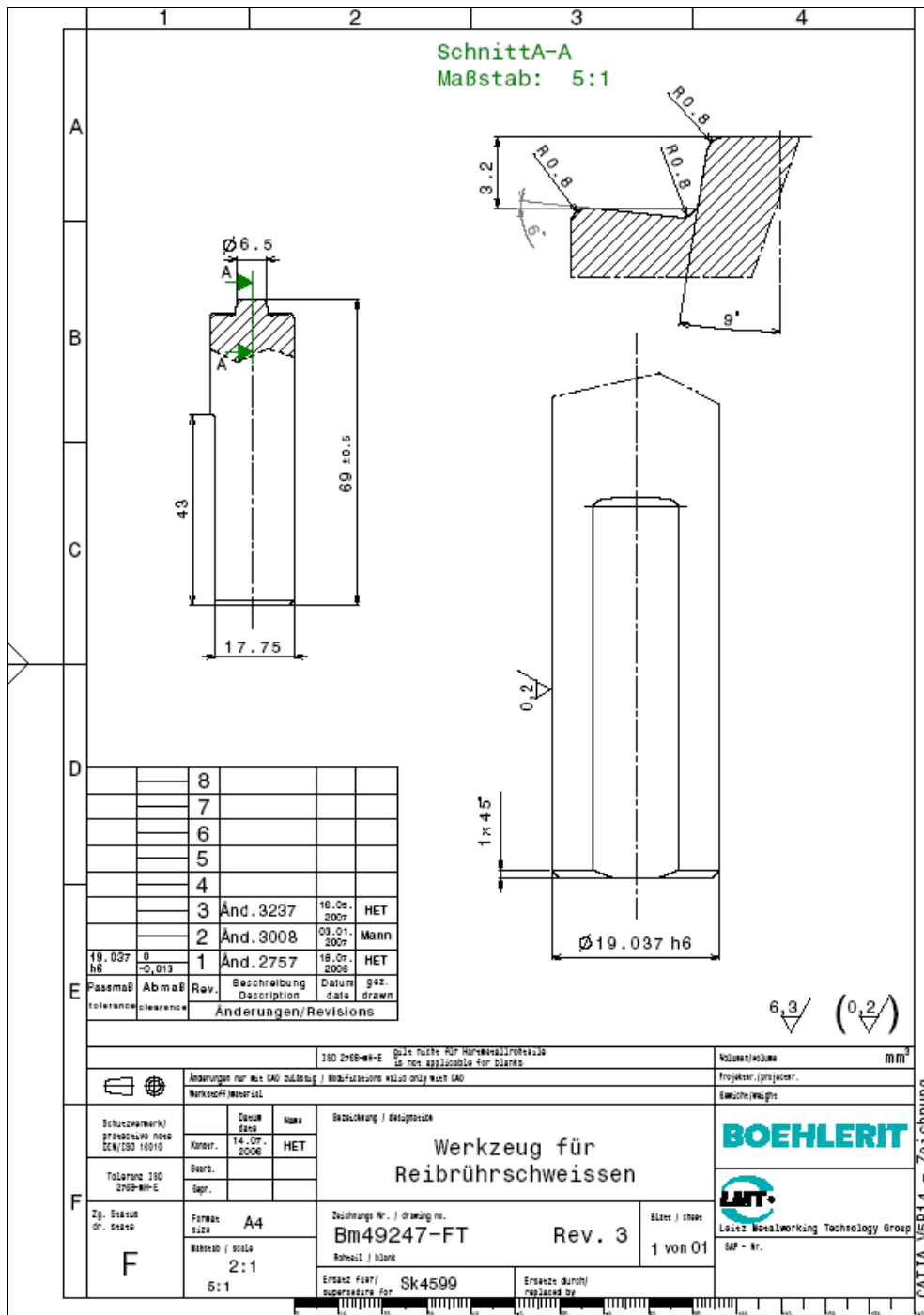
1.2.   Tool drawing for friction stir welding of 4 mm thick steel sheets with a three-flat pin
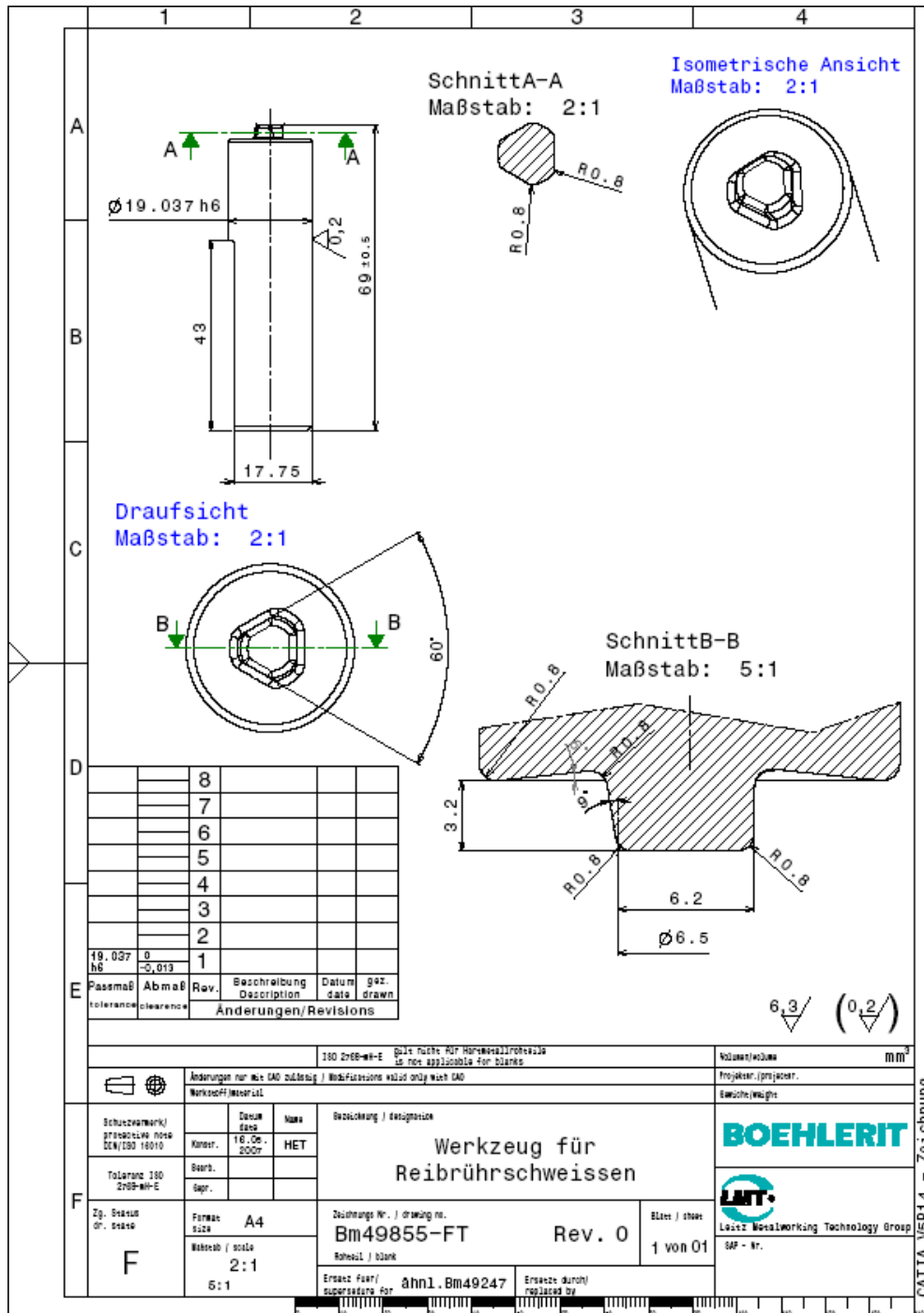
1.3.   Tool drawing for friction stir welding of 2.6 mm thick steel sheets
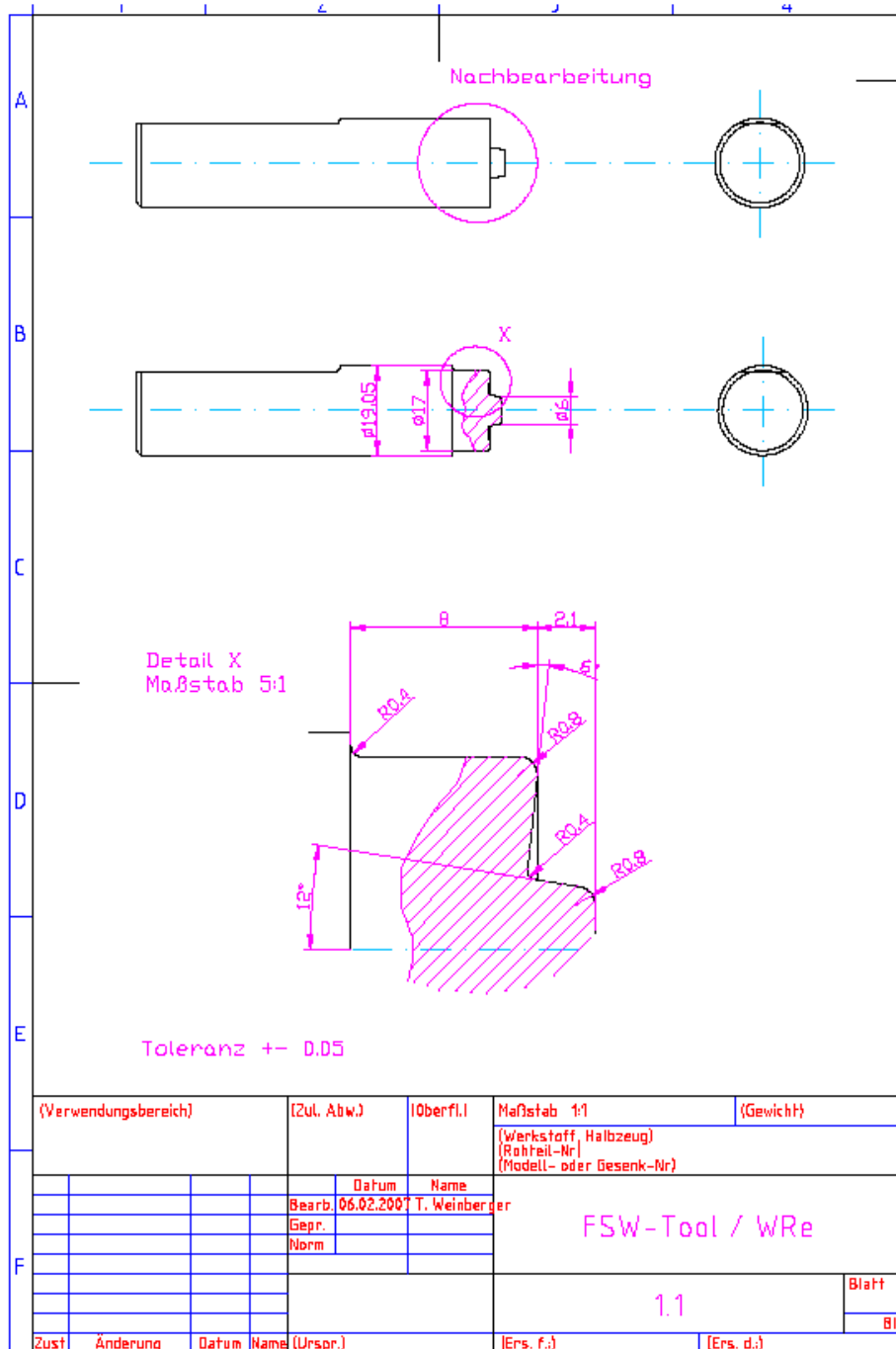
1.4.   Tool drawing for friction stir spot welding of two 0.8 mm thick steel sheets
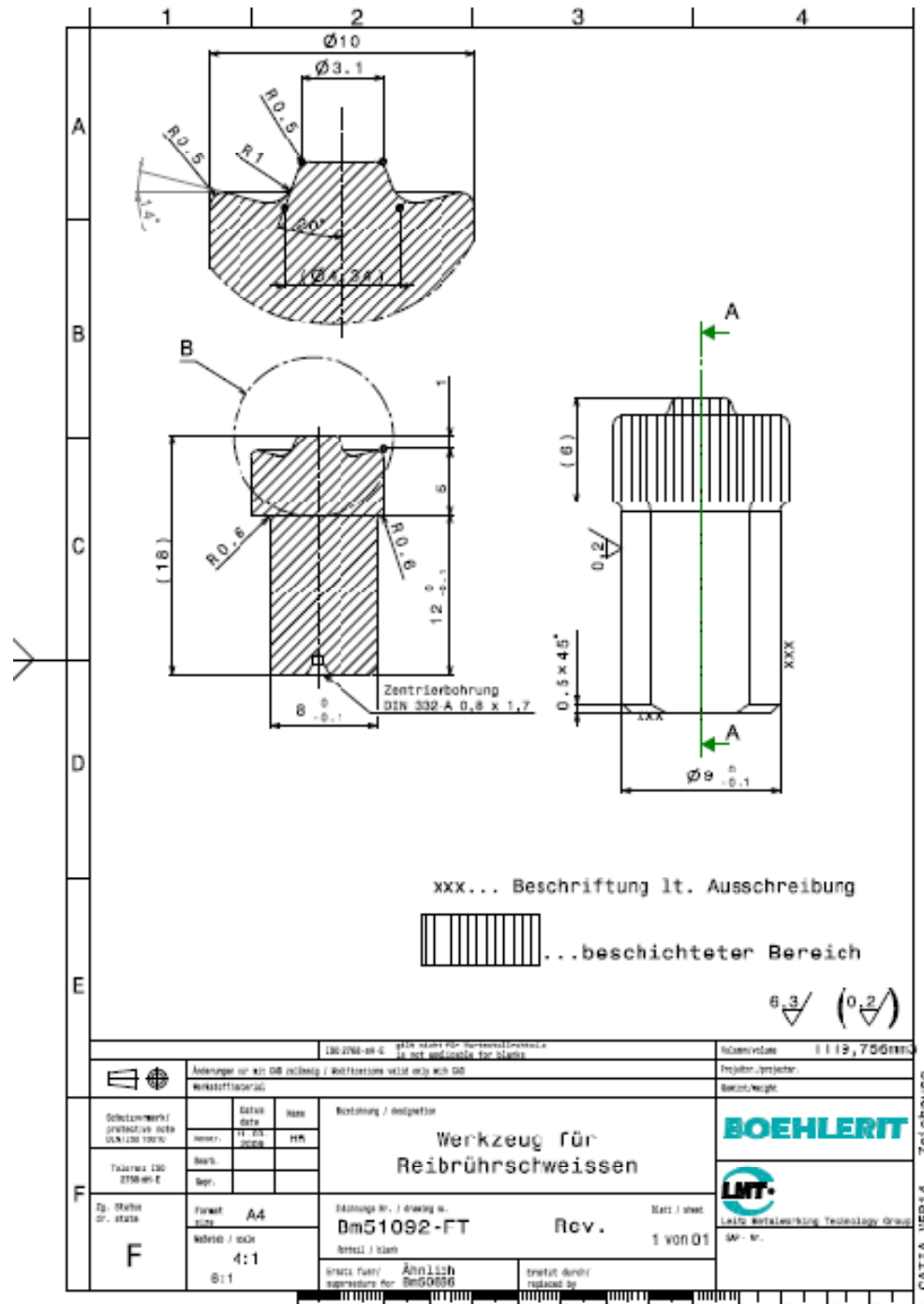
1.5.   Tool holder drawing for friction stir spot welding
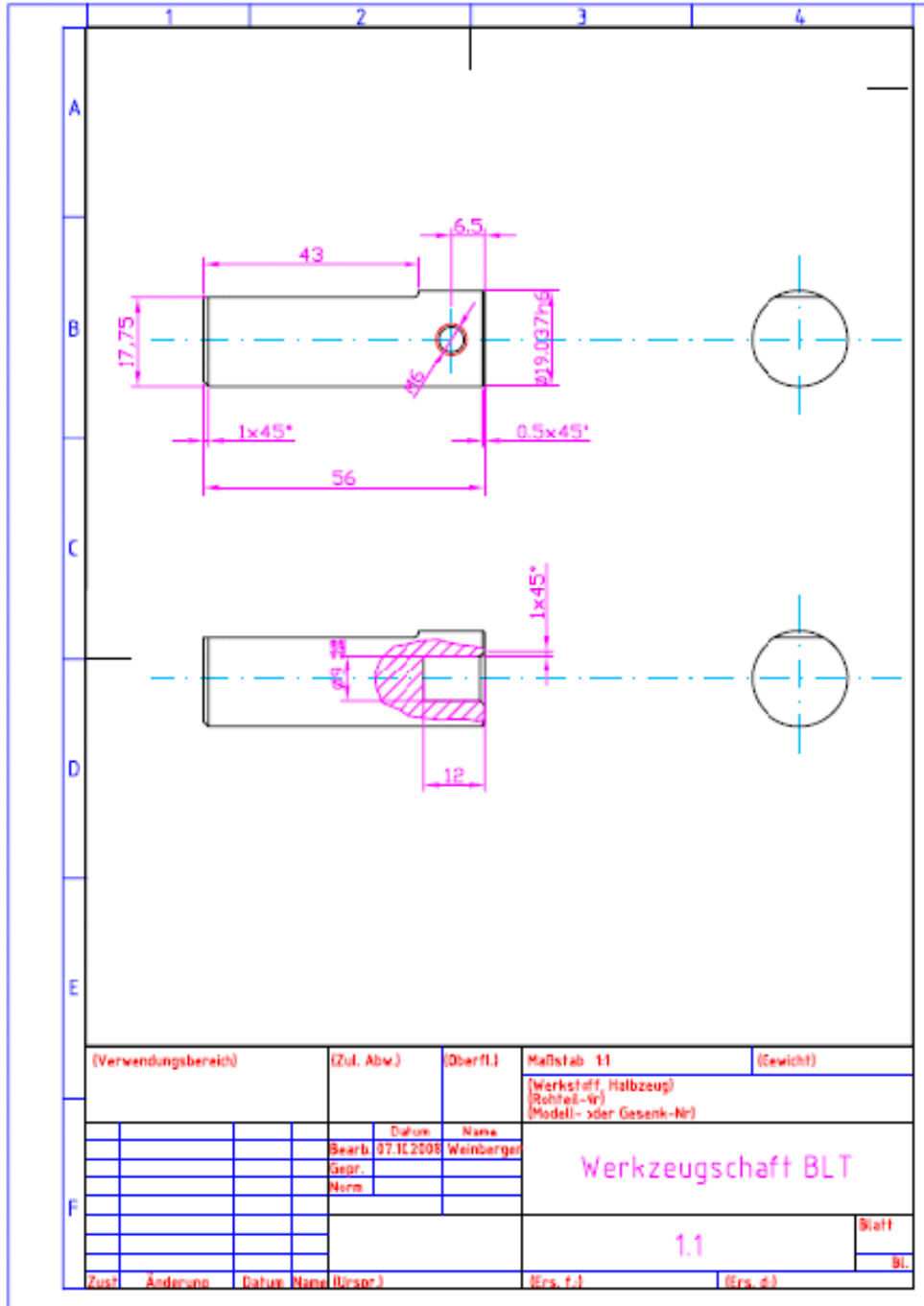
B Heat Treatments

1.1. Heat treatment of 15-5PH steel, thermal cycle

B607 Join, Auslagerung, Ofen 3, 12.6.2007
Probe S001,S002,S003,S004,S005,S006 - 520°C/1h; Luft

Schlieber; Ke; 20.6.2007
b607c_S014Auslagern.xls

Reglerparameter:
Xp1: 20
Xp2:1,2
Tn1: 400
TV1:100
T:1

Ofentemperatur [°C]

Zeit [h]
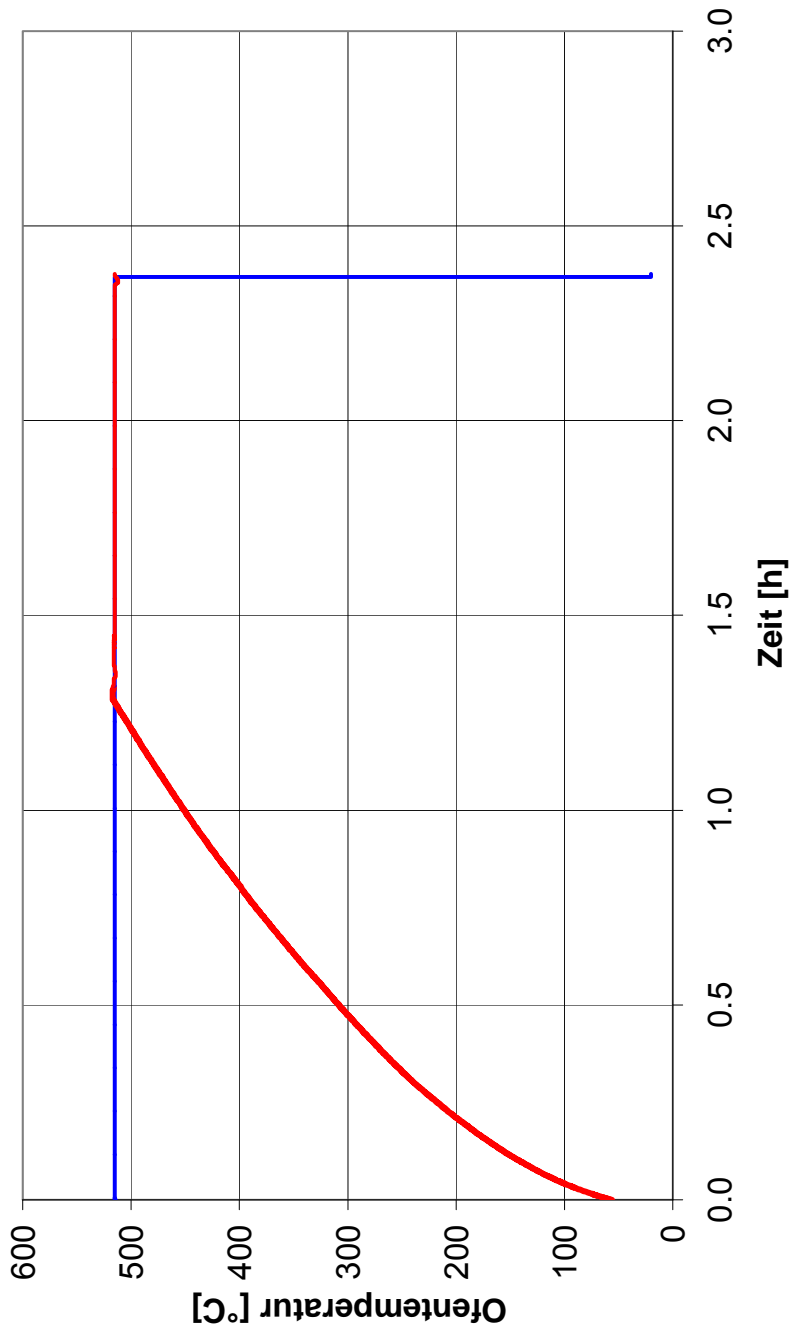
C SEM Pictures

2.1.   Macrograph and corresponding SEM pictures for friction stir butt weld of 2.6mm thick steel 15-5PH, condition A (Weld n. B6_0706_S004)
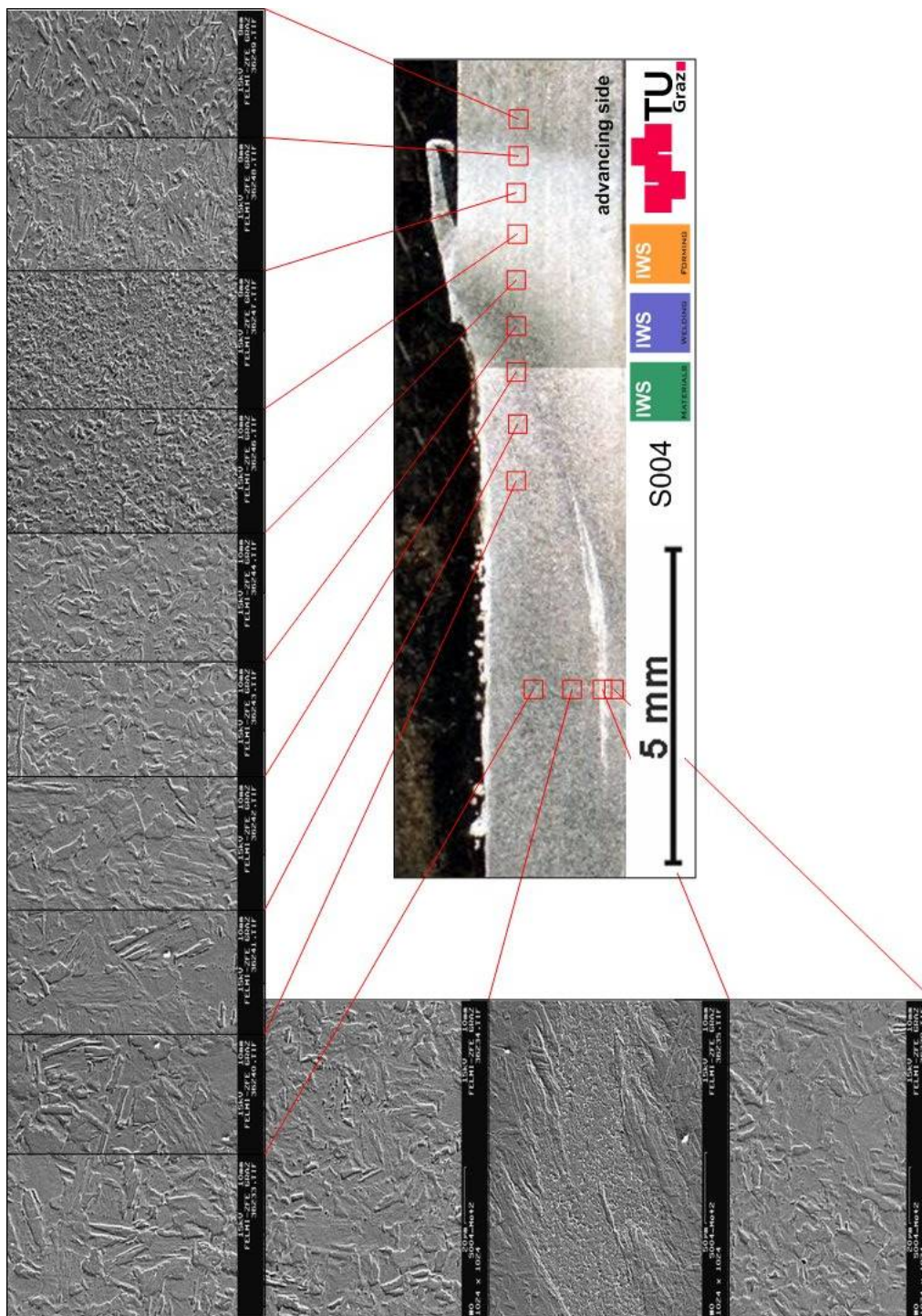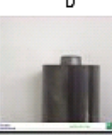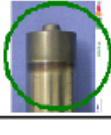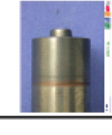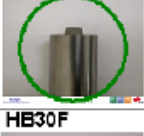
2.2. Macrograph and corresponding SEM pictures for bead on plate welded steel DIN 1.4301 with 4.0 mm plate thickness (Weld n. B7_0709_S010_135)
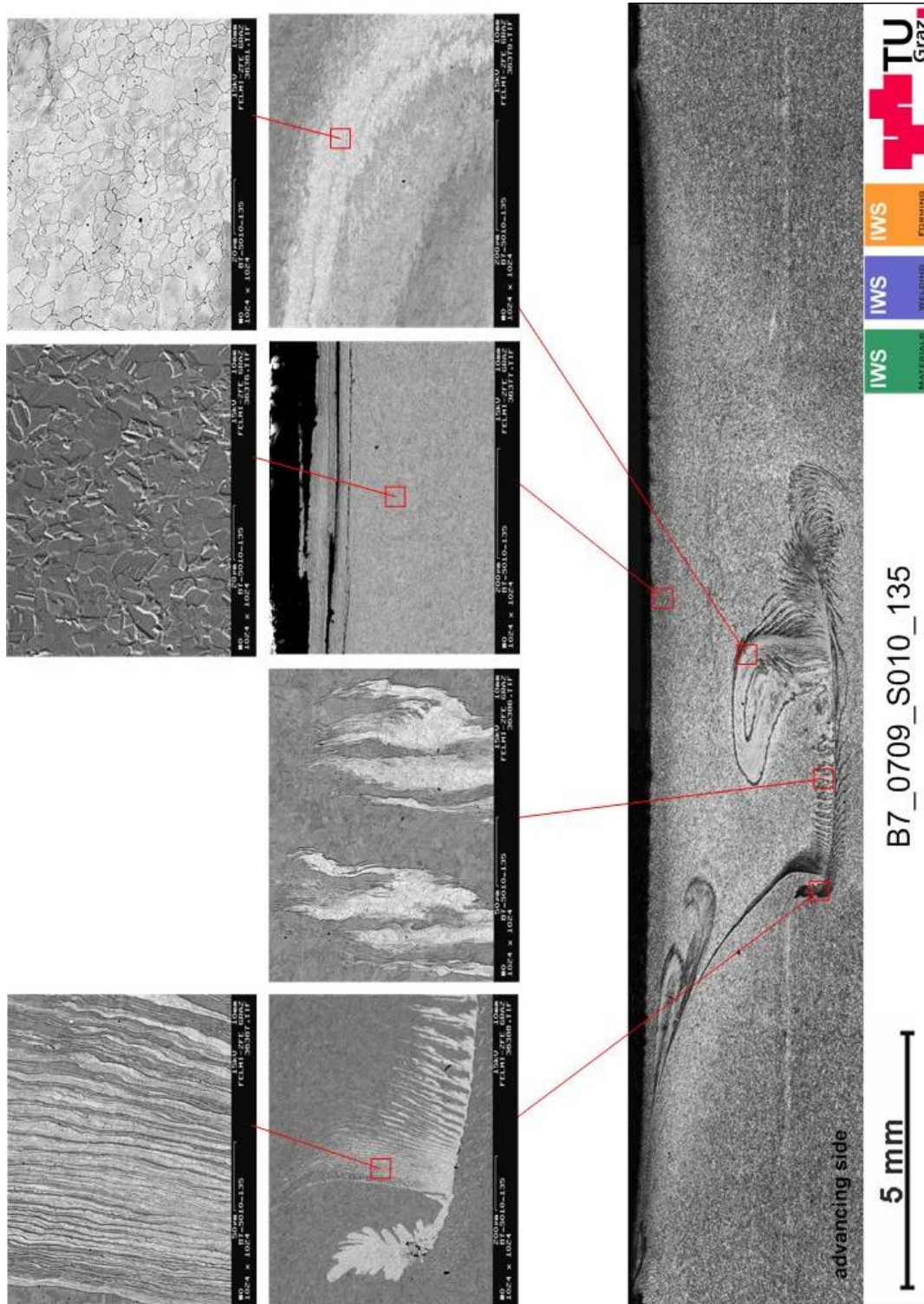
D Tool Development Matrix

FSW tool development matrix I
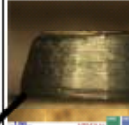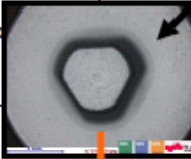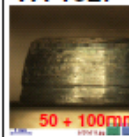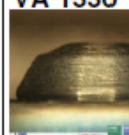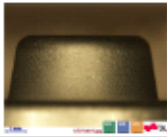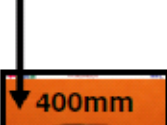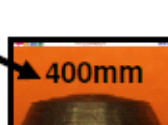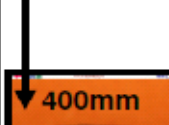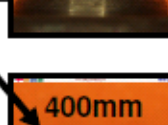
3.1.   FSW tool development matrix II

Beschichtung	A	I	G+	B	„Extra P"
Substrat			20 + 50mm	✗	
BB10	VA 1274	VA 1275	20 + 50 + 80mm VA 1259	Pin-Bruch nach ca. 85mm VA 1162	nicht vorhanden
BB40 (Aussehen vergleichbar BB10)	VA 1276	Pin-Bruch nach ca. 85mm VA 1277	20 + 50 + 80mm Pin-Bruch nach Σ ca. 145mm VA 1278	Pin-Bruch nach ca. 25mm VA 1279	nicht vorhanden
SB40 (Aussehen vglb. BB10)	VA 1280	VA 1281	20 + 50 + 80mm VA 1282	Pin-Bruch nach ca. 48mm VA 1156	nicht vorhanden
GB56 (Aussehen vglb. BB10) !nicht zielführend!	20mm VA 1283 !nicht zielführend!	20mm VA 1284 !nicht zielführend!	20mm VA 1285 !nicht zielführend!	nicht getestet VA 1286	20mm !nicht zielführend!

3.2. FSW tool development matrix III

Beschichtung Substrat	keine (Aussehen vergleichbar G+)	A (Aussehen vergleichbar G+)	I (Aussehen vergleichbar G+)	G+	„Extra P" (Aussehen vergleichbar G+)	AlCrO (Aussehen vergleichbar G+)
BB10		VA 1274	VA 1275	VA 1259	VA 1349	
WS08C00 (Aussehen vergleichbar BB10)	nicht vorgesehen	nicht vorgesehen		VA 1327 50 + 100mm	nicht vorgesehen Σ 550mm 7 50U/min	
GB20 (Aussehen vglb. BB10)	nicht vorgesehen	nicht vorgesehen	nicht vorgesehen	VA 1330	nicht vorgesehen	nicht vorgesehen
GB30 (Aussehen vglb. BB10)	nicht vorgesehen	nicht vorgesehen		VA 1333	nicht vorgesehen WRe(25%) (40mm)	en

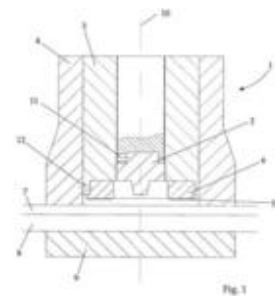## 3.3.   FSW tool development matrix IV

E Patent description

(WO/2009/126981) DEVICE AND METHOD FOR THE FRICTION STIR SPOT WELDING OF TWO WORKPIECES WITH A HOLLOW CYLINDER HAVING A DETACHABLE FRICTION LINER AND WITH A TOOL

Abstract:

(EN) The invention relates to a device (1) and a method for connecting at least two workpieces (7, 8) by friction welding. The device here comprises an axis (10) which can be driven in a rotating manner and on which a friction welding tool (1) is arranged, wherein the friction welding tool (1) has at least one pin-like tool (2), which can be driven in a rotating manner and is surrounded by at least one hollow cylinder (3), which can be driven in a rotating manner. The friction welding tool (1) can be moved along its axis of rotation (10) by the plastifying workpieces (7, 8), wherein the pin-like tool (2) and the hollow cylinder (3) can be moved independently of each other in the axial direction. The hollow cylinder (3) has on its side facing the at least one upper workpiece (7) a detachable friction liner (6) with a friction surface (5).

(DE) Die Erfindung betrifft eine Vorrichtung (1) bzw. ein Verfahren zum Verbinden von mindestens zwei Werkstücken (7, 8) durch Reibschweißen. Die Vorrichtung umfasst dabei eine rotierend antreibbare Achse (10), an der ein Reibschweißwerkzeug (1) angeordnet ist, wobei das Reibschweißwerkzeug (1) zumindest ein rotierend antreibbares stiftartiges Werkzeug (2) aufweist, das von zumindest einem rotierend antreibbaren Hohlzylinder (3) umgeben ist. Das Reibschweißwerkzeug (1) ist entlang seiner Drehachse (10) durch die sich plastifizierenden Werkstücke (7, 8) bewegbar, wobei das stiftartige Werkzeug (2) und der Hohlzylinder (3) unabhängig voneinander in axialer Richtung bewegbar sind. Der Hohlzylinder (3) weist an seiner dem zumindest einen oberen Werkstück (7) zugewandten Seite einen lösbaren Reibbelag (6) mit einer Reibfläche (5) auf.

Designated States: AE, AG, AL, AM, AO, AT, AU, AZ, BA, BB, BG, BH, BR, BW, BY, BZ, CA, CH, CN, CO, CR, CU, CZ, DE, DK, DM, DO, DZ, EC, EE, EG, ES, FI, GB, GD, GE, GH, GM, GT, HN, HR, HU, ID, IL, IN, IS, JP, KE, KG, KM, KN, KP, KR, KZ, LA, LC, LK, LR, LS, LT, LU, LY, MA, MD, ME, MG, MK, MN, MW, MX, MY, MZ, NA, NG, NI, NO, NZ, OM, PG, PH, PL, PT, RO, RS, RU, SC, SD, SE, SG, SK, SL, SM, ST, SV, SY, TJ, TM, TN, TR, TT, TZ, UA, UG, US, UZ, VC, VN, ZA, ZM, ZW.
African Regional Intellectual Property Org. (ARIPO) (BW, GH, GM, KE, LS, MW, MZ, NA, SD, SL, SZ, TZ, UG, ZM, ZW)
Eurasian Patent Organization (EAPO) (AM, AZ, BY, KG, KZ, MD, RU, TJ, TM)
European Patent Office (EPO) (AT, BE, BG, CH, CY, CZ, DE, DK, EE, ES, FI, FR, GB, GR, HR, HU, IE, IS, IT, LT, LU, LV, MC, MK, MT, NL, NO, PL, PT, RO, SE, SI, SK, TR)
African Intellectual Property Organization (OAPI) (BF, BJ, CF, CG, CI, CM, GA, GN, GQ, GW, ML, MR, NE, SN, TD, TG).

Publication Language: German (DE)

Filing Language: German (DE)